Towards the SQL Interferometer
Length Stabilization at the AEI 10 m-Prototype

Der Fakultät für Mathematik und Physik
der Gottfried Wilhelm Leibniz Universität Hannover

zur Erlangung des akademischen Grades
Doktorin der Naturwissenschaften
Dr. rer. nat.

genehmigte Dissertation von

Dipl.-Phys. Sina Maria Köhlenbeck

2018

Referent:	Prof. Dr. Karsten Danzmann
Korreferentin:	Prof. Dr. Michèle Heurs
Korreferent:	Prof. Dr. Kenneth Strain

Tag der Promotion: 29. Juni 2018

Kurzfassung

Neue Technologien zur Verbesserung der Empfindlichkeit von Gravitationswellendetektoren werden weltweit in Prototypenanlagen entwickelt und charakterisiert. Klassische Rauschquellen in den erdgebundenen interferometrischen Detektoren werden bald bis unterhalb der fundamentalen Quantenrauschgrenze unterdrückt werden. Diese entsteht bei niedrigen Frequenzen durch Quantenstrahlungsdruckrauschen und bei hohen Frequenzen durch Schrotrauschen. Diese beiden Quantenrauschquellen schneiden sich an einem Punkt auf dem Standardquantenlimit (SQL). Das SQL ist die Ortskurve, welche von den Schnittpunkten der beiden Rauschquellen für verschiedene Laserleistungen gebildet wird. Der AEI 10 m-Prototyp wird ein Michelson Interferometer mit Fabry-Perot Resonatoren beherbergen um das SQL zu vermessen und einen Prüfstand zur Verfügung stellen um Technologien zu testen, welche es übertreffen können.

Die Experimente des AEI 10 m-Prototyp sind auf drei seismisch isolierten optischen Bänken installiert. Die Spiegel der Hauptexperimente sind einzeln an kaskadierten Aufhängungen aufgehängt, die über diese Bänke verteilt sind. Der Betrieb des Hauptinterferometers erfordert eine genaue Kontrolle der Spiegelpositionen.

Diese Arbeit befasst sich mit der Längenstabilisierung am AEI 10 m-Prototyp, getrennt in aktive seismische Vorisolierung und Ansteuerung der aufgehängten Resonatorspiegel.

Die Differenzbewegung zwischen den seismisch isolierten optischen Bänken wird durch ein Suspension Platform Interferometers gemessen und liefert ein Steuersignal, das zur aktiven Stabilisierung genutzt werden kann. Im Rahmen dieser Arbeit wurde die Auslese-Empfindlichkeit des Suspension Platform Interferometers verbessert und die ursprünglich vorgesehene Stabilität übertroffen. Diese Stabilität wird durch ein Feedback-System auf die Experimente am AEI 10 m-Prototyp übertragen. Es steuert die optischen Tische relativ zueinander und unterdrückt die Differenzbewegung um mehr als vier Größenordnungen bis $10\,\mathrm{pm\,Hz^{-1/2}}$ bei 100 mHz.

Die Bewegung der Aufhängepunkte der optischen Resonatoren wandelt Winkelverschiebungen in Änderungen die Resonatorlänge um. Diese Winkelfreiheitsgrade werden durch eine Reihe von optischen Hebeln gesteuert und die Entwicklung, Implementierung und Charakterisierung dieser Sensoren wird demonstriert. Zusammen mit dem Suspension Platform Interferometer wurde die restliche Bewegung der Aufhängepunkte eines optischen Resonators um bis zu drei Größenordnungen unterdrückt. Die aktive seismische Vorisolierung ist vollständig in Betrieb.

Ein neues Konzept für einen elektrostatischen Aktuator (ESD) wird untersucht und die Funktionsweise der mehrstufige Spiegelaufhängung, der Aktuatoren sowie der ESD-Technik wird mit einem Vorversuch zur Nachahmung eines Arms des Sub-SQL-Interferometers charakterisiert. Es wurden zwei mehrstufige Spiegelaufhängungen aufgebaut, mit jeweils einer Testoptik ausgestattet. Sie wurden dann im AEI 10 m-Prototypen installiert und bilden einen Fabry-Perot-Resonator mit einer Länge von 10,8 m, das so genannte Single Arm Test Experiment. Dieses demonstriert Schlüsseltechnologien und ermöglicht zusätzlich eine schnelle Inbetriebnahme des Sub-SQL-Interferometers durch das installierte Detektionsverfahren und den neu aufgebauten Eingangspfad.

Schlagwörter: Erdgebundene Gravitationswellenmessung, Laserinterferometer, Seismikisolation, Spiegelaufhängung

Abstract

New technologies to improve the sensitivity of gravitational wave detectors are developed and characterized in prototype facilities across the world. Classical noise sources in the ground-based interferometric detectors will soon be suppressed below the fundamental quantum noise limit which arises from quantum radiation pressure noise at low frequencies and shot noise at high frequencies. The two quantum noise sources intersect at a point on the Standard Quantum Limit (SQL). The SQL is a locus formed from the intersection points of the noise sources for different laser powers. The AEI 10 m-Prototype facility will house a Michelson Interferometer with Fabry-Perot cavities to probe the SQL and provide a test bed for technologies to eventually surpass it.

The experiments of the AEI 10 m-Prototype are installed on three seismically isolated optical benches. The mirrors of the main experiments are individually suspended by cascaded suspension chains, distributed across these benches. The operation of the main interferometer requires a precise control of the mirror positions.

This thesis addresses the length stabilization at the AEI 10 m-Prototype, separated into active seismic pre-isolation and actuation to the suspended cavity mirrors.

Differential motion between the seismically isolated optical benches is measured by a Suspension Platform Interferometer and provides a control signal that can be used for its active stabilization. In the scope of this thesis, the readout sensitivity of the Suspension Platform Interferometer was improved and the originally intended noise floor was surpassed. The stability is transfered to the experiments at the AEI 10 m-Prototype by a feedback system. It controls the optical tables relative to each other and suppresses the differential motion by more than four orders of magnitude to 10 pm $\mathrm{Hz}^{-1/2}$ at 100 mHz.

The suspension point motion of the cavities converts angular displacement to the cavity length. These angular degrees of freedom are controlled by a set of optical levers, and the development, implementation and characterization of these sensors is demonstrated. Together with the Suspension Platform Interferometer, the residual suspension point motion of a cavity was suppressed by up to three orders of magnitude. The active seismic pre-isolation is fully commissioned and operating.

A new concept for an Electro Static Drive (ESD) is investigated and the performance of the suspension chain, the actuators as well as the ESD technique is characterized using a preliminary experiment set up to mimic one arm of the sub-SQL interferometer. Two suspensions chains were built, equipped with pilot optics and installed in the AEI 10 m-Prototype system forming a Fabry-Perot cavity of length 10.8 m. The so-called Single Arm Test experiment proves key technologies and additionally the installed detection chain and the input path will allow for a fast commissioning of the sub-SQL interferometer.

Key words: Ground-based gravitational wave detection, laser interferometry, seismic isolation, mirror suspension

Contents

List of Abbreviations

ADC	Analog-to-Digital Converter
AEI	Albert Einstein Institute
aLIGO	advanced LIGO
AOM	Acousto-Optic Modulator
ASD	Amplitude Spectral Density
CDS	Control and Data System
CMM	Coordinate Measuring Machine
CMS	Crystalline Mirror Solutions GmbH
D-Sub	D-Subminiature
DAC	Digital-to-Analog Converter
DTT	Diagnostic Test Tool
DWS	Differential Wavefront Sensing
eLIGO	enhanced LIGO
EOM	Electro-Optic Modulator
ESD	Electro Static Drive
FEM	Finite Element Modeling
FIOS	Fibre Injector Optical Subassemblies
GAS	Geometric Anti Spring
HV	High Voltage
IBS	Ion Beam Sputtering
IGR	Institute for Gravitational Research
IP	Inverted Pendulum
LIGO	Laser Interferometer Gravitational-Wave Observatory
ligoDV	LIGO Data Viewer
LISA	Laser Interferometer Space Antenna
LVDT	Linear Variable Differential Transformer
NPRO	Non-Planar Ring Oscillator

OPD	Optical Path-length Difference Stabilization
PEEK	Polyether Ether Ketone
PLL	Phase Lock Loop
PM	Polarization-Maintaining
PMI	Phasemeter Interface
PUM	Penultimate Mass
QPD	Quadrant Photo Diode
SAS	Seismic Attenuation System
SM	Steering Mirror
SQL	Standard Quantum Limit
UHV	Ultra-High Vacuum

CHAPTER 1

Introduction

The first observation of gravitational waves in 2015 was achieved decades after the initial construction of a gravitational wave detector. Years of consecutive upgrades, developed by thousands of scientists, later the advanced Laser Interferometer Gravitational-Wave Observatorys (LIGOs) finally became sensitive enough to allow for this first detection [Aas15; Abb16].

The Albert Einstein Institute (AEI) is home to many fields of gravitational wave detection research, for both spaceborne and ground-based detectors. The scientific work performed at the AEI spans from theoretical work on numerical simulations of waveform models over data analysis of compact binaries and continuous gravitational waves as well as gravitational wave bursts, to the experimental divisions of ground-based detectors, such as GEO 600 [Lüc10; Wil02] and the spaceborne Laser Interferometer Space Antenna (LISA) project [Ama17].

Technologies for gravitational wave detectors need to work reliably before they can be implemented. In bench-top experiments and prototype facilities, the technologies can be tested in separate experiments.

To fully test the required instruments for the LISA mission, a technology demonstrator satellite named LISA-pathfinder, was launched [McN08]. Within this mission crucial new hardware and technologies were tested, such as the caging system, the release and the discharging of the test masses and the satellite positioning with micro-Newton thruster. A major achievement for the LISA mission was the interferometric readout sensitivity, which exceeded all expectations and already reached the required readout sensitivity of the LISA mission [Arm16].

For ground-based interferometers, prototype facilities have provided a test bed for technologies to be implemented in large-scale detectors [Rob95; Sho88; War08]. One example are the quasi-monolithic silica mirror suspensions for GEO 600, which were developed at the Institute for Gravitational Research (IGR) of Glasgow University, and were first tested in their 10 m prototype facility [Bar02]. Upon the successful implementation at GEO 600, they were also integrated into the LIGO during their upgrade to advanced LIGO (aLIGO) [Cum12].

Interferometric gravitational wave detectors are limited by quantum noise, which causes shot noise at high frequencies as well as radiation pressure noise at low frequencies [Sch17]. Currently operating gravitational wave detectors are not yet sensitive enough to measure radiation pressure noise. By introducing non-classical light, the interferometer can be operate beyond the shot-noise limit. To do so, the vacuum fluctuations at the open port of the interferometers beam splitter have to be replaced with squeezed vacuum states [Cav81]. The generation of squeezed vacuum states is now a standard technique to surpass the shot noise limit and is been

used at GEO 600 for years [Aff14; Vah10; Vah16].

The final upgrade level of aLIGO and the future gravitational wave detectors such as Einstein Telescope (ET) are expected to be limited by both quantum quantum radiation pressure noise and shot noise. New technologies are required to overcome this fundamental limit. Since upgrades at the detector site are invasive and take valuable time barring the detector from accumulating data a test facility is required such as the AEI 10 m-Prototype dedicated to testing technology to reduce quantum noise [Goß10]. The two associated observables, phase and amplitude of the interferometer output, cannot be measured with arbitrary precision at the same time. They are limited by the Heisenberg uncertainty principle. The minimum of the sum of the radiation-pressure noise and the shot noise is the SQL, and can be probed by variation of the input power [Cav81]. In the following section, the ambitious project of building a prototype system only limited by the SQL in the gravitational wave detection band, is described.

The AEI 10 m-Prototype facility is still under construction. The first part of this thesis describes the active stabilization of the differential and inertial motion of two optical tables supported by the AEI-Seismic Attenuation System (SAS) units using optical sensors. The optical sensors are split into two categories. An interferometric sensor, the Suspension Platform Interferometer, to control the longitudinal displacement of the two AEI-SAS units relative to each other and two optical lever signals for control of rotational degrees of freedom. By using the signals of these sensors in a feedback control system, the motion of the three most important degrees of freedom for the suspended optics installed on the AEI-SAS can efficiently be reduced. By making the suspension point quieter, the mirror motion and therefore the actuation force onto the interferometer mirrors can be reduced. The second part of this thesis contains the assembly and testing of the suspension chain for the interferometer mirrors. Two pilot optics are currently installed in the two SQL suspensions, which are located on different optical tables inside the AEI 10 m-Prototype vacuum system. They form a Fabry-Perot cavity, with the equivalent properties as intended for the final interferometer. The system to actuate on the suspension is characterized, featuring a novel ESD at the mirror. The stabilization of the cavity using the actuators on the suspension is demonstrated.

1.1 AEI 10 m-Prototype

The AEI 10 m-Prototype is designed to test novel techniques to surpass the SQL. By adjusting the optical components and the size of the interferometer and its core optics, it is designed to reach the SQL in the measurement band of gravitational wave detectors. This will allow for a direct transfer of knowledge and technologies to the large-scale interferometers. The risk of failure, when scaling to the large interferometers, is therefore almost negligible. To build an interferometer only limited by quantum noise, all classical noise sources need to be suppressed below the SQL. The setup to achieve this at the AEI 10 m-Prototype is discussed in the next sections.

1.1.1 Sub-SQL interferometer

The design of the AEI 10 m-Prototype is kept close to the large scale interferometers, with an L-shaped Michelson interferometer [Mül03]. In figure 1.1 a simplified sketch of the optical layout is shown. By using light weight mirrors of only 100 g and building up laser power with cavities in the interferometer arms the radiation pressure noise of the interferometer is enhanced. In contrast, aLIGO uses 40 kg test mass mirrors in order to reduces the susceptibility to quantum radiation pressure noise.

The interferometer is housed in an Ultra-High Vacuum (UHV) system, decoupling it form air fluctuations, acoustic disturbances and thermal drifts. A panoramic photo of the full vacuum system can be seen in figure 1.2. The three vacuum chambers are 3 m in diameter, separated by 11.65 m. Since the quadratic optical tables within each vacuum chamber have dimensions of 1.75 m × 1.75 m, enough space remains to allow access to the optical components after their initial installation inside the vacuum system. To use the space on the optical table efficiently, the tubes connecting the tanks are 1.5 m in diameter [Goß10]. This allows for several beam paths next to each other.

Outside the vacuum system, the light for the interferometer is generated by an enhanced LIGO (eLIGO) 35 W Laser system. Up to 10 W of the laser light is sent into the vacuum system via a polarization maintaining photonic crystal fiber. Using a fiber instead of a free beam coupling of the laser light into the vacuum system was mainly motivated by reduced beam pointing between the outside and the inside of the vacuum system. It comes with the additional benefit of additional mode filter capabilities [Opp17; Rus03].

To further suppress higher-order spatial modes, a triangular ring mode cleaner is used in the input path [Opp17]. The 35 W Laser system includes two actuators, an Acousto-Optic Modulator (AOM) for intensity stabilization and an Electro-Optic Modulator (EOM) for frequency stabilization. The two stabilization systems are briefly explained, and the current status is summarized in section 1.1.2.

The noise budget of the individual contributions to the readout of the sub-SQL interferometer and their suppression is described in the following sections.

1.1.2 Noise contributions in the sub-SQL interferometer

The first design study for the sub-SQL interferometer of AEI 10 m-Prototype was performed in 2009, followed by the prosed experimental setup in [Goß10]. Since then, the optical layout has been revised and a new noise analysis, was performed by D. Wu using the GWINC. The results of this noise projection are shown in figure 1.3.

Seismic noise reduction

The mirrors of the interferometer are moving with the local the seismic noise, which is equivalent to the ground motion. In Hannover, the seismic noise, at 50 Hz varies from 1 nm $\mathrm{Hz}^{-1/2}$ to 0.1 nm $\mathrm{Hz}^{-1/2}$, and would dominate the readout of the sub-SQL interferometer. To suppress this motion, each mirror is suspended from a cascaded pendulum chain [Gos02]. Three stages

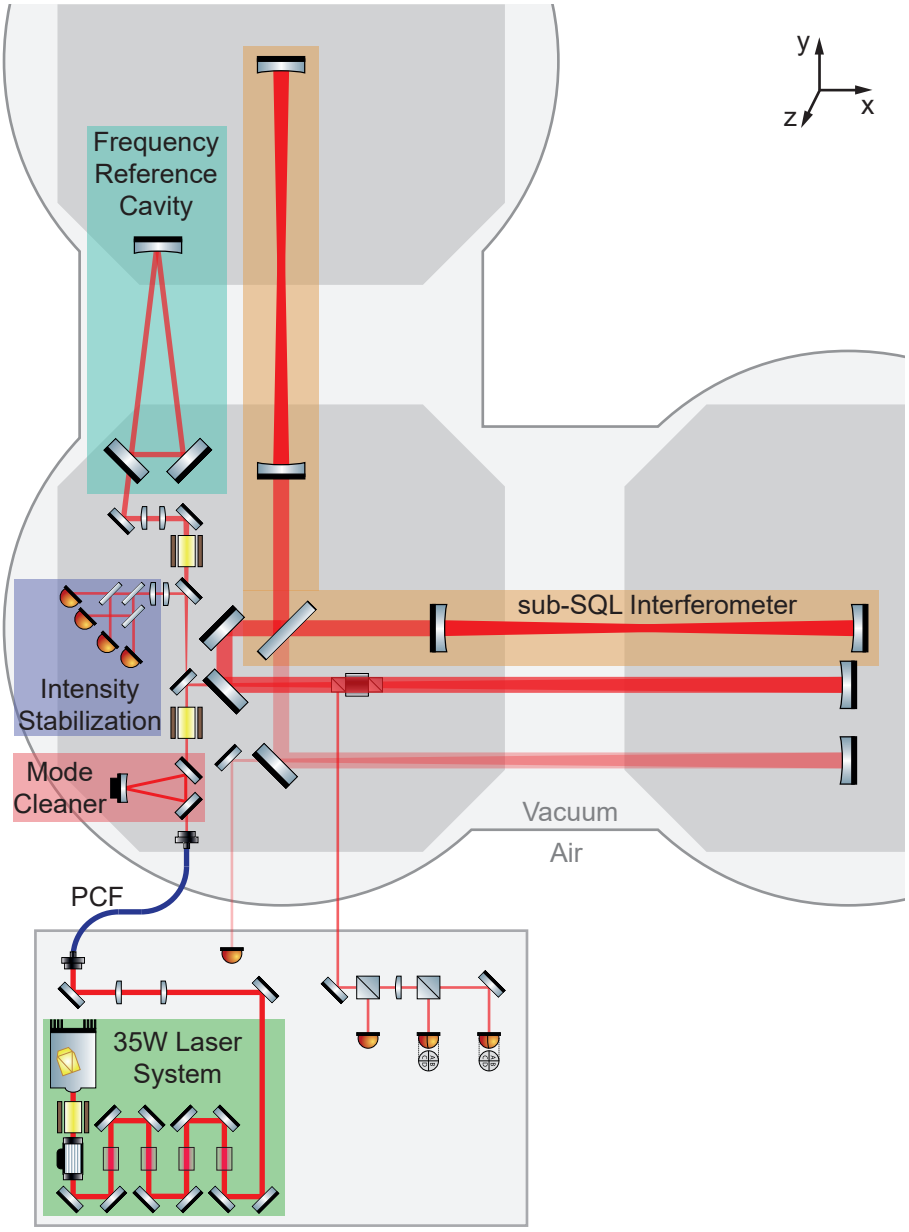

Figure 1.1: Simplified overview of the optical configuration for the sub-SQL interferometer and the sub-systems. The laser light is prepared outside of the vacuum system and than guided into it by a photonic crystal fiber. It is spatially filtered by a Mode Cleaner Cavity. A fraction of the laser beam is split off for the Intensity Stabilization and the Frequency Reference Cavity. The main part of the laser beam is expanded by traveling along the x-arm of the AEI 10 m-Prototype. The beam height is raised from 10 cm to 22 cm. A curved mirror with a radius of curvature of 24 m is collimating the laser beam. It is reflected back to the central table onto the beam splitter and then entering the sub-SQL interferometer.

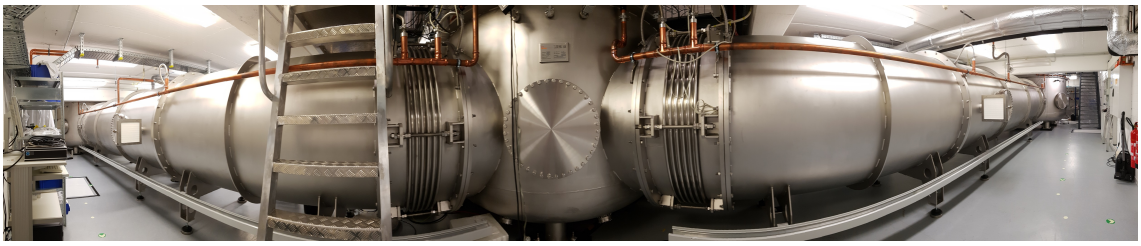

Figure 1.2: Panoramic picture of the vacuum system at the AEI 10 m-Prototype. The sub-SQL interferometer is being installed inside, distributed across the three tanks. Picture courtesy by P. Oppermann.

of horizontal isolation attenuate the ground motion induced mirror displacement. Two vertical isolation stages attenuate the vertical degrees of freedom and suppress the introduction of motion from these to the longitudinal degree of freedom. A detailed description of the pendulum chain is given in section 3.1. The seismic noise reduction is shown in the orange-red line in figure 1.3.

The optical tables supporting the mirror suspensions include a seismic pre-isolation system, the AEI-SAS. It provides passive isolation from the seismic motion for all degrees of freedom of the optical table, spanning from 0.1 Hz to 10 Hz. The performance and assembly of the AEI-SAS is described in detail in [Ber18; Wan13]. The AEI-SAS has two stages of isolation. Mirror suspensions at the AEI 10 m-Prototype have resonance frequencies at about 0.7 Hz. To already provide isolation from the AEI-SAS, the passive filters are tuned to frequencies below these. The first stage uses Inverted Pendulum (IP) legs as a low-frequency harmonic oscillator for the horizontal isolation of the optical bench [Tak07; Wan12]. The resonance frequency for this stage can be tuned 100 mHz.

In figure 1.4(a) shows the AEI-SAS during its construction phase, which allows to see the passive filter stages. The IP legs are visible as rods covered by bell shaped structures. After this stage the filters for vertical isolation follow. Cantilever blades are compressed against each other and form a crown shaped Geometric Anti Spring (GAS) filter. The resonance frequency of this filter stage can be lowered to 300 mHz [Ber18]. The fully assembled AEI-SAS is shown in 1.4(b).

In addition to the passive filter stages inertial and relative sensors are installed and allow active stabilization of the optical bench of the AEI-SAS. The relative sensors are measuring the displacement relative to the ground. To drive the AEI-SAS into position, actuators are co-located with the relative sensors and together they form an Linear Variable Differential Transformer (LVDT) [Wan12]. The passive isolation is additionally improved by active feedback with inertial sensors. For the vertical degrees of freedom L4C-geophones from Sercel are used [Kir17] and for the horizontal degrees of freedom monolithic accelerometers are installed in a stage between the horizontal and the vertical filter stage [Ber06a; Wan12].

The longitudinal degrees of freedom of the sub-SQL interferometer have to be stabilized to operate the interferometer, see 1.1.4. By pre-isolating these degrees of freedom, the feedback control at the interferometer mirrors can be reduced. The suspension point is 82 cm above the

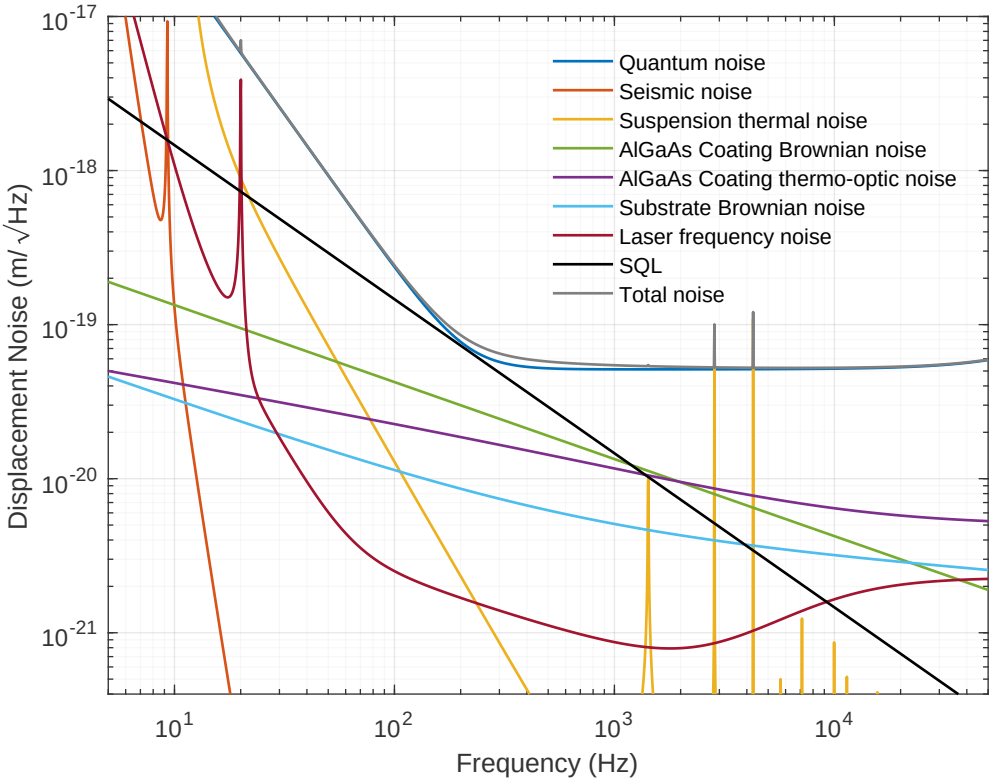

Figure 1.3: Noise projection of the individual noise sources to the readout of the sub-SQL interferometer. All classical noise sources will be suppressed below the SQL in a frequency band from 30 Hz to 900 Hz. To probe the SQL, the input power to the interferometer can be varied. The displayed quantum noise corresponds to an input power of 5 W. A stability factor of the arm cavities of $g = 0.99$ is assumed. The seismic noise will be reduced by cascaded mirror suspensions. The last stage of the suspension will be made out of quasi-monolithic fused silica suspensions, to reduce the suspension thermal noise. The coating thermal noise calculation is assuming crystalline coatings. The mirror material is fused silica. To suppress the laser frequency noise sufficiently, a suspended cavity with 21 m round trip length and heavy mirrors is used as a reference for the laser frequency. This noise analysis was performed by D. Wu using Gravitational Wave Interferometer Noise Calculator (GWINC).

optical table and pitch motion of them is displacing the suspension point longitudinally. Optics that are not placed on the rotational axis, experience also a longitudinal displacement. The suspended cavities are most sensitive to the longitudinal, pitch and yaw degrees of freedom of the optical table. These are additionally stabilized using optical sensors. The detailed description and performance analysis is one of the main topics of this thesis and is described in detail in section 2 and section 4.1.

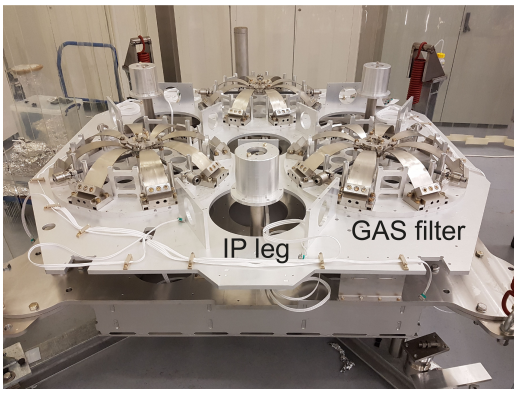

(a) View at the passive filter components of an AEI-SAS. The crown-shaped cantilever blades are forming three GAS filter. The pillars, covered by bell-shaped structures are the IP legs.

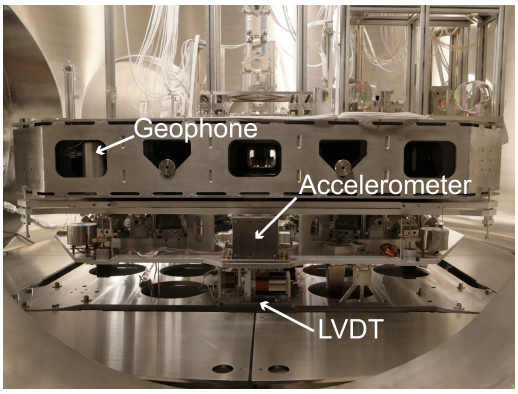

(b) Completely assembled and installed AEI-SAS. The passive filter stages are hidden by the sensors and support structure. At the bottom, a horizontal LVDT and above that an accelerometer are visible. To the left a vertical geophone is installed in the support structure of the optical table.

Figure 1.4: Two pictures of the AEI-SAS.

Intensity and frequency stabilization

The sensor for the intensity stabilization of the laser is a photodiode array developed at the AEI for aLIGO. The assembly was prepared at LIGO and consist of four photodiodes which measure the laser power fluctuations, sensing a total power of 145 mW. The signal of each of the photodiodes is converted to a voltage and then added. This signal is used as an error signal for an analog controller. The control signal is fed back to an AOM included in the 35 W Laser system. Four additional photodiodes function together as one out-of-loop reference detector and measure the laser power fluctuations. The relative power noise using this assembly was measured at the AEI 10 m-Prototype and is found to be $1.8 \times 10^{-9}\,\mathrm{Hz}^{-1/2}$ [Jun17].

A detailed description of the frequency stabilization design can be found in [Kaw12]. For the frequency stabilization, multiple actuators are required to achieve a bandwidth of up to 900 kHz with a suppression of 120 dB [Pöl14]. The feedback signal is differentiated into three frequency regions. The EOM is used at the highest frequencies, up to a unity gain frequency of 300 kHz to 900 kHz. For mid frequencies, ranging from 1 Hz to 50 kHz, the refractive index of the NPRO crystal is modulated by a piezoelectric element. For frequencies below 1 Hz, the NPRO crystal length is modulated by temperature variation. The resulting stabilization has a high bandwidth with a suppression of up to 120 dB at 100 Hz. The reference for the frequency is the length of a triangular cavity. It has a round trip of 21 m and is also located in the vacuum system of the AEI 10 m-Prototype, see figure 1.1. The mirrors of the Frequency Reference Cavity are individually suspended by a three stage pendulum, isolating the mirrors from seismic motion and therefore creating a quiet reference in the frequency band of the SQL. Heavy mirrors with a mass of 850 g are used to reduce their susceptibility to radiation pressure

noise [Kaw12]. The achievable frequency stabilization as seen by the sub-SQL interferometer using the suspended Frequency Reference Cavity is plotted as dark red curve in figure 1.3. The length of the suspended cavity is used as the reference for the laser frequency. The analysis of the noise performance of the frequency stabilization is work in progress.

Monolithic mirror suspensions

The concept of passive filtering to reduce ground motion at the mirror by cascaded pendulum stages is a standard technique for in gravitational wave detectors [Ast12; Pli00]. As already mentioned, the seismic noise is attenuated by mirror suspensions which is described in section 3.1 in detail. The design of the suspension chain was provided by the IGR at the University of Glasgow. To reduce the thermal noise coupling to the interferometer readout through the suspension, a material with very low mechanical loss is required [Gil93; Veg18]. The thermal noise is reduced below the SQL by the use of thin silica fibers of only 20 µm diameter. The friction between the fibers and the optics must preserve the low mechanical loss of silica by reducing mechanical losses due to friction [Cum09]. The fibers are welded onto ears and then bonded to the mirror and the Penultimate Mass (PUM). The fabrication of the silica suspension is prepared in Glasgow and will also be used for their Speed Meter experiment [Grä14; Hen18]. The expected suspension thermal noise is plotted in the solid yellow line in figure 1.3.

Reduction of coating thermal noise

The initial design of the sub-SQL interferometer included anti-resonant cavities, forming a compound end-mirror for the arm cavities. With this, the number of required layers of tantala/silica coatings could have been reduced, while the reflectivity of the compound mirror would have been conserved [Har02]. Recently a new single-crystal GaAs/AlGaAs multilayers coating became available. These coatings have a significantly reduced coating Brownian noise as published in [Col13]. The compound end-mirror is not required any more. The coupling of Brownian coating noise to the interferometer output was also intended to be reduced by using laser beam sizes of up to a radius of 9.7 mm. With the reduced Brownian coating noise of the crystalline coatings, the beam size can be reduced to 6 mm resulting an a shorter cavity. The stability factor of the arm cavities is reduced from $g = 0.998$ to $g = 0.99$ [Kog66]. The expected noise contributions of the coating Brownian noise (green), the substrate Brownian noise (light blue) and the effective thermo-optic noise (purple). The thermo-optic noise is minimized by the coherent cancellation of the thermo-elastic and thermo-refractive noise [Cha16]. The design of the mirror coating layer thickness was done in close collaboration with Crystalline Mirror Solutions GmbH (CMS).

For the experiment described in this thesis, the AlGaAs mirrors were not yet available and substituted by pilot mirrors. These pilot mirrors are identical to the final AlGaAs mirrors with respect to the radius of curvature as well as their cavity parameters such as Finesse, fundamental mode profile and higher order mode spacing. The reflectivity of the input and end mirror of the cavity is identical resulting in an impedance matched cavity. A detailed description of these

preparatory experiment the Single Arm Test and the used optics is presented in section 3.2.

1.1.3 Control and Data System

The complexity of the AEI 10 m-Prototype facility is comparable to a large-scale gravitational wave detector. Many different subsystem need to be in a controlled state, while the interferometer is operated. Therefore a small-scale version of the Control and Data System (CDS) developed for and by LIGO, has been set up for the AEI 10 m-Prototype [Bor01]. It allows real-time control and data acquisition. Several user interfaces give access to the data, and allow the setting up of control loops. The digital real-time system is interfaced with Analog-to-Digital Converter (ADC) and Digital-to-Analog Converter (DAC) cards. CDS is capable of doing multi-input multi-output data processing among all connected channels with a sampling frequency of up to 65 kHz. The control loop bandwidth is limited by the phase delay of the anti-aliasing and anti-imaging filters and is usually below 2 kHz. To generate a digital filter, the software tool *Foton* is used. It accesses software filter modules interfaced into the digital data stream. The acquired real-time data can be accessed by the Diagnostic Test Tool (DTT) optimized for computation of spectral densities and transfer functions, and the MATLAB based application LIGO Data Viewer (ligoDV), allowing mathematical operations before the computation of the spectral density. Time series data can be accessed through *DataViewer*. It also has the functionality of an oscilloscope, thereby showing live streams of the acquired and processed data.

This thesis has used DTT and ligoDV to obtain the necessary transfer functions and Amplitude Spectral Density (ASD). All control loops were implemented digitally, using *Foton* as a filter design tool.

1.1.4 Coordinate system and naming convention

To operate a large scale experiment like the AEI 10 m-Prototype a global coordinate system is used to express the orientation of components, beam paths and signals in this reference frame. In figure 1.5 a schematic overview of the orientation of the coordinate system of the AEI 10 m-Prototype is shown on the left hand side. The origin of the coordinate system is set to the central vacuum chamber and the x-axis is oriented to the west chamber. The y-axis is pointing towards the south chamber. Angular displacements are named r_x, r_y and r_z and translational displacements d_x, d_y and d_z. In some instances the local coordinate system of one component is required. This is illustrated in the drawing to the right hand side at the example of a mirror. Translational displacements along the beam path are named longitudinal displacements. Angular rotations around the horizontal axis are named pitch and around the vertical axis yaw.

Outline of this thesis

In chapter 2 the concepts of the two optical sensors for stabilization of the installed AEI-SAS units are presented. An interferometric sensor, the Suspension Platform Interferometer is

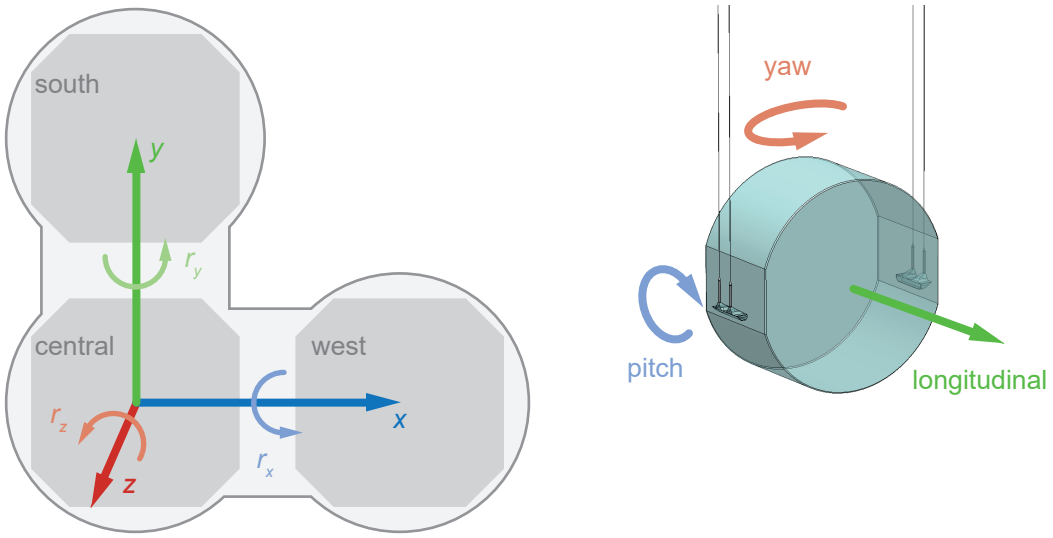

Figure 1.5: Global and local coordinate system naming convention. On the left side a schematic overview of the vacuum system is shown. The x-axis is pointing from the central to the the west chamber and the y-axis is pointing form the central to the south chamber. The z-axis is pointing out of the drawing plane. Angular displacements around these axes are named r_x, r_y and r_z. Translational displacement along these axis is named d_x, d_y and d_z. For instances where the local coordinate system is required the drawing on the right hand side explains the displacement names used in this thesis for the example of a mirror. The translational displacement along the beam axis is named longitudinal displacement and the angular rotations are named pitch and yaw. Right hand side drawing exported from the technical drawing of the SQL suspensions. Courtesy of the IGR.

measuring the differential displacement of the central and south AEI-SAS relative to each other. The quasi-monolithic assembly was prepared before hand in a prevision PhD thesis. In this thesis an Optical Path-length Difference Stabilization (OPD) stabilization was integrated, to achieve and surpass the desired readout noise of $100\,\mathrm{pm\,Hz^{-1/2}}$ from 10 Hz to 10 mHz. Hardware modifications were performed to allow a reliable operation of all interferometers at the same time and to protect quasi-monolithic assembly. Optical levers are integrated in the AEI 10 m-Prototype system controlling the angular displacement of the AEI-SAS in r_x and r_z.

In chapter 3 the preparatory experiment named Single Arm Test is presented. Within this thesis, two fully operational SQL suspensions were set up in the vacuum system forming a linear Fabry-Perot cavity with 10.8 m length. The suspensions are equipped with pilot optics substituting the AlGaAs opics for the sub-SQL interferometer. The coil/magnet actuators at the PUM and the ESD at the mirror are characterized by the measured transfer function to the cavity length.

In chapter 4 the results of the stabilization of the differential length changes of two AEI-SAS relative to each other by the Suspension Platform Interferometer and the angular displacement by the optical levers are presented. Out-of-loop sensors are installed to characterize the residual displacement noise. The according reduction in suspension point motion of the

Frequency Reference Cavity is analyzed by measuring the cavity length. Furthermore the length stabilization of the Single Arm Test cavity, by the ESD and the PUM actuators, to the laser frequency are presented. The error and the feedback signal are analyzed.

CHAPTER 2

Optical sensors for active seismic pre-isolation

All experiments at the AEI 10 m-Prototype are distributed across three optical tables separated by 11.65 m each. To provide a stable test bed for all experiments at the same time, a pre-isolation of the optical tables from ground motion is established. Interferometric sensors are used to readout the differential motion between them and optical levers are used to inertially control the angular displacement around the x- and z-axis.

The construction and implementation of the AEI-SAS and the control of it with the built-in senors was not part of this thesis and is briefly recapitulated as an introduction to the seismic isolation concept. In this thesis the design and implementation of optical levers and the improvement of the readout noise of the Suspension Platform Interferometer as well as the feedback control with the them was performed.

Every optical table is isolated by a AEI-SAS [Wan13]. The isolation of an AEI-SAS starts at the fundamental resonances of the passive isolation stages at 0.3 Hz for the vertical degrees of freedom and at 0.1 Hz for the horizontal degrees of freedom. Above these frequencies, the ground motion is suppressed with the transfer function of an harmonic oscillator. The amplitude response above the resonance frequency is $\sim 1/f^2$. A complete description of the design, assembly and improvements can be found in [Wan12], [Wan13], [Ber17] and [Ber18].

At the resonances of the passive filter stages, input ground motion is amplified and need to be actively suppressed. With the sensors build into the AEI-SAS, the motion at the resonance frequency and above is suppressed. For the active control sensors are used to control the position and suppress motion. The inertial sensors need to be combined with the LVDTs to create one virtual sensor in the control band. The LVDTs are always measuring the table motion against the ground motion. Therefore they will only provide a useful signal, if the table motion is larger than the ground motion, i.e. on the resonance frequency. Additionally, an LVDT provides a position signal relative to ground. The inertial sensors are measuring the actual motion of the optical table. For the horizontal degrees of freedom monolithic accelerometers [Ber06b] are installed and for the vertical degree of freedom L4C-Geophones from Sercel are used [Kir17]. Due to their frequency response they cannot measure below 0.1 Hz. The noise of the inertial sensors becomes dominant at and below the fundamental resonance frequency of the AEI-SAS. The blending filters cannot attenuate the noise of the LVDTs and the inertial sensors sufficiently, and the feedback is limited by the noise induced by the sensors.

To improve the active stabilization for the suspended cavities of the Frequency Reference Cavity and the sub-SQL interferometer, a set of optical sensors has been developed and inte-

grated into the feedback of the AEI-SAS. The optical sensors are divided into two categories. The first is using an interferometer to measure the relative displacement of two AEI-SAS and is therefore not an inertial sensor. This sensor is the Suspension Platform Interferometer and is described in section 2.1. The other sensor category is using the position detection of an optical lever on quadrant photodiodes. This is described in section 2.2. Both methods are explained, and an overview over the methods themselves, the limitations and the integration into the existing feedback system are discussed.

2.1 Suspension Platform Interferometer

The future experiments at the AEI 10 m-Prototype, such as the sub-SQL interferometer, are carried out among the three optical tables. The cavities are orientated along the tubes connecting the vacuum tanks. The displacement of the mirrors on each optical table is filtered by the suspensions described in section 3.1. The suspension system is providing sufficient isolation in the measurement band of the sub-SQL interferometer. To keep the interferometer and the arm cavities at their operation points, the actuators at the pendulum stages have to actuate on the suspended masses, forcing them to follow the residual seismic motion. With seismic pre-isolation, less ground motion has to be compensated.

The Suspension Platform Interferometer is measuring the differential motion of the two satellite optical tables relative to the central optical table by interferometric readout. Differential motion is therefore measured, such that the cavities of the sub-SQL interferometer have to follow. By feeding back the signal to the satellite optical tables, the differential table motion is reduced. The design and assembly of the Suspension Platform Interferometer was performed in a former PhD thesis and is described in [Dah13] and only briefly recapitulated in section 2.1.1. The chosen design is mainly using hardware developed at the AEI for the LISA pathfinder mission. According to the test of the LISA Pathfinder group, the readout of the Suspension Platform Interferometer can be sensitive to 100 pm $\mathrm{Hz}^{-1/2}$ between 10 mHz to 100 mHz. A detailed description of the LISA pathfinder test hardware can be found in [Aud14].

2.1.1 Design and working principle

The Suspension Platform Interferometer is an interferometric sensor using heterodyne Mach-Zehnder interferometers. In figure 2.1, a schematic overview of the optical layout, outside and inside the vacuum system, is shown. Starting at the light source for the interferometers, a commercially available Nd:YAG Non-Planar Ring Oscillator type P2000NE from InnoLight with a wavelength of 1064 nm is used.

A Faraday Isolator and a set of waveplates protects the laser from back reflections of optical components in the beam path. A beam splitter divides the power of the light into two equal parts. These are the two interferometer arms, for all interferometers of the Suspension Platform Interferometer.

One arm of the Mach–Zehnder interferometer travels to the remote table and back, as shown in the yellow lines. The other arm is located on the central optical table and is shown

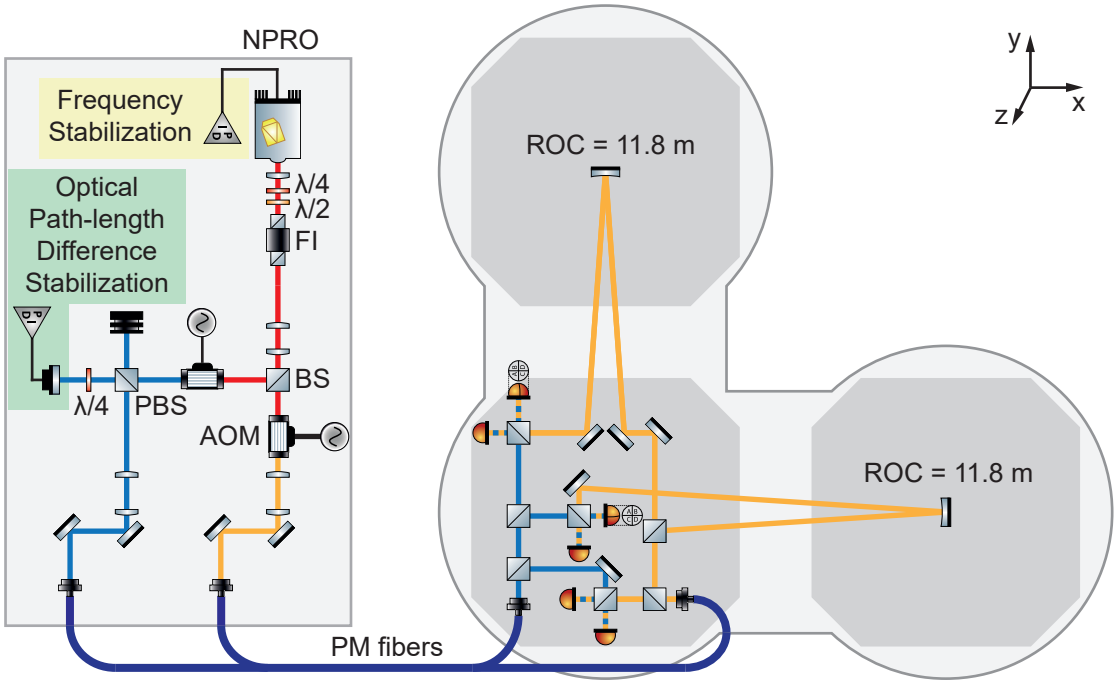

Figure 2.1: A schematic sketch of the optical part of the Suspension Platform Interferometer. The left part is showing the laser light preparation outside of the vacuum system. A frequency stabilized NPRO generates light at 1064 nm. The light is split into two beams of equal power by a beam splitter (BS). Each beam is shifted by an AOM by 80 MHz. A frequency offset between the two AOM drivers of $f_{\mathrm{het}} \approx 15$ kHz is generating a heterodyne beat. Two Polarization-Maintaining (PM) fibers are guiding the light into the vacuum system. Fibre Injector Optical Subassemblies (FIOS) are coupling the light out of the fiber. On the central table the two beams are further split into four interferometers namely two reference and two measurement interferometers. The second reference interferometer is redundant and not shown. A detailed overview of the optical assembly on the central optical bench is shown in figure 2.2. To measure the relative displacement of the two satellite optical tables from the central table, one beam of the west and south interferometer travels to the satellite table and back, while the other beam is staying on the central optical table. To reduce phase-noise coupling to the Suspension Platform Interferometer through the input path, the reference interferometer signal is used in a feedback control loop. A piezoelectric element is driving a mirror on the laser preparation table with the control signal, stabilizing the interferometer arms to each other.

in blue. The interferometer arms of the Suspension Platform Interferometer therefore have an inherent arm length mismatch of 23 m. The frequency noise of the NPRO laser would dominate the interferometer readout and a frequency stabilization is therefore required to reach 100 pm $\mathrm{Hz}^{-1/2}$. A stabilization unit type I2 MTS V2.0, also manufactured by InnoLight and housed together with the laser, uses an Iodine hyperfine transition as a frequency reference. Measurements made by the LISA pathfinder group with two of these units demonstrate a sufficient frequency stability for the arm length difference. A projection of the laser frequency noise introduced through the 23 m delay to the readout noise of the Suspension Platform

Interferometer can be found in appendix A.1.

A heterodyne beat note is required for the readout of the interferometers. The two interferometer arms are therefore different in frequency by an offset of $f_{\mathrm{het}} = 15.34\,\mathrm{kHz}$. Two AOMs, one in each interferometer arm shift the light by 80 MHz each. The frequency offset for the heterodyne interferometry is controlled by a Phase Lock Loop (PLL). This stabilizes the difference of the two AOM driver signals to an offset of f_{het}. The effective difference in frequency between the interferometer arms is therefore f_{het}.

The two interferometer beams are guided into the vacuum through optical fibers. On the central optical table they are released by Fibre Injector Optical Subassemblies (FIOS) [Bog09]. All optics on the central optical table for the Suspension Platform Interferometer are attached to a low-thermal expansion base plate (Clearceram-Z HS) and fixed by hydroxide catalysis bonding, optically contacting or gluing. Figure 2.2 shows the bare assembly without the photodiodes. For the design of the Suspension Platform Interferometer, one constraint is the size and height of the optical assembly. The base plate is 250 mm × 250 mm × 30 mm and the beam height is 45 mm. The Suspension Platform Interferometer length readout needs to be decoupled from the other degrees of freedom. The position is therefore chosen to be as close to the rotation axis of the optical bench as possible. The Suspension Platform Interferometer is therefore located in the center of the optical bench. The lower beam-height and compact assembly allows it to fit below the beam splitter for the sub-SQL interferometer. The disadvantage of this location is the difficulty in performing a later alignment or regular maintenance. With the quasi-monolithic assembly, all components are permanently attached to the low-thermal expansion glass base plate. Once the optical components are set, the alignment is fixed. The quasi-monolithic assembly unifies the desired thermal stability with the space constraints.

On the path to the quasi-monolithic base plate, phase fluctuations are introduced. To measure these optical path-length differences, a reference interferometer is included on the base plate. As pictured in figure 2.1 it consists of the two launched beams, that are then directly interfered with each other.

Two more interferometers are pictured, measuring the displacement along the x- and y-arms of the AEI 10 m-Prototype. One arm of these measurement interferometers located on the monolithic assembly. The other arms reach to the center of the south and west optical tables. Curved mirrors with a radius of curvature of 11.8 m reflect the beams back to the central optical table. The curved mirror matches the reflected Gaussian beam with the beam remaining on the base plate at the recombining beam splitter. The measurements of the south and west optical table are independent of each other.

The natural motion of the central optical table relative to the satellite tables is typically around $1\,\mu\mathrm{m\,Hz}^{-1/2}$ at the micro-seismic peak [Wan13]. Another constraint is therefore the ability to measure over multiple fringes of the interferometric signal. The heterodyne signal read by the photodiodes is constantly measured by a phasemeter. This was also developed for tests of the LISA pathfinder mission [Hei04]. The phase shift ϕ measured by the phasemeter, is

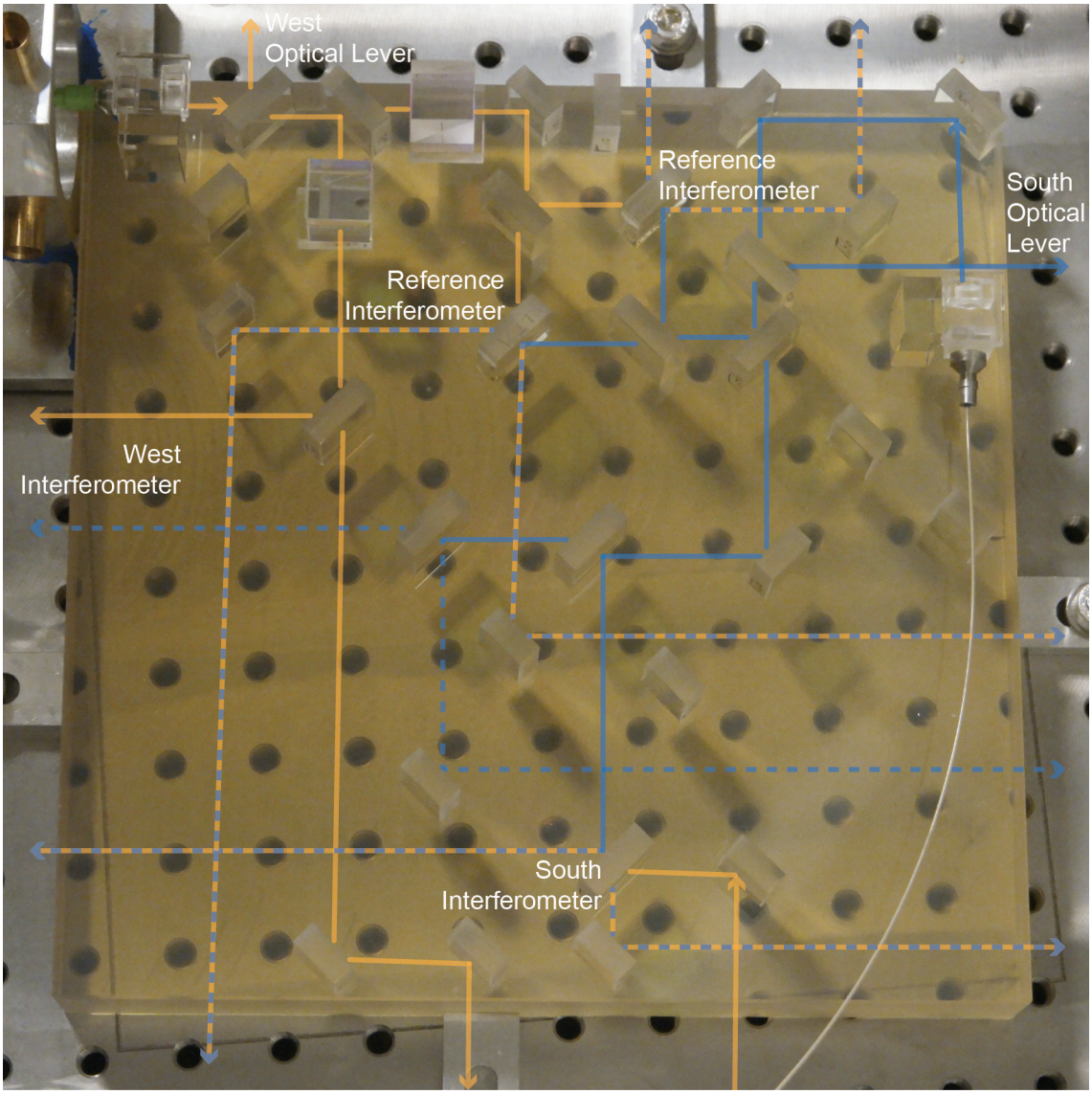

Figure 2.2: The optics of the Suspension Platform Interferometer on the central optical table are all attached to an ultra-low thermal expansion glass-plate. The majority of the optics are attached by hydroxide catalysis bonding. The FIOSs are optically contacted, the polarizing beam splitter, as well as the mirror, reflecting the incoming beam of the south interferometer, are glued. The yellow and blue lines are marking the beam path of light coupled out of the two FIOS. In total, four interferometers are formed. Two reference interferometers, where both arms stay on the monolithic base plate, and two measurement interferometers, where one arm is staying on the base plate and the second is sent to one satellite table and back. The interference at the recombining beam splitters is marked by the dashed yellow/blue line. The west AEI-SAS is not yet installed, and the completion of the west interferometer therefore postponed. The recombining beam splitter for the west interferometer is splitting the local arm, marked by the dashed blue lines.

directly proportional to the differential length change d of the interferometer:

$$d = \frac{\lambda}{2\pi}\phi, \tag{2.1}$$

with λ being the wavelength of the laser. A detailed description can be found in [Aud14] on page 46. The phasemeter has 20 individual channels. Data from the phasemeter are interfaced with the CDS by the Phasemeter Interface (PMI). The control loops for the feedback to the AEI-SAS are achieved through the CDS.

The original design of the Suspension Platform Interferometer readout had included two Quadrant Photo Diodes (QPDs) for every interferometer. The phasemeter includes a transimpedance amplifier for each of the channels. The individual phase signals from the QPDs are then combined in the CDS to a common phase signal and the two differential signals of the Differential Wavefront Sensing (DWS) provide the pitch and yaw signals. These signals can be processed by the CDS and applied to the actuators of the AEI-SAS.

The alignment of the quasi-monolithic assembly was performed with a Coordinate Measuring Machine (CMM), a manual positioning device with three ball tips, and a template. Reference components were placed with the CMM. The majority of the optics were afterwards bonded using a template aligned to the reference components. The recombining beam splitters were placed with the manual alignment tool to have control of the interference of the individual interferometers. The measurement interferometers therefore had to be installed in situ. The west AEI-SAS is not yet installed, and the installation of the west interferometer postponed. The beam splitter reflecting the beam to the west optical table shifts the beam to the south interferometer and was installed at a dummy position. In figure 2.2 the beam for the west interferometer is not coming back, and therefore the recombining beam splitter is splitting the local arm of the west interferometer, indicated by the dashed blue lines. For the south interferometer, the steering mirror before the recombining beam splitter was used for alignment and glued in situ.

This work was performed in a former PhD thesis [Dah13]. A detailed description of the design considerations and the assembly are described in [Dah13]. In the next section the modifications to the existing hardware done within this thesis are presented.

2.1.2 Commissioning and Improving the Suspension Platform Interferometer

The Suspension Platform Interferometer was not reaching the desired readout noise of $100\,\mathrm{pm\,Hz^{-1/2}}$ in the frequency range from 10 mHz to 100 mHz. An OPD stabilization was required and implemented. In section 2.1.3 the implementation and the improved readout noise of the Suspension Platform Interferometer are shown. For the angular stabilization, the use of DWS signals was foreseen. The contrast of the quasi-monolithic interferometers of the Suspension Platform Interferometer reduced the noise performance. The AEI-SAS is attenuating the angular displacement noise to $1\,\mathrm{nrad\,Hz^{-1/2}}$ at a frequency of 1 Hz. Optical levers were developed within this thesis, allowing to stabilize the AEI-SAS to $40\,\mathrm{prad\,Hz^{-1/2}}$ at a frequency of 1 Hz. The setup and integration of the optical levers is presented in section

2.2 and the results of the active stabilization are presented in 4.1.2. The number of optical signals of the Suspension Platform Interferometer was reduced to the allow a simultaneous readout of all interferometers. The new photodiodes are integrated into a housing, protecting the Suspension Platform Interferometer. This is explained in the next section.

Integration of Hardware Modifications

The original design used QPDs for all interferometers. A quadrant readout of the reference interferometers cannot provide feedback signals and the same applies for the second quadrant photodiode of the measurement interferometers. The readout was therefore changed to single element photodiodes only keeping one QPD for each measurement interferometer. The reduction of the number of signals allows for the readout of all interferometers simultaneously as the phasemeter provides only 20 channels. Before the new photodiodes were integrated, the west interferometer QPDs and the second reference interferometer were not connected.

The beam splitter of the sub-SQL interferometer will be placed above the Suspension Platform Interferometer base plate. To reduce the space consumed by the original setup and to protect it from stray light and physical damage, a housing around the base plate was required. A new layout for the photodiode mounting was developed and directly integrated into the walls surrounding the base plate.

Figure 2.3(a) shows the original QPD mount installed at all eight interferometer ports. The holders are mounted to the optical tables. Strain-relief wire-clamps reduce the tension on the connection point between photodiode pins and cable. The cable was attached by a crimp barrel, and it was easily removed when under tension.

All QPDs had to be removed for the new housing, see figure 2.3(b). The bare base plate is kept in place by clamps, pushing from the side.

In figure 2.3(c) the new walls of the housing are placed around the base plate. Each side is covered by one wall. These are bolted onto the optical table, and are intentionally not connected to each other. This wall concept allows for easy maintenance. If a photodiode needs to be exchanged, the complete wall will be taken out, without disturbing the others. The walls are equipped with photodiodes with a large active area with a diameter of 8 mm. The baseplate and the neighboring walls constrain the spot position well enough that alignment of individual photodiodes is not required. Only the west wall is housing QPDs, and alignment of the sensors will be required. The electrical connection is changed to D-Subminiature (D-Sub) 9-pin connector, which are also attached to the wall. The original cables were removed and replaced by shielded twisted pair cables which adheres into the grounding concept of the AEI 10 m-Prototype system.

The housing is completed by two lids supported by the walls. In figure 2.3(d) the final assembly is shown. All wires are in place and connected. The external optics for the optical levers were also installed. The new cabling reduced the size considerably as a comparison of picture 2.3(a) to 2.3(d) shows. The AEI-SAS can support a limited amount of weight. The new housing and cabling even reduced the weight by 2 kg. Stray-light protection and maintenance accessibility were improved and the monolithic assembly is shielded from mechanical impacts.

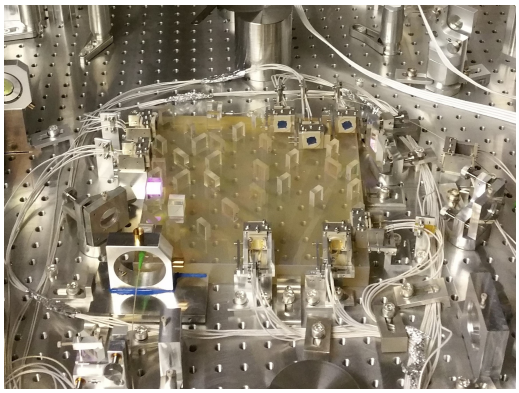

(a) The original setup with an open access to the base plate. All QPDs are fixed by holders mounted separately to the optical table. The QPD assembly, strain reliefs and cables were consuming too much space.

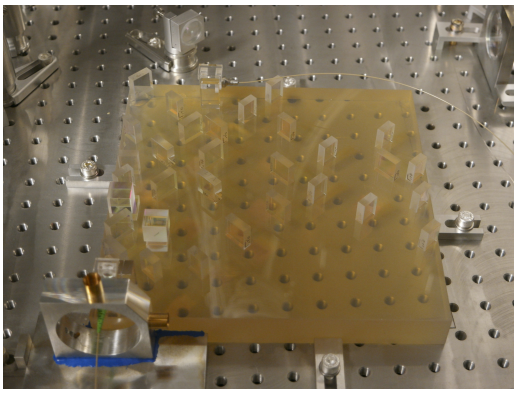

(b) For the installation of the new housing, all QPDs, cables and strain reliefs had to be removed, leaving the bare base plate.

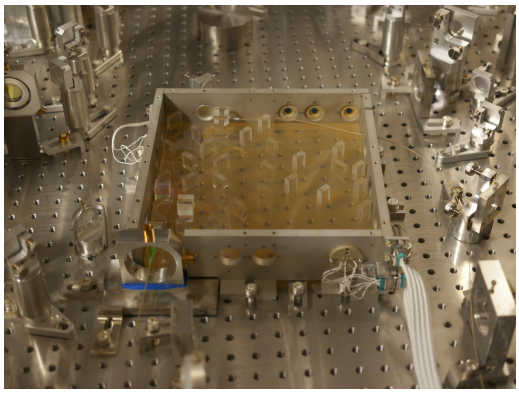

(c) The walls of the new housing were placed around the base plate. All photodiodes, as well as the lenses for the optical levers were integrated into theses walls. Most of the QPDs were replaced by single-element photodiodes. All photodiodes in one wall were connected to a D-Sub 9-pin plug. Every wall itself can now be taken out for maintenance and easily be reinstalled.

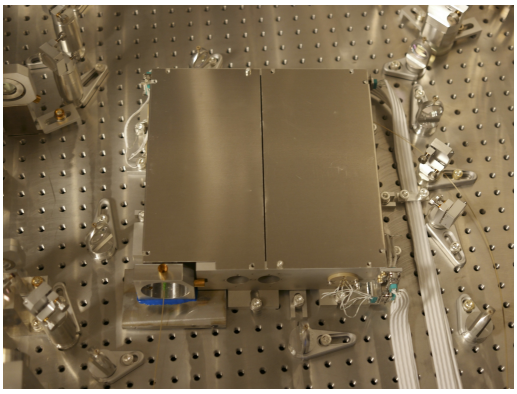

(d) On the walls of the housing two lids were mounted, sealing the base plate from stray light and damage. All required cables and the optics of the optical levers were newly installed.

Figure 2.3: Installation of a housing for the Suspension Platform Interferometer base plate. Along with this most of the QPDs were replaced by single-element photodiodes. This reduced the number of signals without compromising the available feedback signals. The number of phasemeter channels is now sufficient to read out all interferometers simultaneously.

The light preparation for the Suspension Platform Interferometer was also revised. The original AOMs had been thermally isolated from the mounting unit leading to an overheating of the crystals. This led to a fast degradation in deflection efficiency, even cracking one crystal. To enhance the lifetime of the AOMs, they were thermally contacted to the supporting mounting unit. To ease the alignment, each AOM is mounted on a Four-Axis Tilt Aligner from Newport (type 9071-M). It was anticipated that the Tilt Aligner would require occasional alignment, but no significant drift was observed. The input path also had used about 500 mW optical power of the laser. The optical power consumption was reduced to 200 mW by rebuilding the input path and thereby improving the losses. In figure 2.4 the new setup is shown. It uses less than half of the available space on the optical table, leaving enough space and optical power for other experiments, such as the optical levers introduced in 2.2.

2.1.3 Implementation and characterization

During the first commissioning phase, the Suspension Platform Interferometer had reached the desired $100\,\mathrm{pm\,Hz^{-1/2}}$ only above 300 mHz, see figure 7.2 on p.102 in [Dah13]. By implementing an OPD, the sensing noise of the interferometers was reduced below $10\,\mathrm{pm\,Hz^{-1/2}}$ down to 10 mHz. A test interferometer with a deliberate arm length mismatch of 1 m was installed to validate the performance of both the OPD and frequency stabilization systems. The test interferometer furthermore allowed a comparison of the quasi-monolithic assembly of the Suspension Platform Interferometer to regular optics mounts. The results are presented in the following sections.

Optical Path-length Difference Stabilization

The input optical paths accumulate differential phase noise due to, for example, thermal expansion of optical components and stresses in the optical fibers. The reference interferometer can be used to subtract these fluctuations from the measurement interferometers, but due to non-linearities in the readout, the subtraction is imperfect. To improve performance, the relative phase is stabilized by taking the reference interferometer output and controlling the position of a mirror on the injection bench with a piezoelectric drive.

The phase measurement of the reference interferometer is sent from the phasemeter to the CDS. A feedback controller is implemented through the CDS and the feedback signal is converted to a voltage by a DAC. This signal is amplified by a High Voltage (HV) amplifier and applied to the piezoelectric element actuator (type PI P-601.3S). The optical set up of theOPD is shown in figure 2.1. A mirror is glued to the piezo actuator. The interferometer arm is transmitted at a polarizing beam splitter, guided through a quarter-waveplate and reflected under 0° at the mirror on the piezoelectric element. Passing the quarter-waveplate again, the polarization is rotated by 90°, and the light therefore reflected by the polarizing beam splitter.

In figure 2.5 the phase measurement of the reference interferometer is shown, demonstrating the reduction of phase noise by the OPD. Every interferometer has two photodiodes at the output ports of the Mach-Zehnder interferometer. Two reference interferometers are placed

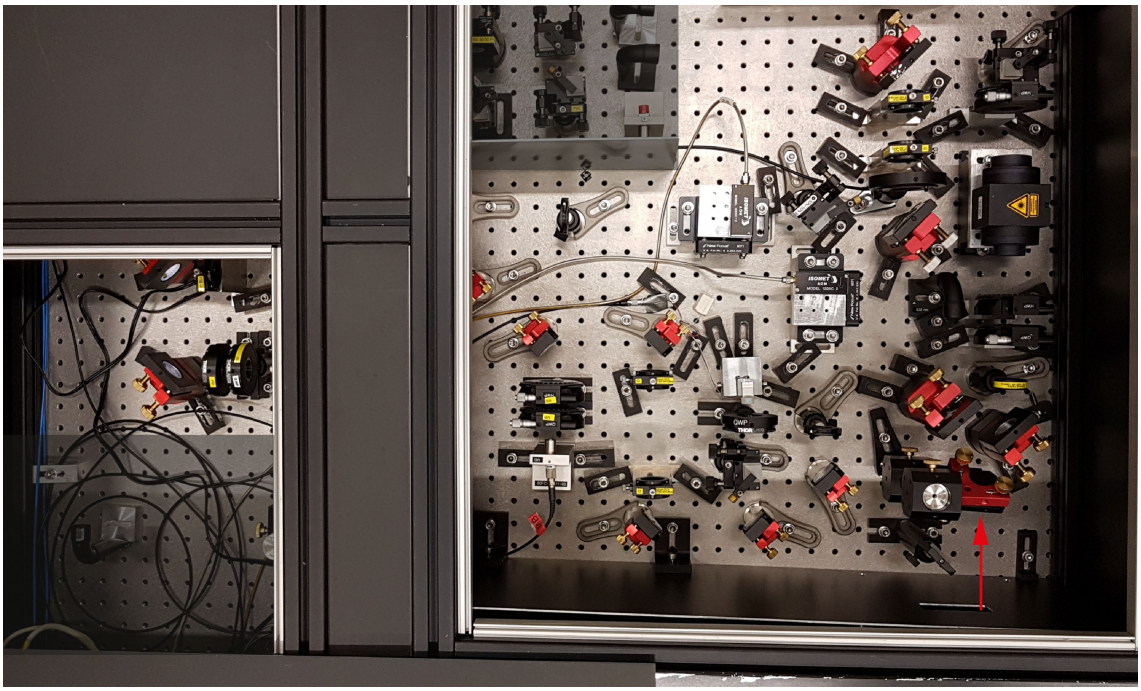

Figure 2.4: Picture of the newly setup laser preparation. The setup was compacted to allow space for other experiments, such as the optical lever. The consumed laser power was reduced from 500 mW to 200 mW. The laser itself is located in the bottom of the picture. A simplified sketch of the laser preparation can be found in figure 2.1.

on the base plate. The first interferometer has a contrast of 8 % and its readout is limited to 100 pm $\mathrm{Hz}^{-1/2}$. The second reference interferometer has a contrast of 30 % and was used for all measurements. The two photodiodes of the other interferometer served as the in- and out-of-loop measurements for the OPD. To reduce the noise outside of the of the control bandwidth, the phase measurement of the in-loop photodiode is subtracted from all interferometers of the Suspension Platform Interferometer. All shown measurements of the Suspension Platform Interferometer are always corrected by this method.

The measurements demonstrated that the phase noise was reduced below 10 pm $\mathrm{Hz}^{-1/2}$ from 0.01 Hz to 1 Hz. Below 0.01 Hz, thermal effects become dominant. The noise induced by temperature changes is due to the low-thermal expansion base plate, lower than 100 pm $\mathrm{Hz}^{-1/2}$ down to approximately 3 mHz. The Suspension Platform Interferometer readout noise surpassed the expected noise performance with the OPD stabilization, even reaching 5 pm $\mathrm{Hz}^{-1/2}$. The noise floor is not constant over time. Temperature drifts are changing the overall noise floor. The performance is typically at or below 20 pm $\mathrm{Hz}^{-1/2}$. The interferometer is providing a measurement of the current readout sensitivity and is therefore shown in the all presented results of the Suspension Platform Interferometer. A test interferometer was set up to further prove the measured stability. This is presented in the next section.

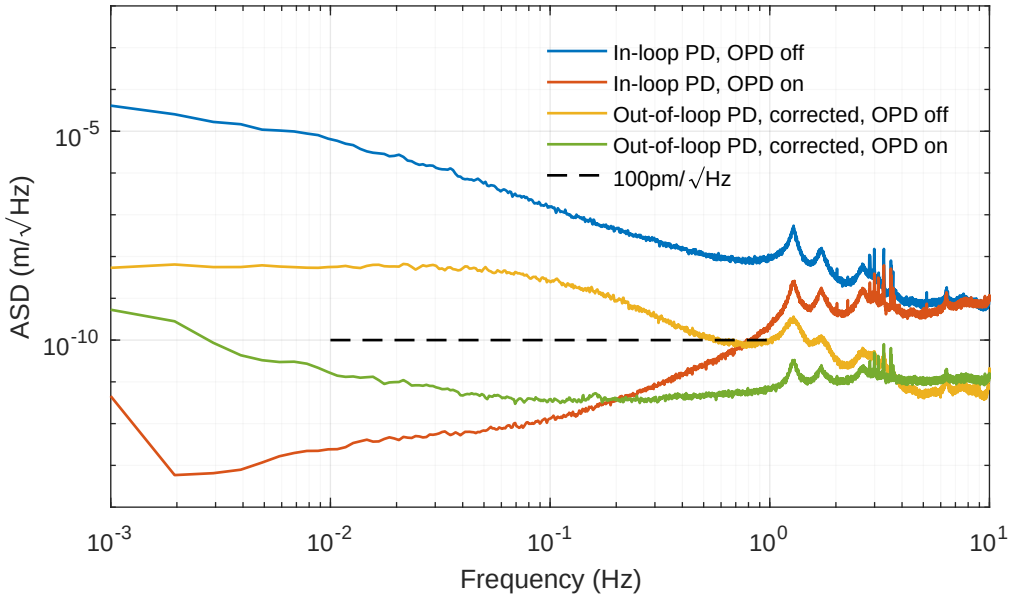

Figure 2.5: Displacement measurement of the Reference Interferometer of the Suspension Platform Interferometer, with and with out the OPD. The OPD stabilization is feeding back the measured phase from the reference interferometer to a piezoelectric element driven mirror in one of the interferometer arms of the Suspension Platform Interferometer. Thereby it stabilizes the arms relative to each other. In blue the equivalent length change in the reference interferometer is shown. The OPD stabilization reduces it to the red line. As an out-of-loop sensor the second photodiode of the reference interferometer is displayed in yellow for the free running case and in green for the active OPD stabilization. The out-of-loop measurements were additionally corrected by subtracting the in-loop measurement. With these two techniques, the sensing noise of the Suspension Platform Interferometer is reduced below 100 pm $\mathrm{Hz}^{-1/2}$, even reaching 5 pm $\mathrm{Hz}^{-1/2}$ at 100 mHz.

Non-monolithic Interferometer

The low-frequency stability of the Suspension Platform Interferometer is transfered to the displacement of the center of the optical tables relative to each other. Since the experiments at the AEI 10 m-Prototype will be distributed across the three optical tables this stabilization is creating one virtual platform. The thermal stability of the optical table itself, the regular optic mounts and the suspension frames are not expected to be as good as the stability of the low-thermal expansion glass and can introduce path length changes due to expansions in the material. To test the stability of regular optics mounts an interferometer using these mounts was set up. Furthermore, it was used for testing the functionality of the frequency stabilization. The two reference interferometers have equal arm lengths and hence both are affected equally by frequency noise. The equal arm length also minimizes the influence of frequency noise due to common mode rejection. The test interferometer used unequal arm length, with a 1 m mismatch.

In figure 2.6 the beam paths of the non-monolithic test interferometer are drawn. The beams

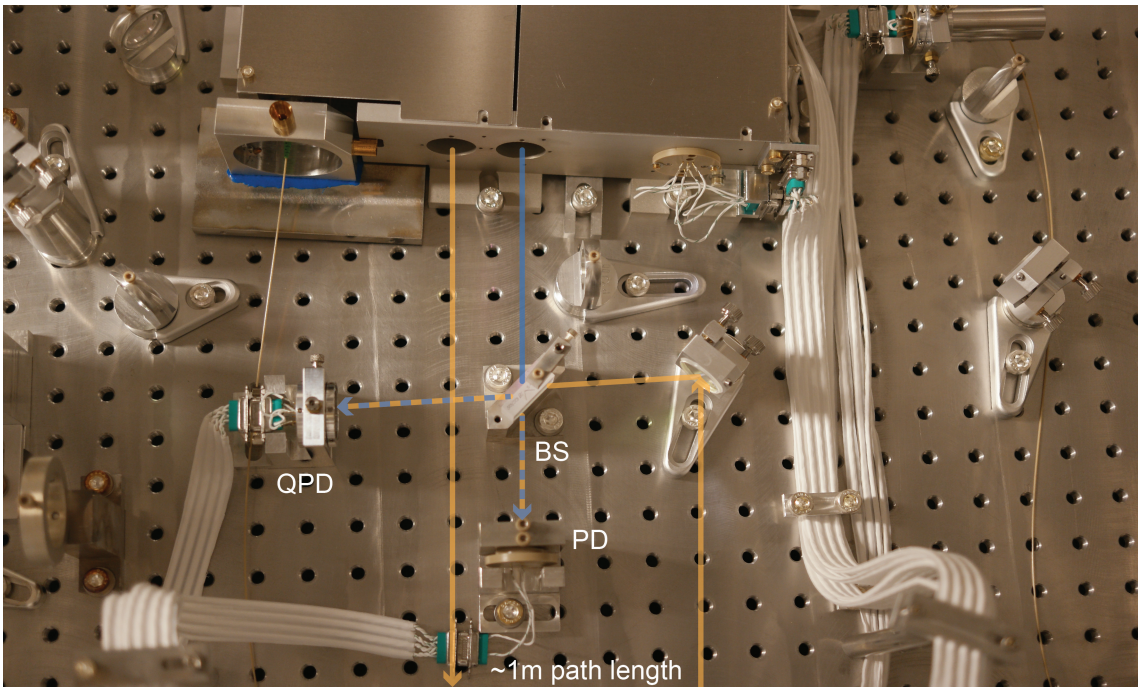

Figure 2.6: Picture of the non-monolithic test interferometer. The two beams of the west interferometer are leaving the quasi-monolithic assembly. A beam splitter is recombining the two arms, and two photodiodes are detecting the light. The arm shown in yellow is guided by steering mirrors on the central table while the arm shown in blue is kept short. The arm length mismatch is 1 m. With this test interferometer the functionality of the laser frequency stabilization and the stability of regular optics mounts was tested.

of the west interferometer were used to form the interferometer. One arm is kept short, while the other is reflected from steering mirrors near the west edge of the central table. The two arms were combined at the beam splitter and a QPD and a photodiode were used for readout. The beam shown in blue is approximately half the power of the beam shown in yellow, because the intended recombining beam splitter of the west interferometer had already been bonded onto the base plate splitting the blue beam.

The readout sensitivity is displayed in figure 2.7. For comparison, the simultaneous measurement of the two reference interferometers are shown. The out-of-loop measurement of the first reference interferometer is shown in blue. At frequencies above 20 mHz the noise is at and even below 20 pm $\mathrm{Hz}^{-1/2}$. The contrast of the test interferometer is higher than in the reference interferometers, because it was adjusted by steering mirrors. The contrast of the quasi-monolithic assembly is fixed. Even the interferometer with only 8 % contrast is sensitive to 100 pm $\mathrm{Hz}^{-1/2}$. The contrast determines the signal to noise ratio at the phasemeter. As shown in the measurement, the noise of the test interferometer was lower than in the reference interferometers down to 50 mHz, below thermal effects started to dominate the displacement noise. Nevertheless, the non-monolithic interferometer fulfilled the expectations and could measure as low as 10 pm $\mathrm{Hz}^{-1/2}$ at 200 mHz, rising to 100 pm $\mathrm{Hz}^{-1/2}$ at 10 mHz. Above 10 Hz

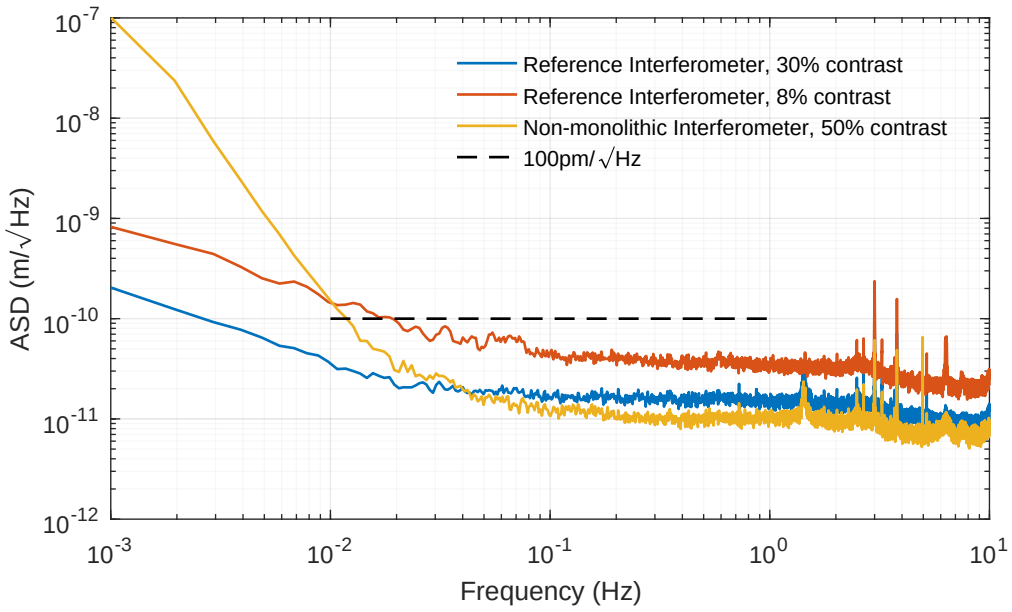

Figure 2.7: Displacement ASD of the two reference interferometers and the non-monolithic test interferometer. In blue, the out-of-loop measurement of the reference interferometer, performing as desired, typically at and below 20 pm $\mathrm{Hz}^{-1/2}$ is shown. In red the second reference interferometer with a contrast of 8 % is shown. It is limited in its sensitivity due to the contrast, but still exceeded 100 pm $\mathrm{Hz}^{-1/2}$. In yellow, the interferometer using standard optic mounts is shown. The contrast is 50 %. It showed lower noise than the monolithic interferometers only below 100 mHz the readout is spoiled due to the thermal drifts. The test interferometer demonstrated, that even without a low-thermal expansion base plate the desired noise of 100 pm $\mathrm{Hz}^{-1/2}$ could be fulfilled, even reaching 10 pm $\mathrm{Hz}^{-1/2}$.

resonances are appearing and some of them seam to be caused by table motion, but the majority is unexplained and even varies with time. They are outside of the control bandwidth of the Suspension Platform Interferometer and are not of interest.

The sensing of the Suspension Platform Interferometer fulfilled and surpassed the expectations. The feedback control, using the Suspension Platform Interferometer south interferometer is discussed in chapter 4.1.1.

2.2 Optical Lever

The Suspension Platform Interferometer is stabilizing the longitudinal degree of freedom along the beam tubes with its interferometric readout. Optical levers are used to control the angular displacement around the x- and z-axis r_x and r_z of the two AEI-SAS. A test of the performance led to a permanent installation in the AEI 10 m-Prototype. When the west AEI-SAS is installed it will be equipped with optical levers to control the angular displacement around the y- and z-axis. The central AEI-SAS will than have an additional optical lever to stabilize its angular

displacement around the y-axis.

The suspension point of the mirrors is approximately a meter above the optical table. A pitch of the suspension frame therefore shifts the suspension point, which leads to an effective change in the length of the cavity. The suspensions for the sub-SQL interferometer will be aligned along center of the x- and y-axis and near the center of the optical table. In contrast, the Frequency Reference Cavity suspensions, are located at the outer corner with a maximum offset in x and y direction from the center, approximately 0.65 m in both directions. A yaw displacement affects the length of the cavity, and therefore couples to the laser frequency. The pre-isolation of these two degrees of freedom has a direct effect on the feedback signal used to stabilize the suspended cavities.

In the original design of the Suspension Platform Interferometer a position read out, based on QPDs behind the curved mirrors had been foreseen. However, the transmission through the curved mirror is 0.2 %, resulting in a transmitted power of approximately 2 µW. This low power is difficult to detect and the south interferometer had been aligned to the position of the curved mirror and exchanging it could have made realignment impossible. Instead, beams originally intended for power monitoring could be used, without risking a failure of the interferometer itself. The tests with these beams were successful and led to a permanent usage. The position sensing of the QPDs by power sensing of the phasemeter had been intended for coarse alignment of the remote table. The sensitivity of the DWS is limited to approximately 10 nrad $\mathrm{Hz}^{-1/2}$. The passive isolation of the AEI-SAS is better above 0.5 Hz. With the dedicated optical lever, discussed in the next section, the control band was broadened up to 5 Hz and they achieved a sensitivity of 1 nrad $\mathrm{Hz}^{-1/2}$ at 100 mHz and below 100 prad $\mathrm{Hz}^{-1/2}$ at 1 Hz.

2.2.1 Design and working principle

The optical set up for the optical levers can be seen in figure 2.8. The laser light is fiber-coupled into the vacuum system onto the central table. It is focused by a set of lenses with a beam radius of approximately 1.4 mm on the QPD at the south table. The individual quadrants of the QPD are converted to a voltage, and an analogue whitening filter from 0.33 Hz to 33 Hz is amplifying the signal above the ADC noise before digitization. Within the CDS, the normalized pitch $\Delta s_{\mathrm{pitch}}$ and yaw Δs_{yaw} signals are calculated as

$$\Delta s_{\mathrm{yaw}} = \frac{P_{\mathrm{left}} - P_{\mathrm{right}}}{P_0} \text{ and} \tag{2.2}$$

$$\Delta s_{\mathrm{pitch}} = \frac{P_{\mathrm{upper}} - P_{\mathrm{lower}}}{P_0} \,. \tag{2.3}$$

with P_0 being the total power of the laser beam measured by the QPD and P_{left} being the power on the left side of the it and accordingly P_{right} on the right side, P_{upper} on the upper half and P_{lower} on the lower half. If the beam is in the center of the QPD, $\Delta s_{\mathrm{yaw}} = 0$ and $\Delta s_{\mathrm{pitch}} = 0$ are fulfilled. Following [Gon13] and [Dah13], the absolute position from the center of the QPD can be calculated from the radius of the laser beam w and the laser power on the two halfs P_{left}

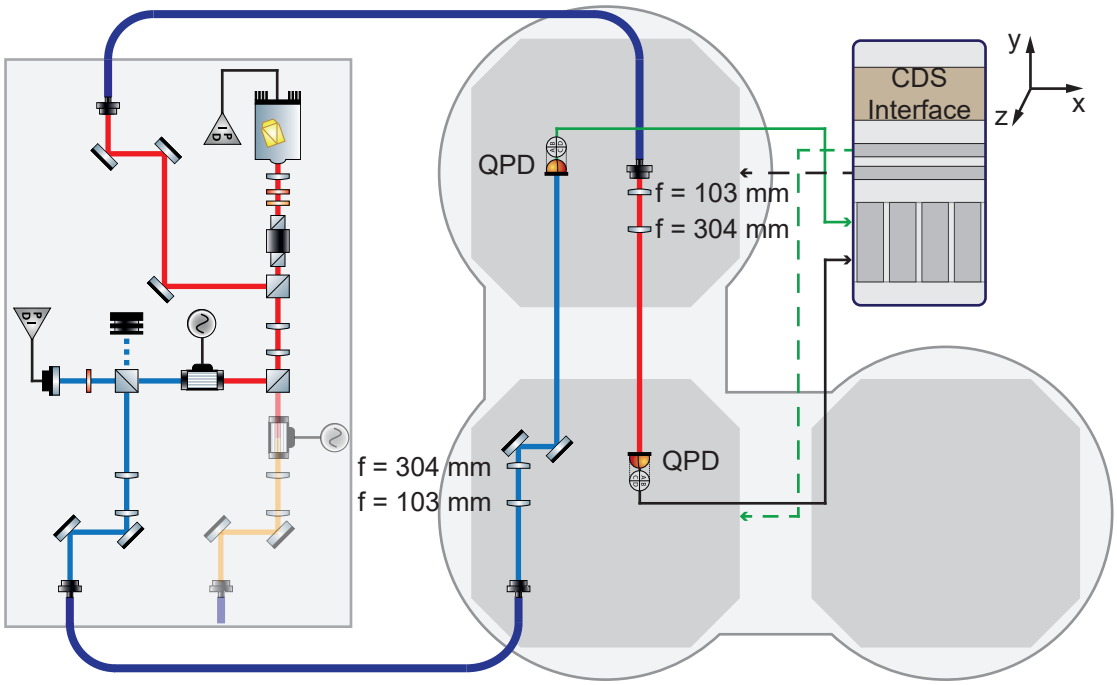

Figure 2.8: Schematic overview of the optical levers. The optical lever to control the central table is taken from the quasi-monolithic assembly of the Suspension Platform Interferometer and guided by steering mirrors to the south optical bench. The signal from the QPD shown in the green line is digitized by the CDS and the control signal is calculated. It is converted to a voltage by the CDS and applied to the central optical table as shown in the dashed green line. For the optical lever of the south optical table a fiber feed through is used to bring the light to the optical table. It is launched by a commercial fiber collimator mounted to an adjustable mount. The QPD signal shown in the black is digitized by the CDS. The feedback is applied to the south AEI-SAS as represented by the dashed black line. For both optical levers two lenses are used to produce a sufficiently small spot on the remote QPD.

and P_{right} of the QPD using

$$P_{\text{left}}(x) = \frac{P_0}{2} + \frac{P_0}{2}\,\text{erf}\left(\frac{\sqrt{2}}{w}(x - x_0)\right) \text{ and} \tag{2.4}$$

$$P_{\text{right}}(x) = \frac{P_0}{2} - \frac{P_0}{2}\,\text{erf}\left(\frac{\sqrt{2}}{w}(x - x_0)\right) . \tag{2.5}$$

x_0 is the center of the QPD, x the position of the center of the laser beam and erf the Gaussian

error function. Inserting this into equation 2.2 leads to

$$\begin{aligned}\Delta s_{\text{yaw}} &= \frac{\frac{P_0}{2} + \frac{P_0}{2}\,\text{erf}\left(\frac{\sqrt{2}}{w}(x-x_0)\right) - \frac{P_0}{2} + \frac{P_0}{2}\,\text{erf}\left(\frac{\sqrt{2}}{w}(x-x_0)\right)}{P_0} \\ &= \text{erf}\left(\frac{\sqrt{2}}{w}(x-x_0)\right) \end{aligned} \tag{2.6}$$

with $x_{\text{yaw}} = x - x_0$ being the displacement of the beam from the center of the QPD:

$$x_{\text{yaw}} = \frac{w}{\sqrt{2}}\,\text{erf}^{-1}\left(\Delta s_{\text{yaw}}\right)\ . \tag{2.7}$$

For $|\Delta s_{\text{yaw}}| \ll 1$, the inverse error function can be approximated by

$$\text{erf}^{-1}\left(\Delta s_{\text{yaw}}\right) \approx \frac{\sqrt{\pi}}{2}\Delta s_{\text{yaw}}. \tag{2.8}$$

Applying this approximation, the absolute position of the laser beam on the QPD is

$$x_{\text{yaw}} = \frac{w}{2}\sqrt{\frac{\pi}{2}}\Delta s_{\text{yaw}}\ . \tag{2.9}$$

The rotational displacement r is calculated using the length of the optical lever l_{OL},

$$\begin{aligned} r_{\text{yaw}} &= x_{\text{yaw}}/l_{\text{OL}} && (2.10)\\ &= \frac{w}{2l_{\text{OL}}}\sqrt{\frac{\pi}{2}}\Delta s_{\text{yaw}} && (2.11)\\ &= \kappa \Delta s_{\text{yaw}} && (2.12) \end{aligned}$$

with

$$\kappa := \frac{w}{l_{\text{OL}}}\sqrt{\frac{\pi}{8}}\ . \tag{2.13}$$

The same applies for pitch on the QPD. The spot size of the optical lever beams on the QPD were measured to calculate the coupling coefficients κ. The optical lever are integrated to the existing control system for the sensors of the AEI-SAS. To obtain the same calibration as for the LVDT, the transfer functions from the LVDT to the optical lever readout were measured. In table 2.1 the beam radius w, the calculated coupling coefficients κ and the measured κ are listed. The calibration of the LVDT was recently measured by a new method and the according κ is listed in the table. The new calibration is not yet integrated. The obtained signals are digital filtered and the feedback signal is transmitted to the AEI-SAS.

The optical lever was designed as a sensor for the full feedback range of the AEI-SAS. The inertial sensors of the AEI-SAS themselves have to be used in a combination with the LVDT because the inertial sensors cannot provide an absolute position signal. The LVDT signal cannot

Table 2.1: Measured beam radius w at the QPDs of the optical lever by using the TaperCamD20-15UCD23. The calculated coupling coefficient κ is calculated from the beam radius. The error of the measurement is estimated to be 5 %. The original coupling coefficient is determined by measuring a transfer function from the calibrated LVDT to the optical lever. A different method of determining the calibration of the LVDTs was recently performed. The new κ was calculated from that. The new calibration is not yet integrated. The optical lever can be used as a calibration reference.

	w (mm)	calc. κ (µrad)	original κ (µrad)	new κ (µrad)
Central AEI-SAS	1.43 ± 0.07	76.9 ± 3.8	54	70
South AEI-SAS	1.13 ± 0.06	60.8 ± 3.0	52	69
Central AEI-SAS out-of-loop	1.34 ± 0.07	72.1 ± 3.6	-	-

be attenuated sufficiently above the cross-over frequency and its noise is therefore limiting the performance of the feedback control from 0.1 Hz to 1 Hz [Ber18]. The limitations to the optical lever sensing are discussed in section 2.2.2. The control benefits are discussed in section 4.1.2.

Tiltable steering mirrors allow coarse alignment of the optical levers. For precise positioning of the QPD an adjustable translation mount is used. Stray light from other experiments, mainly the suspended cavities, can compromise the signals. Tubes reducing the field of view are therefore attached to the QPD. The assembly installed on the south AEI-SAS is shown in figure 2.9(a) .

The optical lever stabilizing the south AEI-SAS is guided into the vacuum system, using a fiber. The beam is emitted by a commercially available fiber coupler type FC60-A11, see figure 2.9(b). The optical lever for the central AEI-SAS originates from the quasi-monolithic assembly of the Suspension Platform Interferometer. Lens systems are installed, to focus the beam to the satellite optical table. The beam radii measured at the QPDs, are listed in table 2.1.

2.2.2 Noise Characterization

To fully explore the limitations of the optical lever the next two sections summarize the noise originating from the electronics and the effect of the transverse degrees of freedom limiting the suppression.

Electronic Noise

The photocurrent generated by each quadrant of the optical lever QPDs is converted to a voltage by a transimpedance amplifier. The amplification was chosen to make full use of the input voltage range of the CDS. The individual quadrants measure the position fluctuations of the laser beam on the QPD due to the ground motion tilt by differential power sensing. The natural shape of the ground motion and the additional passive filtering of the AEI-SAS decreases the signal of the optical lever with higher frequencies. A whitening filter with corner frequencies at

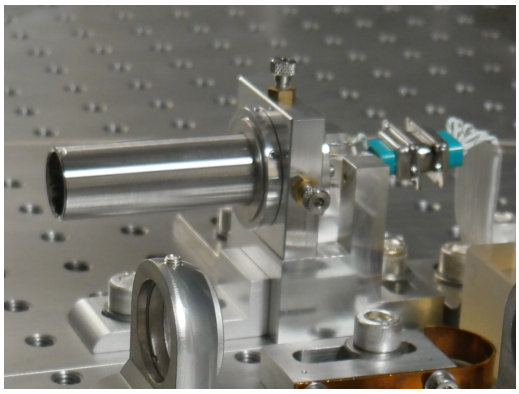

(a) Installed QPD of the optical lever on the south AEI-SAS. The photodiode is protected against stray light by a tube, reducing the field of view. For a precise adjustment the QPD is installed in a translation mount.

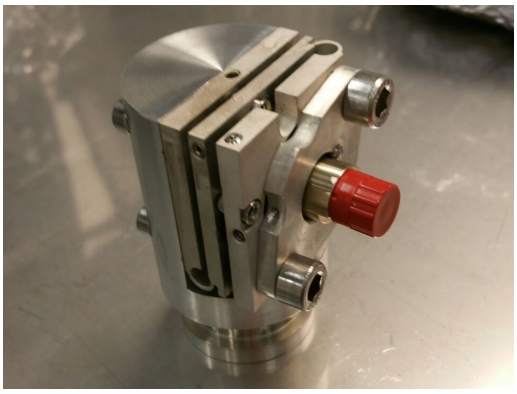

(b) A picture of the fiber coupler of the optical lever in the tiltable mount. The commercially available UHV compatible fiber coupler type FC60-A11 out-couple the beam.

Figure 2.9: All optics mounts for the optical lever are compact mounts allowing to retrofit them while consuming very little space and weight. To align the optical lever commercially adjustable mounts are used to move the beam and the QPD. The beam height is 45 mm as for the Suspension Platform Interferometer.

0.33 Hz and 33 Hz was included into the analogue electronics to amplify the signal above the digitization limit.

To measure the noise performance of the overall electrical path, the current of a single quadrant is sent into all channels. The subtraction of this should show the electronic noise of the readout chain. In figure 2.10, the measurement of the electronic noise projected to the pitch and yaw measurements of the optical levers is shown. The originally envisioned sensitivity for the rotational degree of freedom was 10 nrad $\mathrm{Hz}^{-1/2}$ at 10 mHz. The measured electronic noise was equivalent to 200 prad $\mathrm{Hz}^{-1/2}$ at 100 mHz and rolled off to 2 prad $\mathrm{Hz}^{-1/2}$ above 10 Hz, easily surpassing the original goal. The electronic readout noise is therefore well below the originally intended 10 nrad $\mathrm{Hz}^{-1/2}$. The electronic noise of the optical lever qualifies them for measurements from 0.01 Hz to 10 Hz and therefore over the full control band of the AEI-SAS.

Inherent cross coupling of transverse degrees of freedom

A fundamental limit for all optical lever sensors is the transverse motion of the sending beam and the detecting device, displacing the beam on the QPD. The optical signals from the angular displacement are amplified by the lever length, while transverse degrees of freedom are unaffected. In the case of the AEI 10 m-Prototype optical lever, the x and z degrees of freedom displaced the start and the detection position. The measured displacement d_{QPD} of the beam on the QPD is therefore the transverse displacement $d_{\mathrm{z,x}}$ of the orthogonal degrees of freedom z and x for the central and the optical tables as well as the amplified rotational degree of

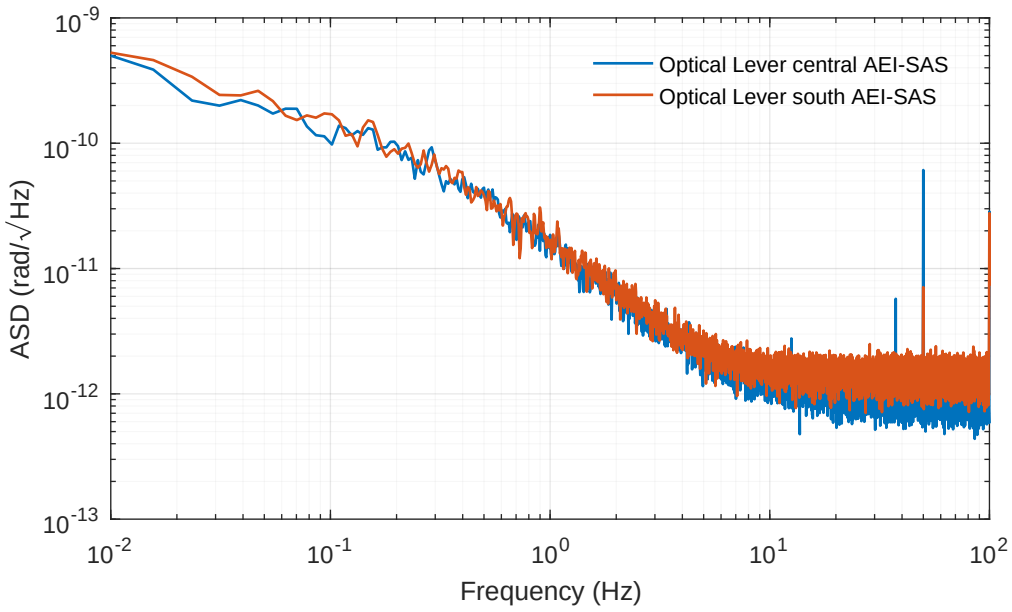

Figure 2.10: Measurement of the electronic noise of the optical levers. In blue, the resulting noise for the projection to the readout accuracy in pitch and yaw for the optical lever stabilizing the central AEI-SAS is shown. Accordingly in red for the optical lever stabilizing the south AEI-SAS. The measurement resolution at 100 mHz is 0.2 nrad $\mathrm{Hz}^{-1/2}$, above 10 Hz reaches 2 prad $\mathrm{Hz}^{-1/2}$.

freedom $l_{\mathrm{OL}} \cdot r_{\mathrm{x,z}}$:

$$d_{\mathrm{QPD}} = l_{\mathrm{OL}} \cdot r_{\mathrm{x,z}} + d_{\mathrm{z,x,central}} + d_{\mathrm{z,x,south}} \,, \tag{2.14}$$

with l_{OL}= 11.65 m being the length of the lever arm. To project the coupling of the transverse degrees of freedom to the rotational degrees of freedom measurement by the optical lever, they need to be divided by the length of the lever arm.

In figure 2.11 the solid and dashed blue and red lines show a typical measurement of the displacement of the x and z degrees of freedom of the two AEI-SAS. The measured displacement in d_{x} and d_{z} is projected to the measurement of r_{z} and r_{x} by the optical lever. The transverse motion at the south and central optical table is caused by common ground motion. The displacement of d_{x} and d_{z} between the tables should therefore be correlated and reduced due to common mode rejection. In figure 2.11 the measurements of the two tables are subtracted and compared to the electronic noise, giving the total expected noise limit for the optical lever measurements. For the optical lever measuring r_{z}, the coupling of d_{x} shown in the dash-dot blue line is larger than the electronic noise in gray. d_{x} was measured by monolithic-accelerometers [Wan12]. Up to 0.8 Hz the measurement was dominated by the sensing noise of the accelerometers. Around the micro seismic peak the motion is above its noise floor. The accelerometers are installed in a stage below the GAS filters. Above approximately 5 Hz, this stage was moving more than the optical table and has strong internal resonances at about

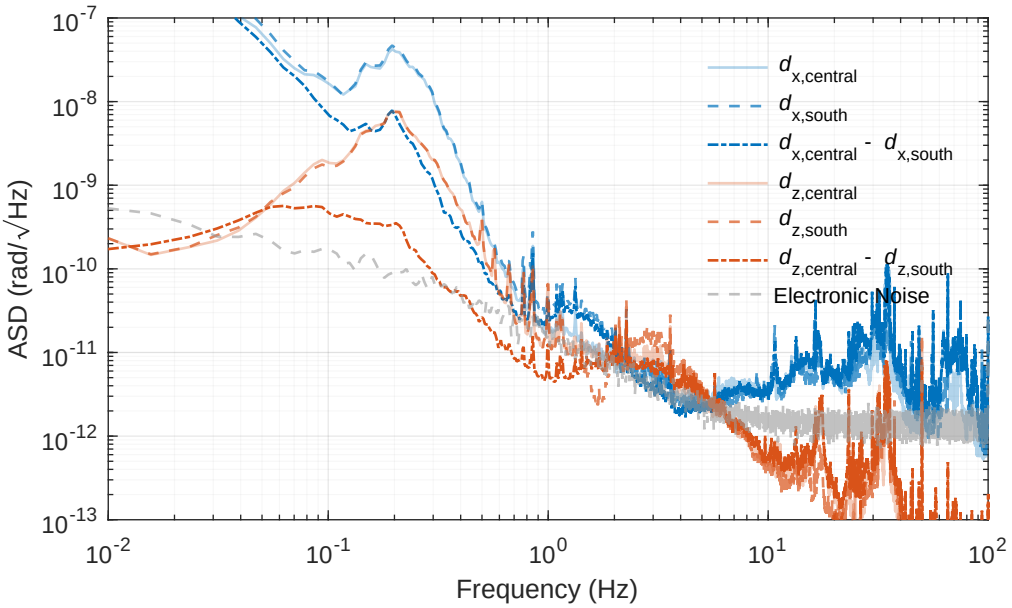

Figure 2.11: Typical inertial measurement of the x degree of freedom the z degree of freedom and their coupling to the optical lever. In the solid light blue and dashed blue line a typical inertial measurement of the x degree of freedom, and in the solid light red and dashed red line for the z degree of freedom are shown. The measurements were performed with the inertial sensors of the AEI-SAS. The measurements were projected to their noise contribution to the optical lever measurement and therefore shown in rad $\mathrm{Hz}^{-1/2}$. The two tables are driven by ground motion. A common-mode rejection of x and z motion is expected. The residual contribution to the optical lever measurement is displayed in the plot in the dash-dot blue for the differential d_{x}, projected to r_{z} and in dash-dot red for the differential d_{z}, projected to r_{x}. The electronic noise of the optical lever is displayed in gray. Due to the sensor noise of the inertial AEI-SAS sensors, a real motion induced noise contribution is mainly expected from 0.8 Hz to 8 Hz.

30 Hz. It is dominating the measurements of the accelerometers. This motion is not directly transfered to the optical table, because of the GAS filter stage in-between. The measurement of the differential motion $d_{\mathrm{x,central}} - d_{\mathrm{x,south}}$ is in the order of the electronic noise from 0.8 Hz to 5 Hz. At the micro seismic peak the contribution can reach 10 nrad $\mathrm{Hz}^{-1/2}$.

The same analysis for the z degree of freedom is shown in the red traces in figure 2.11. The measurement was performed with the L4C-geophones with proven noise performance [Kir17]. Again, the measurements were projected to the equivalent readout of the optical lever. The two independent measurements of $d_{\mathrm{z,central}}$ and $d_{\mathrm{z,south}}$ are subtracted, and the residuals are plotted in figure 2.11 as the red dash-dotted line. These sensors are more sensitive than the accelerometers, but are also not able to provide measurements below 0.2 Hz. The optical lever measurement is therefore expected to be limited by d_{z} from 2 Hz to 6 Hz.

The achieved control loop suppression is verified by a set of optical sensors for the central table. The results are discussed in section 4.1.2 and confirm a stability of 1 nrad $\mathrm{Hz}^{-1/2}$ at a frequency of 100 mHz and 40 prad $\mathrm{Hz}^{-1/2}$ at a frequency of 1 Hz.

Summary

This chapter introduced the two concepts for optical sensors to actively control the displacement of the AEI-SAS in differential longitudinal and angular inertial motion. The interferometric readout of the Suspension Platform Interferometer surpasses the anticipated noise floor reaching down to 5 pm $\mathrm{Hz}^{-1/2}$ at 100 mHz. Together with the hardware modifications and the implementation of the OPD stabilization the Suspension Platform Interferometer is fully commissioned and regularly used. The optical lever sensors were developed to stabilize the AEI-SAS from 10 mHz to 5 Hz for angular displacements. The optical assembly and the integration into the AEI 10 m-Prototype were shown and the expected noise sources presented. The optical lever provide better sensitivity over the full control bandwidth than the foreseen DWS signals, even stabilizing both tables inertially. The optical levers are integrated into the control system of the AEI-SAS and are also fully commissioned. The optical sensors stabilize the two AEI-SAS units, creating a seismically isolated environment for the suspended optics of the AEI 10 m-Prototype. The analysis of the feedback control with a set of out-of-loop sensors is performed in section 4.

CHAPTER 3

Single Arm Test

In this chapter the preparatory experiment for the sub-SQL interferometer, the Single Arm Test is discussed. The sub-SQL interferometer requires a set of well characterized suspension chains to ensure a reliable operation with the monolithically suspended mirrors. Pilot optics were installed in two of them, to test the suspension chain. The weight of the optics has to be (100 ± 2) g per optic. The key difference of the pilot optics compared to the final optics are a poorer surface figure, and the use of an amorphous mirror coating in contrast to the crystaine coating. These amorphous coatings are produced by Ion Beam Sputtering (IBS) and the power reflectivity is 99.5 %. Two suspensions were built, tested and setup in the AEI 10 m-Prototype system. They are arranged to form a linear impedance matched cavity with a comparable finesse. The monolithic suspension is replaced by a steel wire stage, for practical reasons and because suspension thermal noise was not expected to strongly effect testing of the suspension. The construction of the mirror suspensions is described in section 3.1. The optical assembly of the Single Arm Test is discussed in chapter 3.2. The characterization of the suspension actuators is described in section 3.3.

The designs of the mirror suspension as well as the actuator concept were not part of this thesis. The set up of two mirror suspension, their installation in the vacuum system as well as the installation of the input path and the detection chain, the characterization of the actuator range with the Single Arm Test cavity and the length stabilization of it were achieved within this thesis.

3.1 SQL mirror suspension

The 100 g triple mirror suspension has been designed at the University of Glasgow and are also used for the Speed Meter experiment [Grä14; Hen18]. The IGR at Glasgow University has expertise in producing monolithic fused silica suspensions [Aff14; Cum12]. For the sub-SQL interferometer the mirrors will be connected to the Penultimate Masses by two silica fiber sets of 20 µm diameter. This will reduce the suspension thermal noise. The complete assembly will be manufactured in the IGR and sent to the AEI. The other parts of the suspension were manufactured and assembled at the AEI. During the assembly of the suspension and its operation a few changes had to be implemented. All improvements were implemented in close collaboration with the IGR to not compromise the manufacturing of the monolithic suspension stage. The monolithic assembly will be integrated into the suspension chain later. For the

Single Arm Test the monolithic stage was replaced by an aluminum PUM and the pilot optics, connected by steel wire loops.

3.1.1 Suspension properties

The suspensions for the 100 g mirrors proved two isolation stages for the vertical, and three for the horizontal degree of freedom. For vertical isolation, pre-bent maraging steel cantilever blades are used. They provide vertical isolation, from ground motion which is important to reduce the amount of cross coupling to the longitudinal degree of freedom and reduce the excitation of violin modes [Goß04]. The horizontal isolation is provided by wire pendulums which are reducing the mirror motion in the horizontal degrees of freedom.

In figure 3.1 the fully assembled suspension of the input mirror is shown. The technical drawing on the right hand side right illustrates the structure of the assembly. The cross shaped top mass is suspended by wires from two cantilever blades at the suspension point and is shown in figure 3.2. The thickness of the top stage wires is 100 µm. Four coil/magnet actuators are installed at the top mass.

In the top mass, a second set of cantilever blades are installed as shown in figure 3.2(c). From there, the second pendulum stage with a wire diameter of 50 µm suspends the PUM. The wire diameter is thinner at the PUM stage to reduce the thermal noise from the suspension.

Two wire loops support the PUM at the front and back. Another set of coil/magnet actuators at the PUM is installed. The parts of the suspension chain discussed above is the same for the Single Arm Test and the sub-SQL interferometer. The last suspension stage will be replaced by a monolithic stage for the sub-SQL interferometer. It connects a fused silica Penultimate Mass with a high quality crystalline coated fused silica mirrors by silica fibers of 20 µm diameter. For the Single Arm Test pilot mirrors with an amorphous dielectric silica/tantala coating and an aluminum PUM are used. 50 µm steel wires are used to replace the silica fibers for the mirror suspension. The actuator at the mirror is a new concept of an ESD. The actuators used to control the position of the mirror are described in more detail in the next section 3.1.2.

3.1.2 Actuators

Controlling the mirror position is an essential function of the suspension chain. The mirror position needs to be controlled to operate all optical cavities on resonance and keep the interferometer at the desired operating point. Actuators at the suspension are split into two categories. Coil/magnet actuators are used at the first two suspension stages. The displacement noise introduced by the coil/magnet actuator are filtered by the subsequent suspension chains. The mirror actuator is a new concept for an ESD and will fulfill the required displacement noise sensitivity without the need of seismic isolation [Wit15]. The force required from the actuators has already been included into the design of the suspension chain and is not topic of this work. It is briefly discussed in the following section.

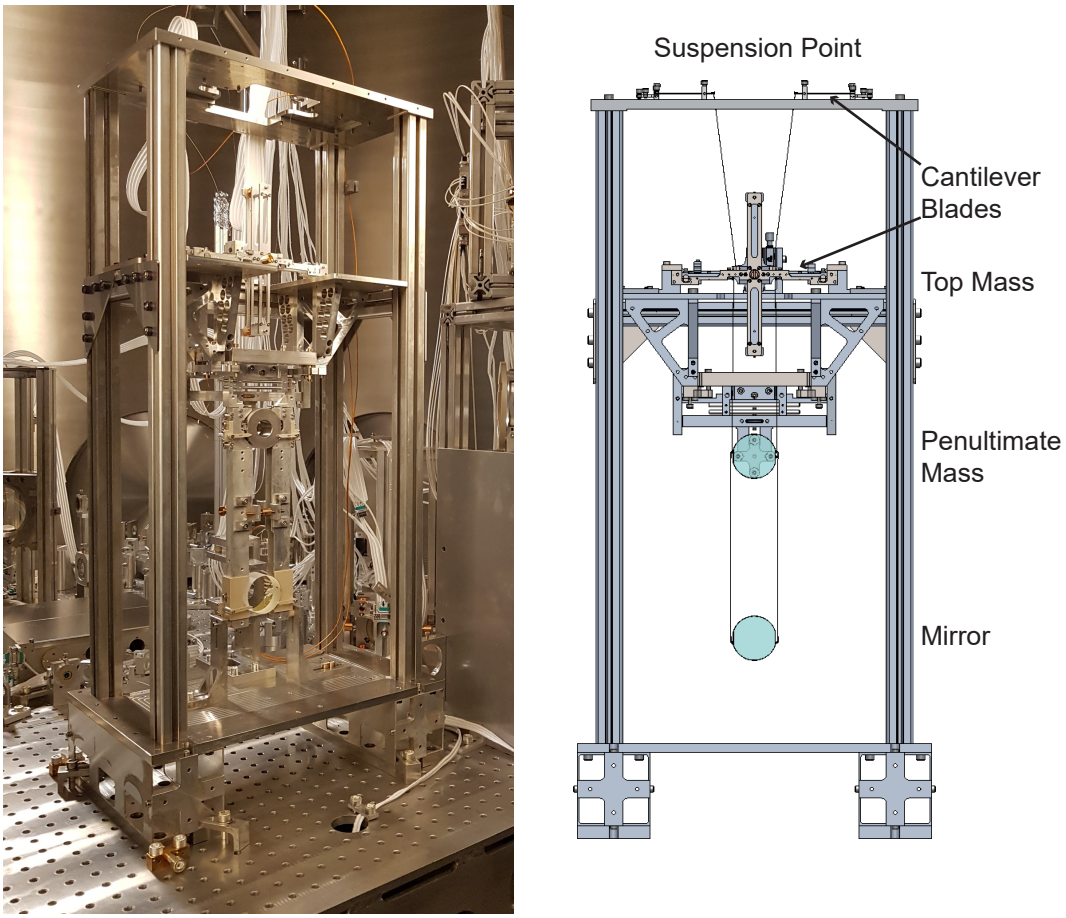

Figure 3.1: The left picture shows the fully assembled and installed input mirror suspension of the Single Arm Test. On the right picture a projection of the technical drawing of the suspension chain, without the fiber guard assembly, is shown. The technical drawing has been provided by the IGR. The horizontal pendulum stages and the two vertical cantilever isolation stages connect the suspension point via cross shaped top mass and aluminum PUM with the mirror. Each suspension stage is 193 mm long.

Coil/magnet actuator at Top Mass and Penultimate Mass

Four pairs of Kapton coated copper-wire coils are placed at the top mass of the suspension. It is shown in figure 3.2. The top mass is cross shaped to provide long lever arms for pitch and yaw displacements. Four pairs of magnets are located at the end of the arms. The coils are wound around a holder made from copper to provide eddy current damping. When the magnet is moving with respect to the coil an eddy current is induced in the copper holder. The suspension and the frame with the attached coils experience the same motion below the fundamental resonances and the magnet moves in common with the eddy current damper. On resonance, the suspended mass motion is strongly enhanced with respect to the frame motion and the induced eddy current is extracting energy from the suspension and therefore damping

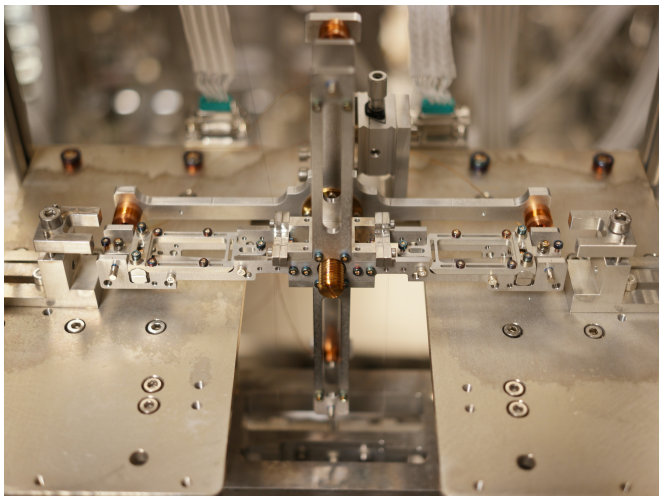

(a) View from the front onto the top mass.

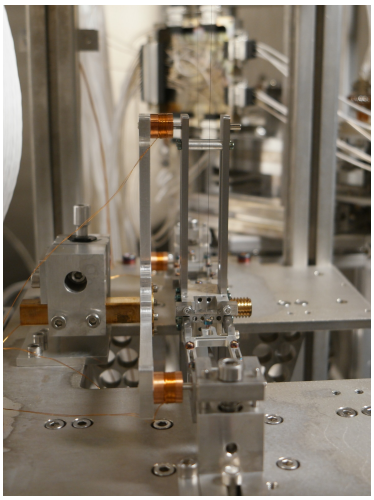

(b) View from the side.

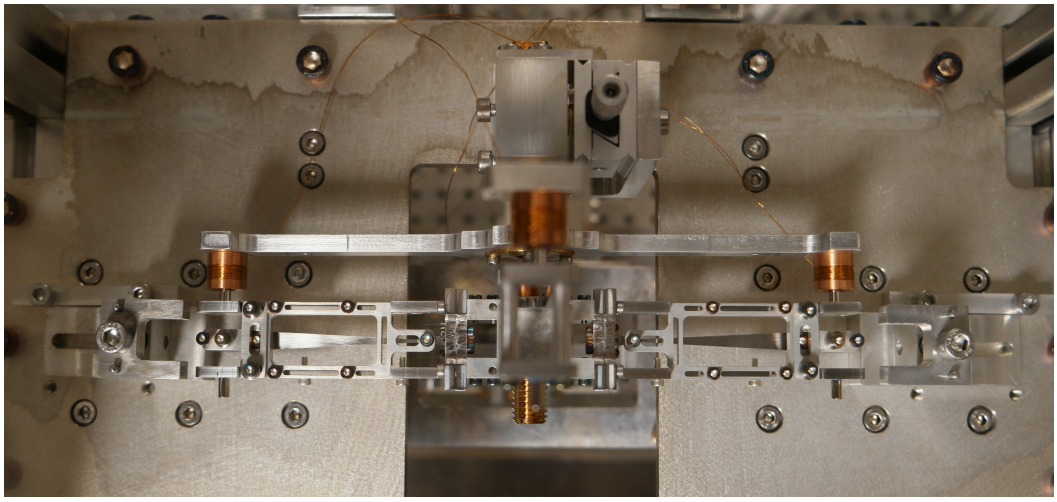

(c) View on top of the Top Mass. From the cantilever blades, the PUM is suspended.

Figure 3.2: Three pictures of the top mass. The cross shaped design provides a long lever arm for the actuation while remaining very light. The actuators are current driven coils which generates a magnetic field and acts an the magnets glued to the top mass. The coils are wound around holders made out of copper. When the magnet is moving inside of the copper holder it will induce a eddy current loop in the copper. Which damps the motion of the magnet and hence the mass. This is reducing the displacement at the fundamental resonances. The top mass actuators are used for positioning of the mirror. Mechanical align of the mirror in pitch is done with a threaded rod in the center of the top mass can be positioned along the central horizontal axis.

the resonance frequencies. Above the resonance frequency the frame moves more than the suspension and the eddy current damping is inducing motion to the suspension. The strength of the eddy current damping is not compromising the seismic isolation in the measurement band of the sub-SQL interferometer.

The coil holders are attached to a support structure located behind the suspension as shown in figure 3.2 and can be pushed over the magnets as a single unit. Each coil/magnet actuator provides a force of $F/I = 0.03\,\mathrm{N\,A^{-1}}$, where the current is limited to 40 mA providing sufficient range for the fine alignment of the mirror [Leh16]. In the top view of the top mass in figure 3.2(c), the blade springs suspending the PUM are shown.

The PUM for the Single Arm Test is an aluminum cylinder with a hole in the center to reduce the weight to 100 g. The two Figures 3.3(a) and 3.2(b) show the PUM from back and side view. The actuators are coil/magnet pairs in a cross shaped configuration. The coil holders are of the same size as the one at the top mass, but made out of a vacuum compatible plastic PEEK which does not introduce eddy current damping. They provide a force of $F/I = 0.0044\,\mathrm{N\,A^{-1}}$ with the maximum current limited to 20 mA improving the signal to noise ratio, due to the bite depth of the ADC [Leh16]. The PUM actuators provide longitudinal actuation force for the length stabilization of the Single Arm Test cavity and will also be used for stabilization of the sub-SQL interferometer degrees of freedom.

Electrostatic Drive

In the sub-SQL interferometer, the beam sizes are large compared to the optic diameter. A Electro Static Drive as used in gravitational wave detectors would reduce the clear aperture of the mirror. Furthermore, it would have to be suspended by a reaction pendulum to isolate it from ground motion. A new concept for an ESD was developed and published in [Wit15]. A plate capacitor is placed around the mirror 3.4. When an electric field is applied a force is acting on a dielectric medium located in an asymmetric inhomogeneous electric field. The force on the mirror is directed in the direction of higher field intensity. The ESD is oriented to pull along the beam axis. The position of the mirror can be modulated bidirectionally by applying a bias voltage to the capacitor plates. The force created by the ESD onto the mirror is proportional to the square of the applied voltage. An approximation for the applied force can be found in [Leh16] following [Wit15],

$$F_{\mathrm{ESD}} = \left(\varepsilon_{\mathrm{m_{eff}}} - \varepsilon_0\right) \frac{b}{2a} U_{\mathrm{ESD}}^2 \tag{3.1}$$

with

$$\varepsilon_{\mathrm{m_{eff}}} = \frac{\pi \cdot r_{\mathrm{m}}^2}{b \cdot a} \varepsilon_{\mathrm{m}}\,. \tag{3.2}$$

The above equation assumes there is no gap between the dielectric medium and the capacitor, and that one end of the dielectric medium is within the homogeneous field of the capacitor. The separation of the two capacitor plates is a and the width is b. The dielectric constant of the

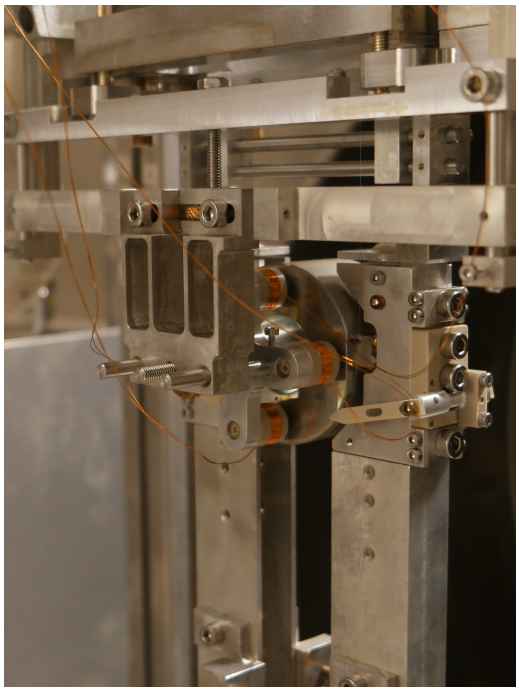

(a) View from the back of the suspension onto the PUM. The coils are attached to a holder and can be moved as one unit. Two degrees of freedom can be adjusted by translational sliders.

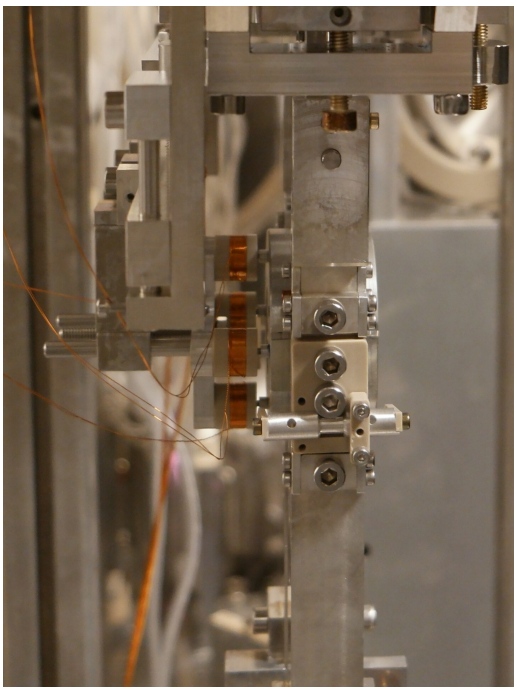

(b) View from the side of the suspension onto the PUM. The magnets are 3 mm × 1.5 mm and would be almost completely covered by the coil holders. The risk of touching the PUM with the coil holders is reduced by gluing the magnets to aluminum cylinders.

Figure 3.3: Two pictures of the coil/magnet actuator at the PUM. The coils are wound around a holder made out of Polyether Ether Ketone (PEEK) and do not provide eddy current damping.

vacuum is ε_0, ε_m is the dielectric constant of fused silica, the material the mirrors are made of. The radius of the mirror is r_m and the voltage difference of the capacitor plates is U_{ESD}. The simple model used for the equation is not directly applicable to the ESD. A fill factor for the mirror in the capacitor is therefore multiplied to the dielectric constant of the mirror resulting in the effective dielectric constant $\varepsilon_{m_{eff}}$. This model is an approximation and the publication [Wit15] includes a detailed Finite Element Modeling (FEM). The force of the ESD pulls the suspended mirror into the capacitor until the force is canceled with the restoring force of the pendulum. The expected force of the ESD is approximately 1 µN.

The force of the ESD onto the mirror depends on relative position between mirror and capacitor plates. If the mirror would be entirely in the homogeneous electric field no force would act onto it. The force would be relatively weak if the mirror would be placed completely out of the capacitor. In between these two cases the ESD force has a plateau with its maximum force. The force onto the mirror is independent of the position of the ESD at this plateau. The coupling of ground motion to the mirror by the ESD displacement relative to the mirror is analyzed in [Wit15]. The analyses shows that seismic isolation of the ESD is not required.

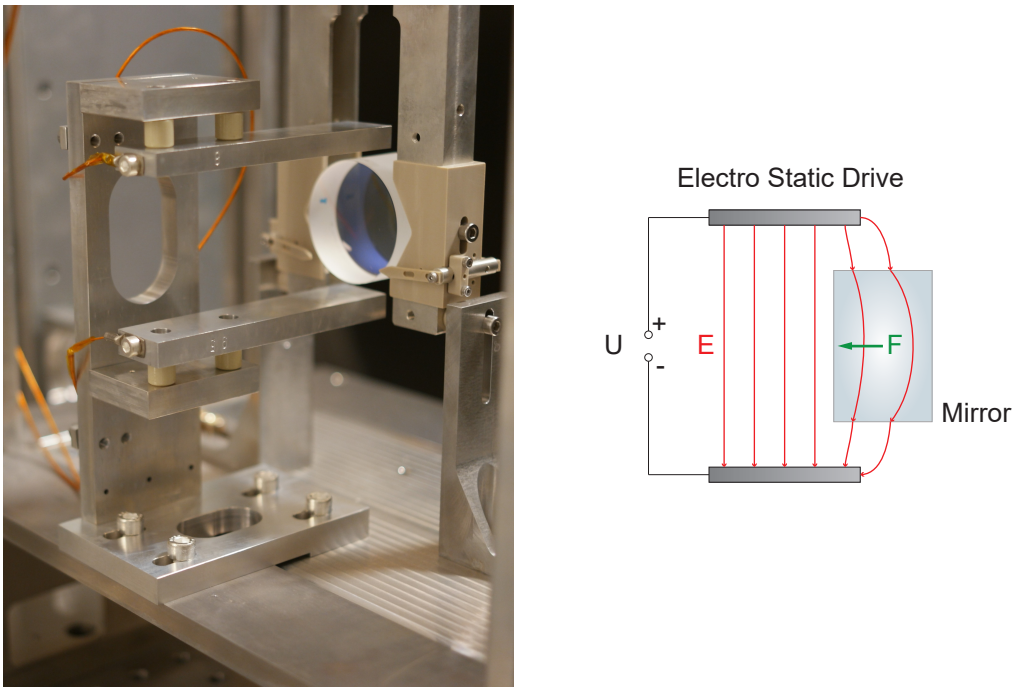

Figure 3.4: Picture of the ESD installed at the input mirror of the Single Arm Test. The ridged mount is defining the distance to the mirror and can be used as a measure of the absolute height of the suspended mirror. Only the position of the ESD along the beam axis can be adjusted. Due to the large spot sizes for the sub-SQL interferometer the clear aperture has to be at least as big as the mirror size. A voltage is applied to the ESD, to actuate onto the mirror. The electric field pulls the dielectric mirror inwards until the force is balancing the restoring gravitational force from the pendulum. The position of the mirror can be used to stabilize the length of the cavity by modulating the applied voltage. The force of the ESD is unidirectional. A voltage offset is applied to allow bidirectional actuation.

The ESD is used as the high frequency actuator on the suspension chain and was used in a feedback loop with a unity gain frequency of up to 100 Hz. A filter is digitally applied by the CDS to generate the feedback signal and amplified by a HV amplifier. Which can provide up to 710 V to the ESD. The electronics are listed in the appendix A.2.

The actuator characterization is discussed in section 3.3.

3.2 Optical assembly and auxiliary optics

The Single Arm Test is installed on only two AEI-SAS and the input path differs therefore from the sub-SQL interferometer input path. The input path is rerouted by positioning the collimating mirror of the beam expansion telescope on the south optical table and orienting the suspended steering mirror accordingly. The EOM crystal is not available yet as the modulation frequencies for the interferometer are not yet decided. The modulation frequencies and modulation index for the sidebands of sub-SQL interferometer need investigation by simulations to provide

separable error signals for control of the individual degrees of freedom of the interferometer. For the Single Arm Test the sidebands of the Frequency Reference Cavity can be used. All detection electronics are non-resonant and can be used up to 20 MHz. This allows a fast transition to a different modulation frequency. The detailed description of the optical set up is discussed in the following section.

3.2.1 Input and output optics

For the sub-SQL interferometer a maximum of 10 W laser power is required. The 35 W Laser system was developed for enhanced LIGO and is also used in GEO 600. Only a fraction of 1 W of the laser light is currently coupled into the photonic crystal fiber and is guided into the vacuum system by a feed-through. The light out of the fiber is spatially filtered by a Mode Cleaner Cavity. A detailed description of the 35 W Laser system, the photonic crystal fiber and the design and performance of the Mode Cleaner Cavity are published in [Opp17].

The Single Arm Test is a Fabry-Perot cavity. The cavity is impedance matched, which is achieved by using cavity mirrors with equal reflectivity. If the cavity is resonant to the laser frequency most of the laser power is transmitted and a fraction is reflected due to mode mismatches and losses in the cavity. An error signal is required, to stabilize the cavity length to the laser frequency, or vise versa. It is generated by imprinting phase modulation sidebands onto the laser light using an EOM. A vacuum compatible EOM from GEO 600 is currently used in the AEI 10 m-Prototype. It consists of a $LiNbO_3$ crystal and was initially installed for the Frequency Reference Cavity and is now also used for the Single Arm Test. The crystal will be replaced later, since it suffers from a permanent optical lens burned into the crystal structure due to operations at high laser powers[Bog13]. The sideband frequency for the Single Arm Test is therefore the same as for the Frequency Reference Cavity with a frequency of 8.047 MHz.

The size of the waist in the Mode Cleaner Cavity is designed to form a collimated beam with the radius of curvature of the first suspended steering mirror. The resulting beam is collimated with the beam size of 9.72 mm for the original design of the sub-SQL interferometer with a cavity g-factor of 0.998 [Grä13]. An additional telescope would not have been required for the sub-SQL interferometer. The Single Arm Test starts with a cavity g-factor of 0.8 and hence the cavity mode is significantly different and requires a different input path . Since the Single Arm Test is using two AEI-SAS the input path had to be extended. A telescope of two lenses, as shown in figure 3.5, is creating a collimated input beam with a radius of $\omega = 3.5$ mm together with the suspended curved mirror. The beam height of the suspended mirrors is 22 cm. All other optics are at a height of 10 cm. The mirror before the first suspended steering mirror (SM1) is therefore tilted, raising the beam height from 10 cm to 22 cm over a distance of more than 10 m. The beam expansion telescope is located before the height raise, to avoid hitting lenses off centered.

The reflected beam from the Single Arm Test cavity is reflected along the same path as the input light. A Faraday Isolator is rotating the polarization by 45° as the light travels through the crystal. The Faraday effect is non-reciprocal and hence the reflected light is accumulating an additional 45° rotation of the polarization for a total of 90° compared to the input of the

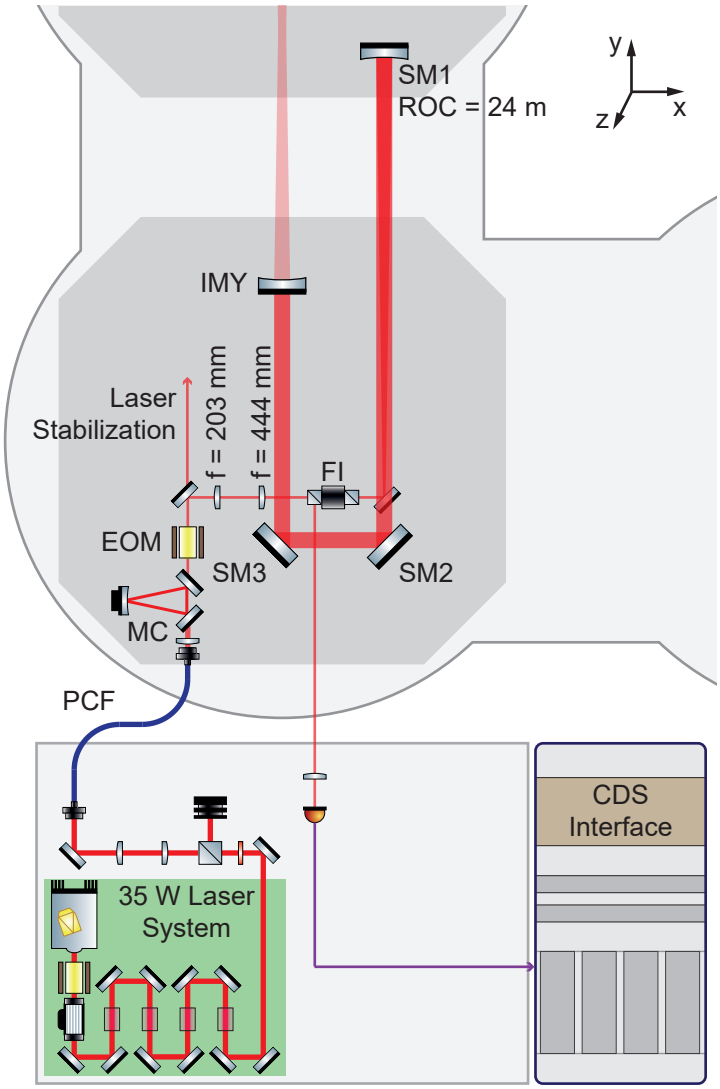

Figure 3.5: Schematic overview of the Single Arm Test input optic path. The 35 W Laser system can produce up to 35 W of laser power at a wavelength of 1064 nm. The light is transmitted through a photonic crystal fiber into the vacuum system. A rigid spacer Mode Cleaner Cavity is spatially filtering the mode of the laser light. The length of the resonator is stabilized to the laser light frequency by a piezoelectric element acting onto the curved mirror [Opp17]. The EOM inside the vacuum system is used to imprint the sidebands for the Pound-Drever-Hall stabilization. Two lenses are expanding the beam and form a collimated input beam with the first suspended curved Steering Mirror (SM) on the south table.

isolator. The returning beam is reflected at the polarizing beam splitter at the front of the Faraday Isolator. It is leaving the vacuum system through a viewport. A lens is focusing the beam to detect it on a photodiode.

3.2.2 Suspended input optics

The beam diameter size expands from the central optical bench to the south optical bench, which requires a change of the 1 " standard optics to optics with an aperture as large as 3 ". Upon reflection from this concave curved mirror with a ROC = 24 m the beam is collimated and not expanding any further. Two mirrors are steering the beam into the cavity and are hit under an angle of 45°. The projection of the beam onto the mirror surface leads to a bigger effective size of the beam and the mirrors have a diameter of 4 ". All three mirrors are suspended by a single pendulum wire loop. Coil/magnet actuators allow remote alignment of the input beam. A copper coil holder is providing eddy current damping. In figures 3.7(a) and 3.7(b) the steering mirrors as well as the end mirror of the SAT installed in the vacuum system are shown. The design is adapted from the steering mirrors of the Frequency Reference Cavity. Transfer functions from the actuation in pitch and yaw show a resonance frequency of 0.68 Hz in pitch and 1.23 Hz in yaw for the suspension of the 4 " mirrors and the Q-factor is 4.1 and 5.7. For the 3 " mirror the resonance frequencies are 0.81 Hz with a Q-factor of 9.2 for pitch and 1.20 Hz for yaw with a Q-factor of 8.7. The resonances are well damp reducing the pointing noise on the Single Arm Test cavity.

Segmented QPD are placed behind the suspended steering mirrors, to ease the alignment when the vacuum system is evacuated. Each current from a quadrant is converted to a voltage by a transimpedance amplifier and whitened before it is digitized by the CDS. The pitch and yaw degree of freedom are computed. Initially the QPDs were installed to allow a precise alignment during the installation of the input optics. In the evacuated vacuum system they allow a fast alignment of the input path. This is resulting in an alignment of the Single Arm Test where light is resonating in the cavity.

In figure 3.6, the installed QPDs are shown. The colors indicate which QPD signal is used to actuate on which mirror. For the initial alignment all were used as position references. Later on, some were equipped with digital control loops to keep the beam path fixed. They are centering the position of the beam on the quadrant photodiodes and are indicated by solid lines. In blue, the measuring detector is installed in the beam transmitted through the second suspended steering mirror (SM2). The control loop is acting onto the first steering mirror (SM1). It is stabilizing the position and damping the resonances in pitch and yaw. For stabilization of the second steering mirror a QPD is detecting the transmitted beam through the third steering mirror (SM3). The other QPD signals are not used in control loop but are instead employed for manual positioning.

The reflected beam from the cavity is detected on the QPD behind the first steering mirror together with the input beam. The separation of the two beams is not large enough to be detected on two separated QPDs. The detector is centered between the two signals. If the cavity is not resonant with the incoming light, the QPD pitch and yaw signals should be zero.

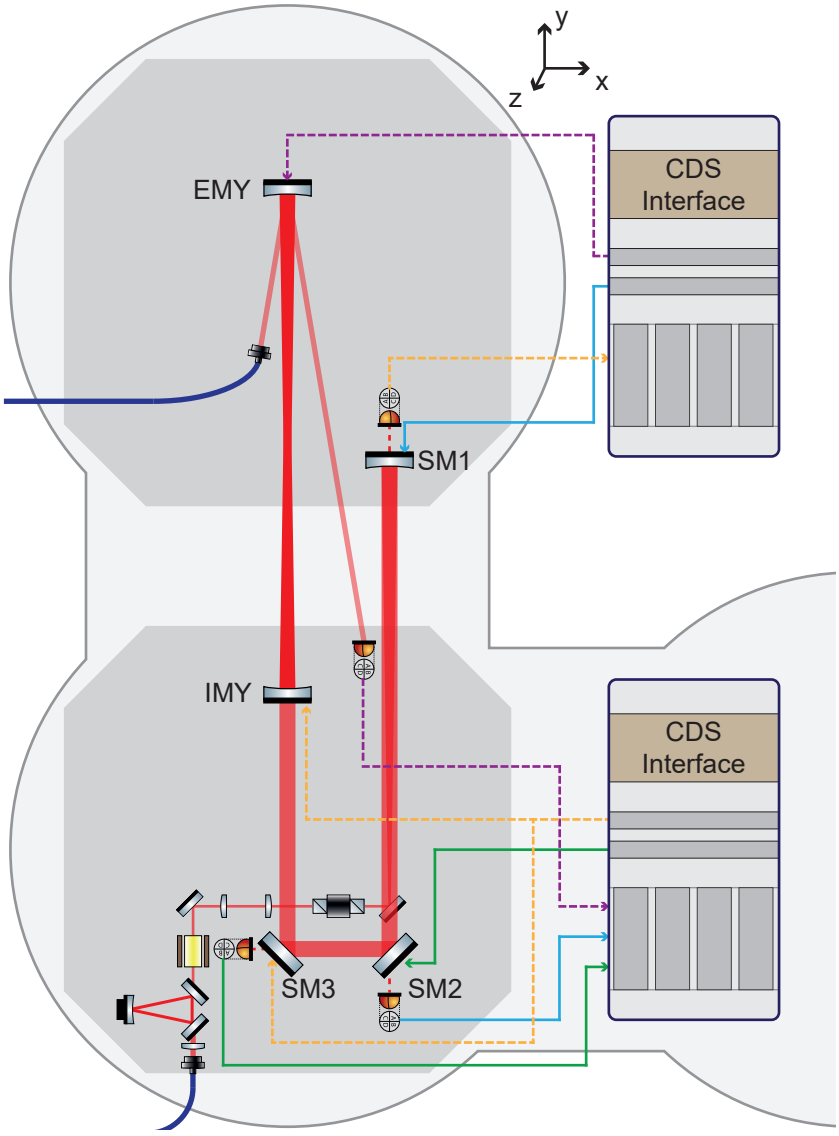

Figure 3.6: Schematic overview of the QPDs installed inside the vacuum system. They allow remote sensing of the beam in the evacuated vacuum system. The solid green and blue lines are indicating the implementation of control loops for permanent positioning and damping of the resonance frequencies of the suspended steering mirrors SM1 and SM2. The other signals with the dashed lines are used for positioning with automated control loops. For the position monitoring of the end mirror a dedicated optical lever was installed. This set of sensors allows a fast and reliable alignment of the Single Arm Test after evacuation of the vacuum system.

This is used to align the input mirror (IMY) of the Single Arm Test after evacuation. For the end mirror (EMY) a separate optical lever is installed. The lever arm amplifies the signal of the pitch and yaw motion of the suspended mirror by keeping the lever arm between the end mirror and the fiber coupler short and the lever to the QPD long.

The suspended steering mirrors and the end mirror of the Single Arm Test are shown in figure 3.7(b) and 3.7(a) installed on the two optical tables. Through the glass of the mirrors the QPDs can be seen as well. In the installation phase also one quadrant photodiode was placed behind the end mirror to align the input path. Afterwards, the input mirror of the Single Arm Test was installed and aligned. The QPD was removed. The pictures were taken between the installation of the end mirror and the input mirror allowing a view onto all steering mirrors.

3.2.3 Cavity readout

A stabilization of the laser frequency to the cavity or a stabilization of the cavity length to the laser light is required, to measure the fluctuations of the cavity length. Error signal are obtained by the Pound-Drever-Hall method [Bla01]. The necessary sidebands are imprinted onto the light by an EOM. Later on a separate EOM will be installed and the side band frequency will likely be shifted. The readout electronics are therefore usable for frequencies in a range of up to 20 MHz. For the readout of the cavity an adapted photo receiver originally developed for the aLIGO Pre-Mode Cleaner detects the reflected light of the Single Arm Test. The transfer function was measured and is shown in figure 3.8 and the circuit documentation and can be found under in the appendix in figure A.2. For demodulation of the Pound-Drever-Hall signal an additional board was developed. An optional whitening filter is implemented and the signal is converted to a differential output signal. The schematic is shown in the appendix in figure A.3 for the error signal and in figure A.4 for the power monitoring of the transmitted and reflected photodiode signals. Two types of stabilization loops were implemented, one acting onto the laser frequency by modulating the piezoelectric element of the 35 W Laser system and the other one acting onto the suspension. They are described in section 3.3 and 4.2. Both control loops were implemented through the CDS.

3.2.4 Cavity Parameters

The radius of curvature of the Single Arm Test mirrors are both $R_{\mathrm{Cavity}} = -5700\,\mathrm{mm} \pm 1\,\%$ on the highly reflective inside of the mirror. The radius of curvature is the same as for the sub-SQL interferometer mirrors. The mirrors form an almost concentric cavity, where the stability parameter will be up to $g = 0.99$ [Kog66]. The Single Arm Test is starting with a conservative set up to obtain a stable cavity. The stability parameter was set to $g = 0.8$ by shortening the cavity to $L_{\mathrm{Cavity}} = 10.8\,\mathrm{m}$

$$g = \left(1 - \frac{L_{\mathrm{Cavity}}}{R_{\mathrm{Cavity}}}\right)^2 . \tag{3.3}$$

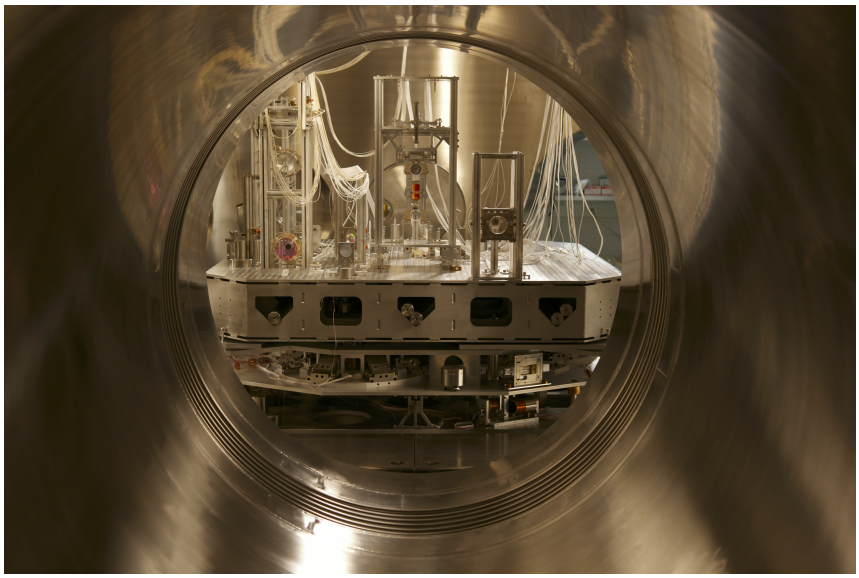

(a) View from the center of the south tube onto the south optical bench. On the right the 3" collimating mirror and in the center the end mirror of the Single Arm Test are installed.

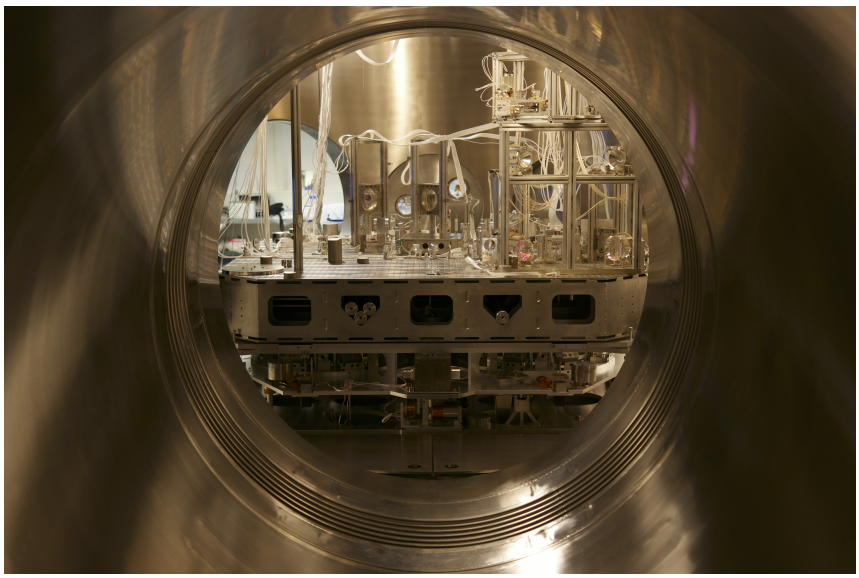

(b) View from the center of the south tube onto the central optical bench. This picture was taken before the input test mass of the Single Arm Test was installed. The view onto the 4" steering mirrors is therefore possible.

Figure 3.7: Pictures taken from the center of the tube connecting the south and central vacuum tanks. The single pendulums holding the steering mirrors and one triple suspension are installed. The pictures were taken during installation and alignment of the input path.

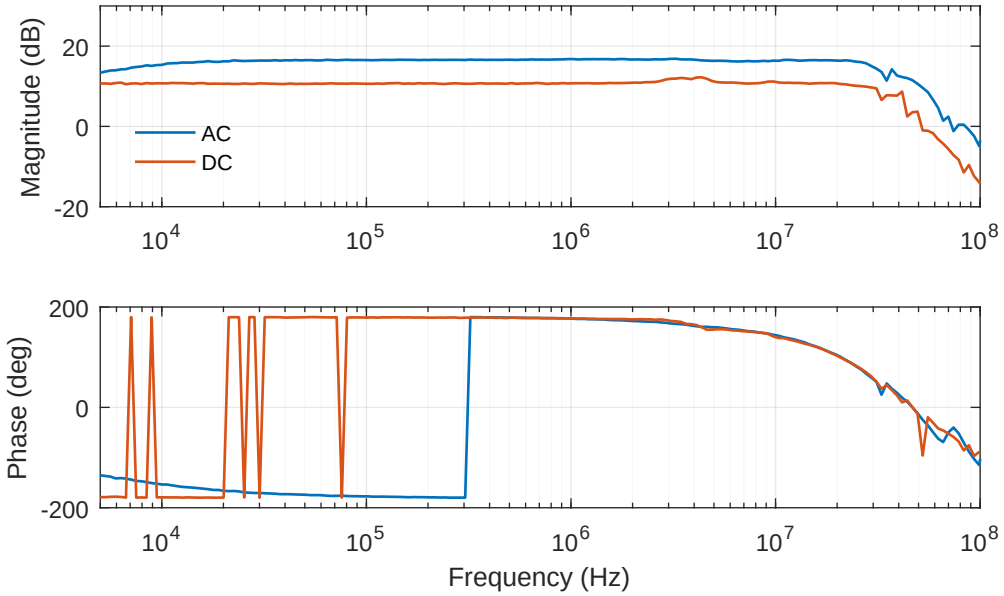

Figure 3.8: Measurement of the Single Arm Test locking photodiode transfer function. The Alternating Current (AC) path is used for the Pound-Drever-Hall signal and the Direct Currnet (DC) path for power monitoring of the Single Arm Test cavity.

The input mirror has a curvature of 1776.3 mm ±1 % on the anti-reflective coated outside to focus the collimated input beam into the cavity. The analysis of different possible input beams as well as the mirror specifications is discussed in [Grä13].

Calibration

The cavity parameters, listed below, of the Single Arm Test are measured by modulating the laser frequency with the piezoelectric element at the NPRO. The modulation depth was chosen to resolve at least four free spectral ranges to eliminate hysteresis effects from the piezoelectric element actuator. In figure 3.9 the measured transmitted and reflected power as well as the error signal are shown. The frequency axis was calibrated by the separation between the sidebands and the fundamental mode. The error signal was amplified to saturated the CDS input at the fundamental mode, thereby giving the impression of being the same sizes as at the sideband frequency. The stabilization of the Single Arm Test is unaffected. The error signal slope was calibrated to the simultaneously monitored feedback signal of the Mode Cleaner Cavity in meter.

With the power reflectivity for $R = 0.995$ and the cavity length of $L = 10.8\,\mathrm{m}$ the calculated cavity parameter are [Sie86]:

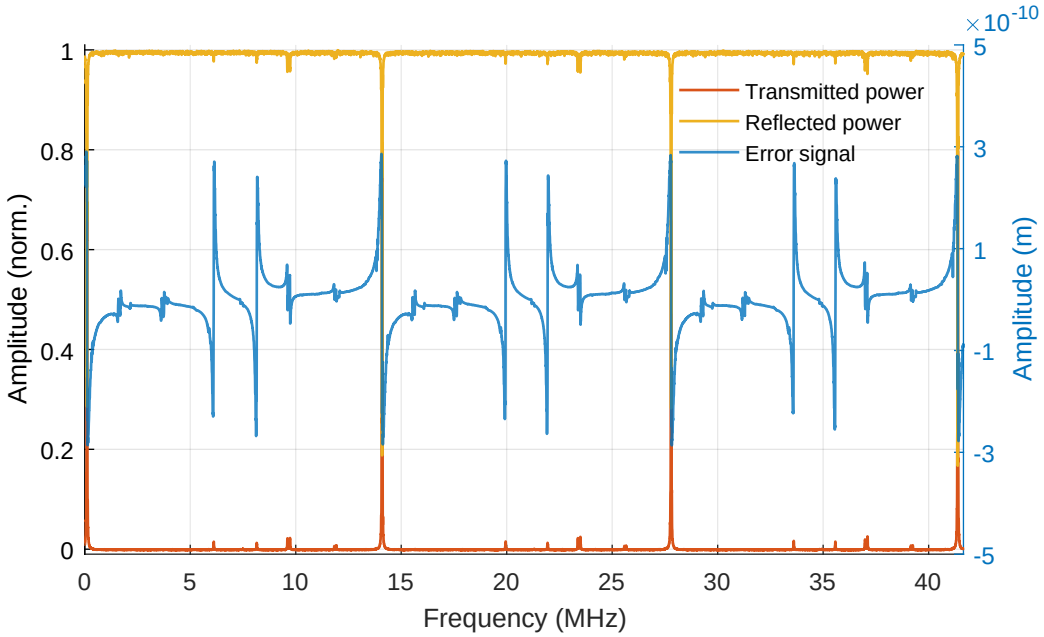

Figure 3.9: Scan of the laser frequency to measured the Single Arm Test cavity parameters. In red the transmitted laser power through the Single Arm Test cavity and in yellow the reflected laser power. The cavity fundamental mode is resonant to the laser frequency and the error signal in blue is crossing the operation point at zero at the maxima of the transmitted power. The sideband frequency is at 8 MHz and is used for the calibration of the frequency axis.

- Free spectral range:

$$\Delta f = \frac{c}{2L_{\text{Cavity}}} \tag{3.4}$$
$$\Delta f = 13.9\,\text{MHz}$$

- Finesse:

$$\mathcal{F} = \frac{\pi\sqrt{R_{\text{Cavity}}}}{1-R_{\text{Cavity}}} \tag{3.5}$$
$$\mathcal{F} = 627$$

- Full Width Half Maximum:

$$\Delta\nu = \frac{\Delta f}{\mathcal{F}} \tag{3.6}$$
$$\Delta\nu = 22\,\text{kHz}$$

The measured values from figure 3.9 are:

- $\Delta f = 13.7\,\mathrm{MHz}$
- $\mathcal{F} = 656$
- $\Delta\nu = 21\,\mathrm{kHz}$

The setup for the Single Arm Test was chosen to be similar to the sub-SQL interferometer to gain experience and troubleshoot possible issues, before the final installation of the monolithic mirror suspension stage. The input path and detection chain are build and can be used for the sub-SQL interferometer commissioning. The transfer function of the actuators to the cavity length were measured, to fully characterize the suspension chain. In the following section the setup for this test is discussed and the results will be presented.

3.3 Actuator characterization

In this section a stabilization of the frequency of the 35 W Laser system to the Single Arm Test cavity length is presented. With the previously explained actuators, the length of the Single Arm Test cavity was modulated and the transfer function to the cavity length was measured.

In figure 3.10 an overview of the optical assembly of the Single Arm Test as well as the simplified feedback loop are shown. For the Single Arm Test experiment a fraction of 200 mW from the 35 W Laser system light was used. Passing the Mode Cleaner Cavity, the EOM, a lens system and a Faraday isolator the beam expands to the curved collimating mirror on the south optical table. The collimated beam is reflected to the suspended steering mirror on the central optical table and aligned to the Single Arm Test cavity. The reflected light from the Single Arm Test is traveling backwards through the input path and is separated from the incoming light by a Faraday Isolator. The reflected light is detected by a photodiode. The imprinted modulation sidebands on the laser light generate an error signal by employing the Pound-Drever-Hall method [Bla01]. The error signal is obtained by frequency mixing with the local oscillator. The signal is digitized by the CDS and a digital filter calculates the feedback signal. This is converted to a voltage by the DAC of the CDS. The feedback signal is applied to a piezoelectric element at the Non-Planar Ring Oscillator laser crystal. The signal from the CDS is amplified to extend the actuator range. The positive path of the HV amplifier developed for the ESD is used. For reference see Appendix A.2. It can produce up to 355 V. The full range is not required due to the active control of the AEI-SAS, discussed in the previous chapter. The control input of the HV amplifier is attenuated to an output of 35.5 V. The noise due to the bit-depth limitation of the DAC is reduced and the signal to noise ratio is improved. It still provides sufficient amplification to keep the laser stabilized to the cavity for hours without interrupt.

The laser frequency is forced to follow the longitudinal motion of the Single Arm Test cavity making it resonant to the cavity eigenmode. The Mode Cleaner Cavity in the input path is stabilized to the laser frequency, see figure 3.10. A piezoelectric element attached to the curved mirror is changing the resonator length according to the frequency fluctuations [Opp17]. A monitoring signal proportional to the feedback to the piezoelectric element of the Mode Cleaner

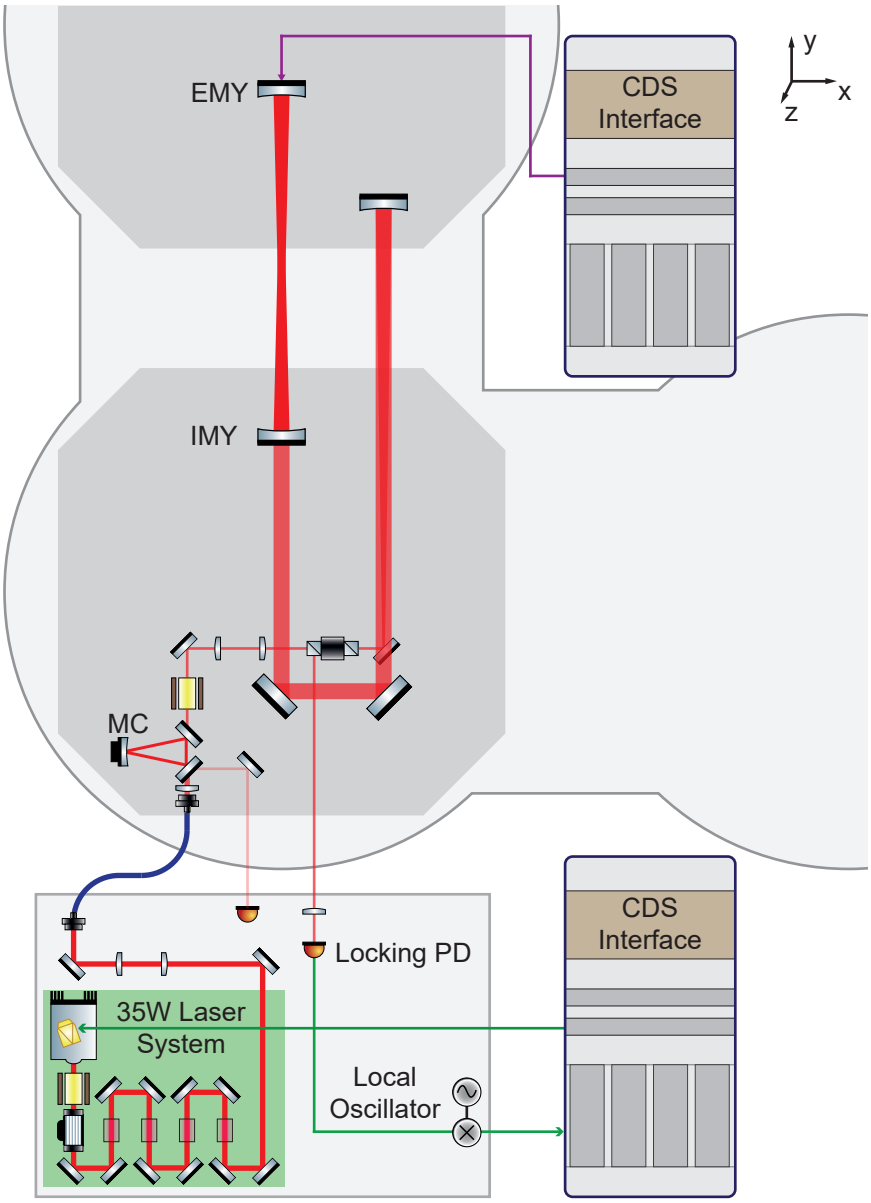

Figure 3.10: Schematic overview of the optical assembly of the Single Arm Test to measure the transfer functions of the suspension actuators. The laser light coming from the 35 W Laser system is entering the Single Arm Test cavity. The fluctuations of the laser frequency relative to the cavity length are detected by the locking photodiode and the signal is mixed with the modulation frequency of the sidebands. This signal is digitized and a filter is applied with the CDS. The feedback signal is converted to a voltage, amplified and applied to the piezoelectric element acting onto the Non-Planar Ring Oscillator crystal in the 35 W Laser system. The laser frequency is forced to follow the length fluctuations of the cavity. Since the laser light has to pass the Mode Cleaner Cavity, the Mode Cleaner Cavity is also forced to follow the laser frequency and therefore the cavity length fluctuations. The cavity length is modulated by actuating onto the suspension actuators of the end mirror. The Mode Cleaner Cavity can be used as a calibrated out-of-loop sensor for the cavity length changes. The suspension actuator transfer functions are therefore measured to this reference.

Cavity is also digitized and recorded by the CDS. This signal is calibrated to equivalent length changes of the Single Arm Test in units of m. The Mode Cleaner Cavity is therefore a calibrated out-of-loop sensor for the Single Arm Test cavity length changes. The length of the Single Arm Test cavity is modulated with the two actuators at the end mirror and the frequency response is measured. The introduced length changes of the Single Arm Test cavity can thereby be measured by the Mode Cleaner Cavity up to 100 Hz. Above this frequency the digitization noise of the monitoring signal of the Mode Cleaner Cavity is masking the length changes of the Single Arm Test cavity.

A detailed analysis of the coil/magnet actuator at the PUM and the ESD at the mirror is shown in the next sections and were performed in assistances of J. Lehmann.

3.3.1 Penultimate Mass

The actuators at the Penultimate Mass are coil/magnet pairs. A magnetic field is induced by applying a current to the coil. The induced magnetic field is acting onto the permanent magnet glued to the PUM. The control input from the CDS is converted to a current by an analogue coil driver. The actuation is bidirectional. In figure 3.11 the measured frequency response of the cavity-length change due to actuation at the PUM in the longitudinal degree of freedom is shown in the red line. The magnitude is calibrated in $\mathrm{m/V_{CDS}}$, calibrating the transfer function of the cavity length to the actuation output of the CDS. The maximum output of the CDS is $U_{\mathrm{CDS,pp}} = 20\,\mathrm{V}$.

The first longitudinal resonance of the suspension is at 0.74 Hz. Below the longitudinal resonance the transfer function is flat with a magnitude of $5.7\,\mu\mathrm{m\,V^{-1}}$. The second longitudinal resonance is at 1.57 Hz. The PUM actuation is filtered by two suspension stages. The actuation force is attenuated by them and is therefore proportional to f^{-4}. The measured magnitude of the transfer function shows exactly this behavior. The phase experiences a total phase loss of $-360°$. The third longitudinal resonance is at 2.39 Hz. All longitudinal resonances are well damped by the eddy current damping at the top mass. Pitch resonances are strongly coupling to the longitudinal degree of freedom at 7.72 Hz and 16.96 Hz. When the monolithic suspension stage will be used, the pitch resonance at 7.72 Hz will shift to lower frequencies. The wire separation of the two slings around the 24.5 mm thick PUM is 20 mm resulting in a stiff pitch mode at 16.96 Hz.

3.3.2 Electrostatic Drive

The laser frequency was stabilized to the Single Arm Test cavity and the ESD was used to modulated the cavity length, to measure the transfer function of the ESD to the cavity length. The input of the HV amplifier is limited to $U_{\mathrm{CDS,pp}} = 10\,\mathrm{V}$. In figure 3.11 the transfer function from the CDS actuation to the length change of the Single Arm Test cavity was measured. The blue line represents the transfer function of the ESD actuation. The magnitude and phase are independent on the frequency below the fundamental longitudinal resonance frequency at 0.74 Hz. Above the fundamental frequency, the frequency response rolls off proportional to f^{-2}.

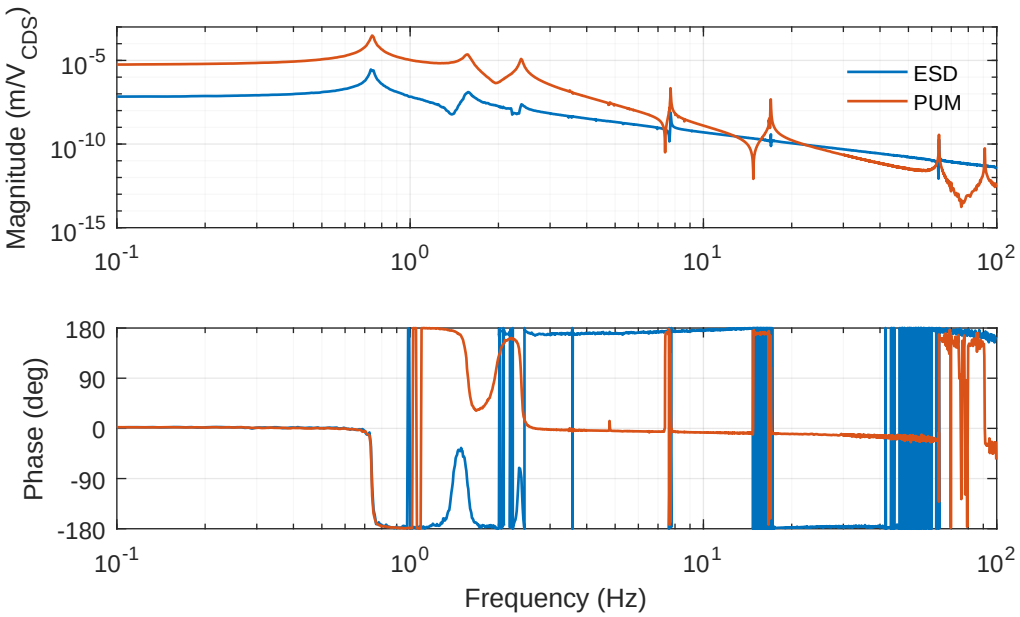

Figure 3.11: Measured transfer function for the suspension actuators at the PUM and the ESD of the end mirror to the length of the Single Arm Test cavity. The transfer function of the ESD proving a similar actuation range as published in [Wit15] with a deviation due to the different geometry of the ESD and the pendulum.

The resonance peaks at 1.57 Hz and 2.39 Hz correspond to the second and third longitudinal resonance. The cross coupling of the pitch resonances introduces the peaks between 6 Hz to 17 Hz. The anti-resonances are caused by the actuation at the actuation point being out of the phase with the mirror mass motion. The phase of the frequency response is accumulating a phase shift of −180°. The force of the ESD onto the mirror is similar to the one presented in [Wit15]. The size of the capacitor plates and the maximum voltage applied to the ESD had to be adapted to the real mirror suspension. This was compensated by bringing the capacitor plates closer to the mirror as simulated in [Ber18]. The magnitude is 69 nm V^{-1} and the longitudinal range is therefore comparable to the simulation of [Wit15] and [Ber18].

Summary

In this chapter an overview of the optical layout of the Single Arm Test was presented. The mirror suspension chain, the Single Arm Test cavity, the input optics, as well as the detection chain were discussed. The actuator transfer functions of the suspension chain were measured by stabilization of the laser frequency to the Single Arm Test cavity length. The ESD actuator range is very close to the simulated actuator range and fulfills the expectations. The PUM actuator provides a much larger range crossing with the ESD at about 10 Hz. The actuator range of the PUM is sufficient for experiments at AEI 10 m-Prototype. In section 4.2 a stabilization of the Single Arm Test to the laser frequency using the two suspension actuators is presented.

CHAPTER 4

Results

In the chapter 2 the description of the general experimental setup and the characterization of the noise limitations of the Suspension Platform Interferometer and the optical levers were presented. This chapter covers the stabilization of the AEI-SAS by using the signals from the optical sensors to apply feedback to them. In section 4.1.1 the Suspension Platform Interferometer provides the feedback for longitudinal stabilization of the two AEI-SAS relative to each other. In section 4.1.2 the stabilization of the angular displacement in r_x and r_z with the optical levers is presented. The noise suppression of the in-loop signals of the Suspension Platform Interferometer and the optical levers are compared to the optical out-of-loop sensors as well as to the inertial sensors of the AEI-SAS. In section 4.1.3 the suspension point motion of the Frequency Reference Cavity is analyzed by measuring its length fluctuations, while the feedback is altered between the optical sensors and the built-in inertial sensors of the AEI-SAS.

In the second section 4.2 the control of the Single Arm Test with the ESD and the PUM actuator is described and the length noise of the cavity is analyzed. The first described stabilization uses exclusively the new concept of an ESD actuator to stabilize the Single Arm Test cavity length to the laser frequency. This is only possible due to the active seismic pre-isolation with the optical sensors developed within this thesis. The low frequency motion is than handed over to the PUM actuator using it together with the ESD to stabilize the cavity length and extend the stabilization duration.

4.1 Feedback stabilization with optical sensors

Two measurements are performed for each degree of freedom, to characterize the feedback with the optical sensors. In the first, the AEI-SAS is not stabilized in the degree of freedom of interest while all other degrees of freedom remain stabilized. The Suspension Platform Interferometer and the optical levers are used to measure the displacement. This measurement is compared to the measurement of the Suspension Platform Interferometer and the optical lever's in-loop signals while they are applied to the AEI-SAS.

The Suspension Platform Interferometer employs two photodiodes at the readout port of the interferometer. One is used as an in-loop sensor and the other one is used as an out-of-loop sensor. To characterize the noise limitations of the optical levers an additional optical lever and an interferometric sensor of the Suspension Platform Interferometer are installed. They are used as out-of-loop sensors. In picture 4.1 the schematic overview of the setup is shown. The

interferometric reference sensor is set up to measure the differential angular displacement $r_{\mathrm{z,diff}}$ of the two AEI-SAS relative to each other. The interferometer beam and the retro-reflecting curved mirror are displaced by 50 cm from the y-axis. This offset leads to a length change of the interferometer arm when the two optical tables rotate around the z-axis differentially with $r_{\mathrm{z,diff}}$. The phase measurement of this interferometer is the superposition of

$$r_{\mathrm{z,diff}} = r_{\mathrm{z,central}} - r_{\mathrm{z,south}} \tag{4.1}$$

and

$$d_{\mathrm{y,diff}} = d_{\mathrm{y,central}} - d_{\mathrm{y,south}} \,. \tag{4.2}$$

By subtracting the out-of-loop measurement of the Suspension Platform Interferometer $d_{\mathrm{y,diff}}$ from the measurement of the interferometric reference sensor, the measurement of $r_{\mathrm{z,diff}}$ can be reconstructed. The subtraction is not as good as a fully decoupled sensors and leaves residual noise above 10 Hz. Together with the additional optical lever this allows an estimate of the residual rotational displacement. The in-loop signals of the Suspension Platform Interferometer and the optical levers are compared to the inertial sensors of the AEI-SAS as well as to the out-of-loop optical sensors.

4.1.1 Suspension Platform Interferometer

The interferometric sensing of the Suspension Platform Interferometer was discussed in chapter 2.1. The readout noise of the Suspension Platform Interferometer is typically below $20\,\mathrm{pm\,Hz^{-1/2}}$. To transfer this stability to the AEI-SAS at a frequency band from 10 mHz to 100 mHz a suppression of approximately 1×10^4 is required. The unity gain frequency of the Suspension Platform Interferometer stabilization is limited by the internal resonances of the AEI-SAS. When the phase delay at these resonances is generating positive feedback they get excited. They appear from 10 Hz on, limiting the unity gain frequency to 4 Hz.

Characterization

The Suspension Platform Interferometer is measuring the differential displacement of the two installed AEI-SAS units relative to each other. They are aligned along the y-axis of the global coordinate system. To characterize the feedback system two measurements are performed. The first measurement is taken while the y degree of freedom is not stabilized. All other degree of freedom are controlled either by the local sensors integrated into the AEI-SAS or the optical levers. This prevents cross coupling from the other degrees of freedom and the introduction of noise into the degree of freedom of interest. The same applies for the measurement with the optical levers.

In figure 4.2 the free running noise of $d_{\mathrm{y,diff}}$ is measured with the interferometer of the Suspension Platform Interferometer. The natural resonance frequency of the passive IP leg filter stage is at 0.13 Hz. The ground motion is amplified on the resonance frequency. A

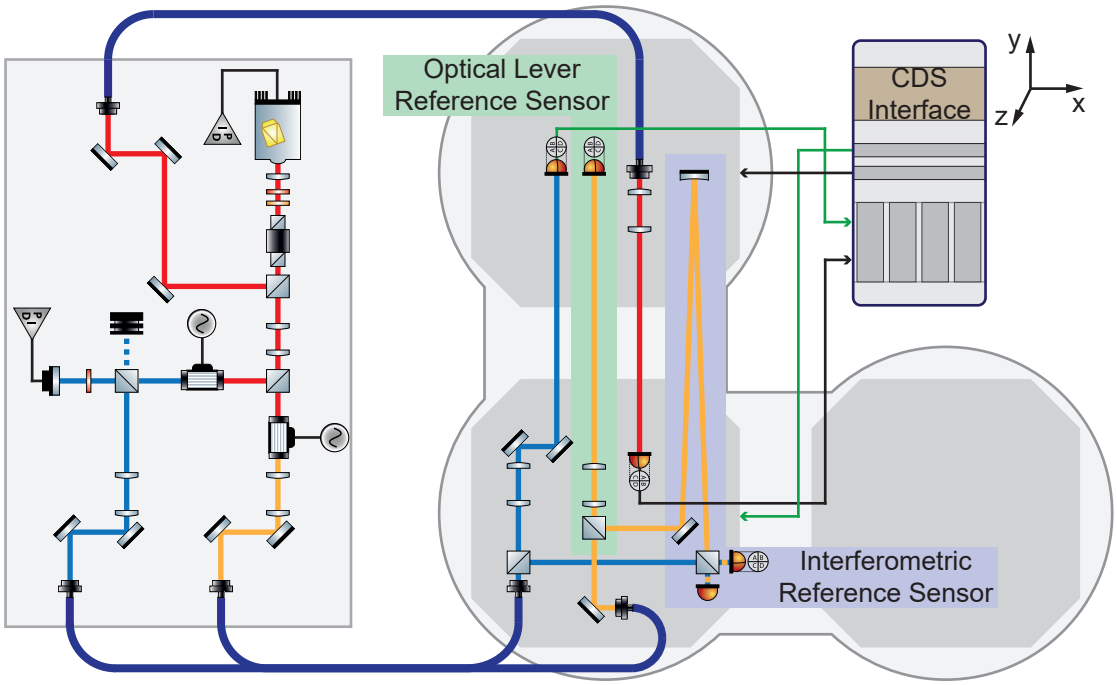

Figure 4.1: Schematic overview of the optical lever positions and the reference sensors. These reference sensor are used to analyze the performance of the stabilization with the optical lever. The optical levers are located as close as possible in the center of the optical tables. The interferometric sensor is deliberately displaced by 50 cm from the y-axis. When the two AEI-SAS differentially rotate the longitudinal displacement in the interferometric sensor is detecting this movement as a phase change.

detailed analysis of the passive isolation is presented in [Ber18]. The Suspension Platform Interferometer is not measuring the inertial motion of one optical table, but the differential motion of the two optical tables relative to each other. Below the fundamental resonance the differential motion is $0.4\,\mu m\,Hz^{-1/2}$ amplified to $3\,\mu m\,Hz^{-1/2}$ at a frequency of 0.13 Hz. The passive isolation system attenuates the ground motion to $30\,pm\,Hz^{-1/2}$ from 5 Hz to 10 Hz. Above 10 Hz the internal resonances of the AEI-SAS are dominating the motion and the readout noise of the Suspension Platform Interferometer starts contributing. The feedback signal from the Suspension Platform Interferometer is applied to the south AEI-SAS via the CDS. It is therefore forced to follow the central AEI-SAS and moving synchronized with it and creating one virtual platform. The unity gain frequency of this feedback system is 4 Hz. Phase loss is inducing positive feedback above the unity gain point, but the amplification is tolerable and allows a suppression of more than 1×10^3 at the micro-seismic peak at 200 mHz, while attenuating the signal at the internal resonances starting at 10 Hz. The displacement is reduced from $700\,nm\,Hz^{-1/2}$ to $300\,pm\,Hz^{-1/2}$ at 200 mHz. The targeted sensitivity of $100\,pm\,Hz^{-1/2}$ is surpassed for the full control bandwidth from below 10 mHz to 4 Hz except for the micro-seismic peak. A simultaneous measurement of the monolithic Reference Interferometer in gray is showing the expected readout noise. At 20 mHz the error signal is reaching the readout noise

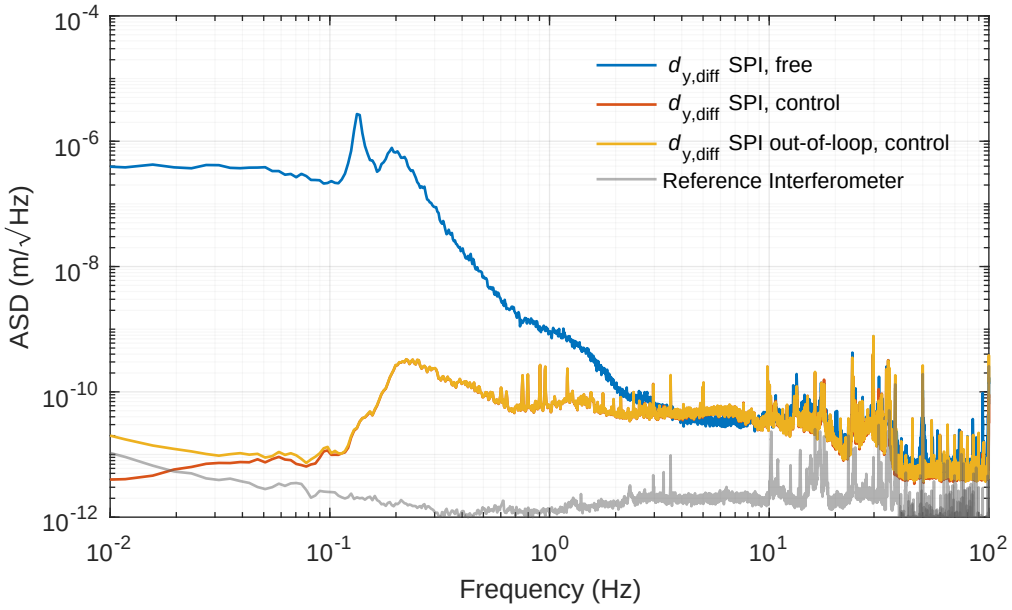

Figure 4.2: ASD for the differential longitudinal displacement along the y-axis measured by the Suspension Platform Interferometer. The solid blue line is a measurement of the Suspension Platform Interferometer, while the central AEI-SAS was actively stabilized by the accelerometers and the south AEI-SAS was uncontrolled and therefore only passively isolated. The solid red line is the in-loop measurement of the Suspension Platform Interferometer. It is hidden behind the yellow solid line, which depicts the the out-of-loop measurement of the Suspension Platform Interferometer performed with the second photodiode of the Mach–Zehnder interferometer. As a measure of the expected readout noise the Reference Interferometer located on the monolithic base plate is shown in gray. The displacement noise of the two optical tables relative to each other is suppressed, reducing it to 300 pm $\mathrm{Hz}^{-1/2}$ at the micro-seismic peak at 200 mHz. From 10 mHz to 100 mHz the motion is 10 pm $\mathrm{Hz}^{-1/2}$, reaching to the readout noise. To achieve the suppression of more than a factor of 1×10^4 amplification above the unity gain frequency is allowed. Due to the excitation of internal resonances of the passive isolation system the unity gain frequency is limited to 4 Hz.

measurement. The second photodiode of the south interferometer of the Suspension Platform Interferometer is shown in yellow and agrees with the error signal until the noise floor of the Suspension Platform Interferometer is reached. The readout noise of the Suspension Platform Interferometer is lower than anticipated and the feedback system is surpassing the expectations of 100 pm $\mathrm{Hz}^{-1/2}$ by even reaching 10 pm $\mathrm{Hz}^{-1/2}$ below 100 mHz.

4.1.2 Optical Lever

The centers of the two optical tables are stabilized to each other by 10 pm $\mathrm{Hz}^{-1/2}$ at 100 mHz. The suspension points of the Frequency Reference Cavity and the sub-SQL interferometer mirrors are located about a meter above the optical tables. A pitch rotation of the AEI-SAS by 1 µrad would result in a shift of 1 µm at the suspension point and therefore introduce longitu-

dinal displacement at the mirror. The rotation around the z-axis also introduces longitudinal displacement. The coupling of a displacement from the rotation around the z-axis r_z to the longitudinal displacement along the y-axis d_y depends on the position of the mirror on the optical table. If the beam axis and the mirror are aligned with the y-axis the rotation around r_z is causing a sideways shift. If the mirror is aligned with x-axis and the beam path is along the y-axis the shift translates to a longitudinal displacement. The sub-SQL interferometer and its beam path are aligned with the x- and y-axis and a coupling from r_z to d_y is negligible. The Frequency Reference Cavity in contrast is located at the corners of the optical tables as shown in 1.1. The rotation around the z-axis is shifting the mirror in longitudinal and sideways displacement equally. The longitudinal suspension point motion below the fundamental resonances of the Frequency Reference Cavity is directly transferred to the laser frequency.

With the optical levers, sensors with a broadband sensitivity improving the stability over a frequency range from 10 mHz to 10 Hz are available. The noise analysis was performed in section 2.2.2. The readout sensitivity is limited by electronic noise and the coupling of the transverse degrees of freedom. Theses two noise sources will be included in the following figures. In section 2.2 the optical layout and the noise sources are presented. With the use of a second optical lever the noise characteristics of the optical lever can be further analyzed. For the third AEI-SAS, an optical lever beam is already available. While the AEI-SAS is not installed, this beam is used as an out-of-loop sensor. The same is done with the west interferometer of the Suspension Platform Interferometer. With steering mirrors, the west arm is guided towards the south table, reflected at the curved mirror and interfere with the second reference arm. This interferometric reference sensor is shifted by 0.5 m from the y-axis to measure $r_{z,\mathrm{diff}}$. The raw signal is corrected by subtracting the measurement of $d_{y,\mathrm{diff}}$. In the schematic overview in figure 4.1 the setup is displayed. In section 4.1.2 the comparison of measurements with the optical lever signals is shown, while the AEI-SAS is uncontrolled and while it is stabilized with the optical lever signals. Afterwards the analysis with the reference sensors is carried out and the achievable stability is analyzed.

Characterization

In figure 4.3 the controlled and uncontrolled displacement in r_x for the central and south AEI-SAS measured by the optical lever is shown. The passive isolation measured by the two optical levers is shown as a dark blue line for the central and as a orange line for the south AEI-SAS. The resonances frequencies of the passive isolation GAS filter stage are at 0.37 Hz for r_x. The microseismic peak is between 100 mHz to 200 mHz. The passive isolation attenuates the ground motion above the resonance frequency to 1 nrad $\mathrm{Hz}^{-1/2}$ at 1 Hz and below 100 prad $\mathrm{Hz}^{-1/2}$ above 5 Hz. Above 10 Hz the internal resonances of the AEI-SAS are showing up. The phase loss of the active stabilization is introducing positive feedback at these frequencies while the unity gain frequency surpasses 3 Hz to 5 Hz. The sensitivity of the optical lever would allow a higher bandwidth. The suppressed motion is shown in blue and yellow.

Figure 4.4 shows the measurement for the central optical table in blue compared to the out-of-loop sensors. As explained in figure 4.1 a second optical lever is installed and shown as

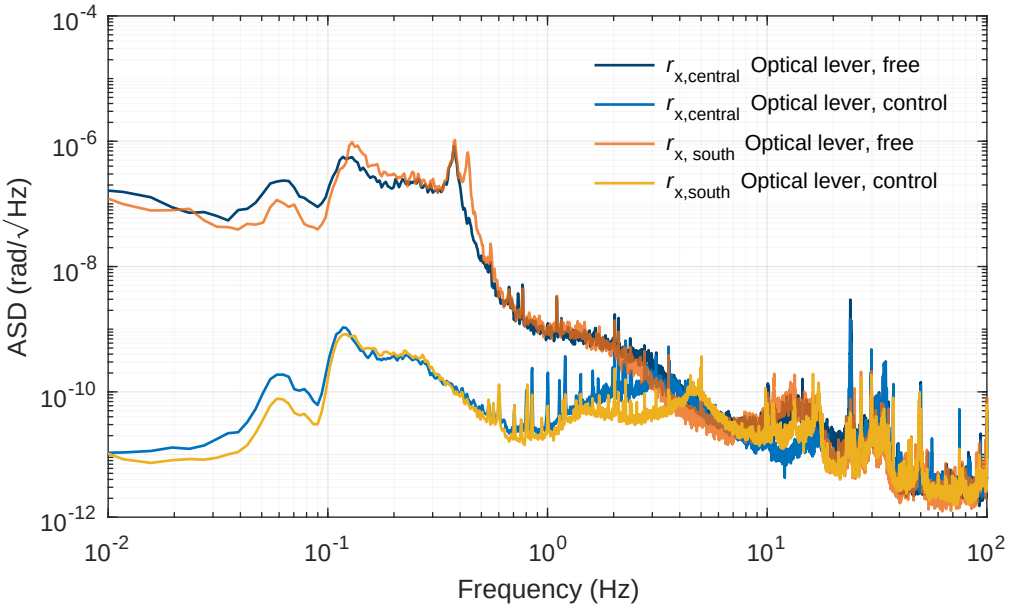

Figure 4.3: ASD of the displacement in r_x for the south and central AEI-SAS. In dark blue the measurement of the optical lever is shown, while r_x of the central AEI-SAS was not stabilized and in orange the optical lever measurement for the south AEI-SAS. In blue and yellow lines, the according measurements, while the optical levers were used as in-loop sensors. The unity gain frequency is at 3 Hz and 3.5 Hz. If the unity gain frequency would be higher, the internal resonances of the AEI-SAS get amplified. At 1 Hz the error signal is suppressed to 20 prad $\mathrm{Hz}^{-1/2}$. At the micro-seismic peak at 120 mHz it is suppressed by a factor of 1×10^3 to 1 nrad $\mathrm{Hz}^{-1/2}$.

a green line. The vertical inertial sensors of the AEI-SAS are geophones and they are shown as a red line. The three measurements agree down to 1 Hz and start to deviate below. The electronic noise in dark gray is giving the expected lower limit of the optical lever sensitivity. The out-of-loop optical lever deviates from the in-loop signal, caused by the sensor noise adding up to the noise of the transversal degrees of freedom. The geophone is limited by its own sensor noise below 0.5 Hz, though measuring a signal at the micro seismic peak [Kir17]. The reference optical lever is not confirming this. The possible introduction of noise through the transversal degree of freedom could be one reason. The measurement of the residual differential motion of d_z is also measured by geophones and projected to the optical lever readout shown in light gray. Since the geophone noise dominates the measurement the projection can only provide an upper limit. The measurement of the geophones in r_x is limited by the residual motion from the other degrees of freedom measured by the same geophones and not real motion of r_x. For the r_z degree of freedom an interferometric sensor is available which supports this interpretation. Below 100 mHz the reference optical lever shows that the electronic noise is not the limitation. The coupling of the transversal degrees of freedom can not be analyzed below 100 mHz due to the sensor noise of the geophones. The cause of the limited sensitivity of the optical lever can therefore not entirely be analyzed. Thermal drifts of the mounts together with the residual

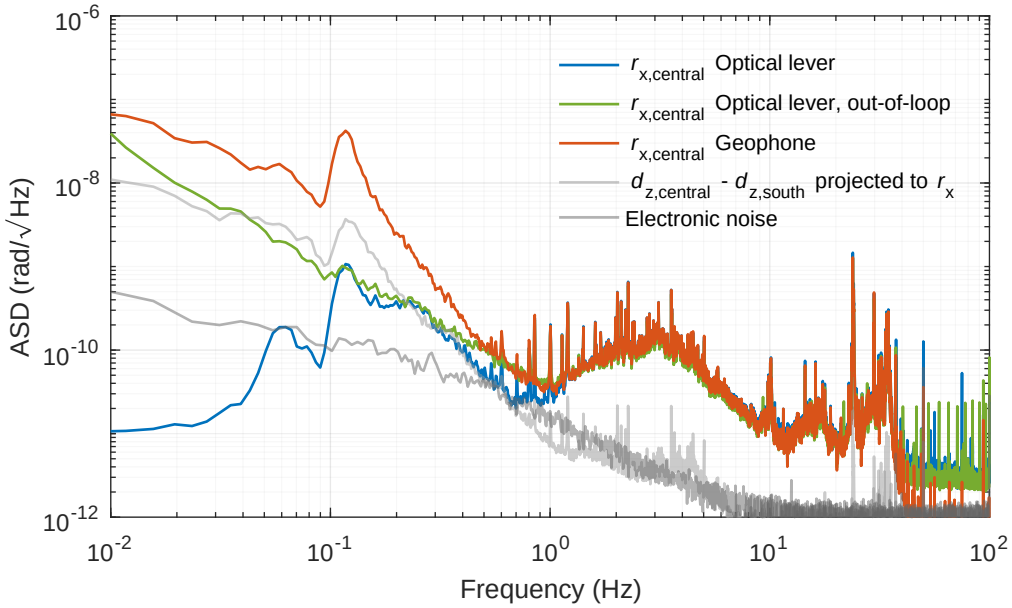

Figure 4.4: Measurement of the angular displacement ASD measured by the in-loop optical lever in blue and the out-of-loop sensors. The electronic noise of the optical lever is show in dark gray. The measurement in light gray is showing the projection of the differential motion of d_z of the two AEI-SAS to r_x. The out-of-loop measurement of the optical lever is shown in green. In red the measurement of the geophones is shown. They agree with the out-of-loop measurement of the optical lever down to 500 mHz. Below, the geophone is deviating from the out-of-loop optical lever due to its sensor noise. The geophone signal is calculated from three sensors measuring all three vertical degrees of freedom. The noise at the micro-seismic peak is likely caused from residuals of the calculation of the degree of freedom. The out-of-loop optical lever is confirming a stability of 1 nrad $\mathrm{Hz}^{-1/2}$ at 100 mHz and 40 prad $\mathrm{Hz}^{-1/2}$ at 1 Hz. Below 100 mHz the out-of-loop optical lever is deviating from the in-loop measurement giving the achievable stability of 30 nrad $\mathrm{Hz}^{-1/2}$ at 10 mHz.

motion of d_z are likely.

For the r_x degree of freedom the same measurements were performed as for r_z. In figure 4.5 the measurement for the central table is shown in dark blue and for the south table in orange. The passive isolation for the horizontal degrees of freedom is provided by IP legs. They can be tuned to lower frequencies than the vertical isolation stage and the resonance frequency for r_z is 0.13 Hz. The ground motion is attenuated by the AEI-SAS to 100 prad $\mathrm{Hz}^{-1/2}$ at 1 Hz. Again, the internal resonances of the AEI-SAS are the limitation to the unity gain frequency. The horizontal passive isolation filter stage is located before the vertical filter stage. After the vertical filter stage vacuum compatible rubber pads are used to suppress the horizontal compliance of the GAS filters. The rubber pads introduce another horizontal isolation stage with a well damped resonance at 9 Hz [Ber18]. For control of the horizontal degree of freedom, this stage must be compensated when having the unity gain frequency close to it. The achieved feedback control with the optical lever as error signals is shown in figure 4.5. The blue line is

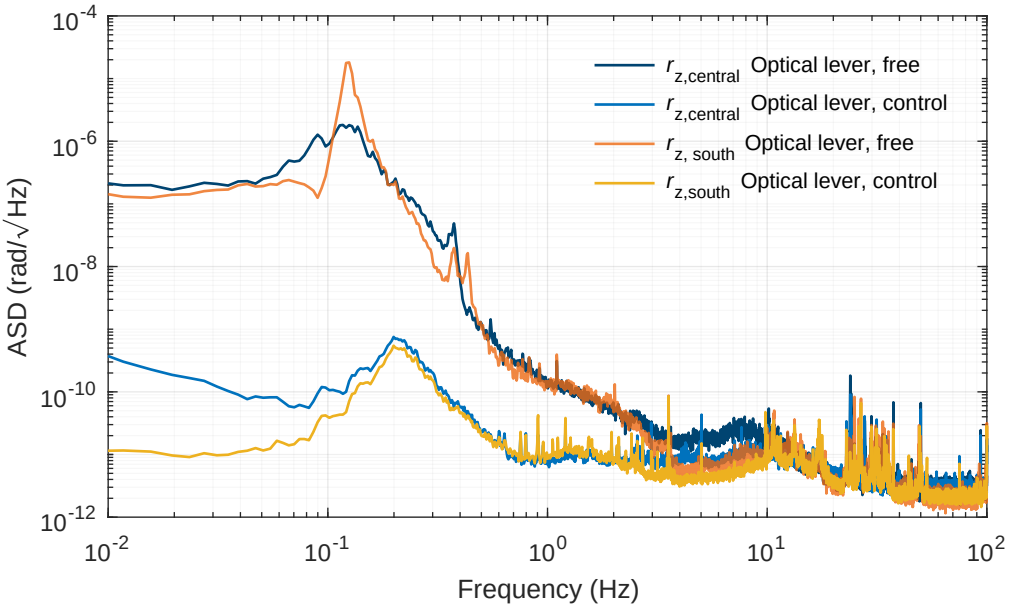

Figure 4.5: Angular displacement ASD measurement of the optical levers in r_z. In the dark blue line the central table was passively isolated without active feedback applied. In orange the same measurement for the south table was done. In blue the suppressed in-loop signal of the optical lever for the control of the central AEI-SAS and in yellow for the south AEI-SAS are shown. The unity gain frequency is at 5 Hz giving a suppression of a factor of up to 1×10^4 at 100 mHz.

for the stabilization of the central AEI-SAS and in yellow for the south AEI-SAS.

In figure 4.6 the blue line shows the in-loop signal of the central AEI-SAS control with the optical lever. In green the out-of-loop optical lever and in purple the interferometric reference sensor. The in-loop signal is suppressed below the electronic noise from 0.4 Hz to 1.3 Hz. The two reference sensors therefore deviate from the in-loop signal giving the real motion of the AEI-SAS. The interferometric sensor is not measuring the inertial motion of the central or the south table, but the differential motion. To reconstruct this, it was corrected by subtracting $d_{y,diff}$ from the measurement. Above 10 Hz residual noise is left, contaminating the $r_{z,diff}$ measurement. The reference optical lever together with the reference interferometric sensor prove the expected noise performance of the optical lever down to 100 mHz. Below 100 mHz the same behavior as for r_x is observed. Thermal drifts or motion from the transversal degrees of freedom are causing this behavior. The inertial sensors for horizontal motion, the accelerometers, are dominated by their sensing noise. They are located in a filter stage before the vertical isolation. Above 5 Hz, they are dominated by the internal resonances of this stage. They are attenuated by the GAS filters. When the AEI-SAS is controlled by the optical levers the accelerometers are not sensitive enough and cannot be used as reference sensors. Also the accelerometers show a signal at the micro seismic peak. Since both optical out-of-loop sensors do not confirm these, it is caused by the other degrees of freedom coupling to the calculated r_z.

The optical lever provides an improvement of over 1×10^3 at 100 mHz for r_z reducing it

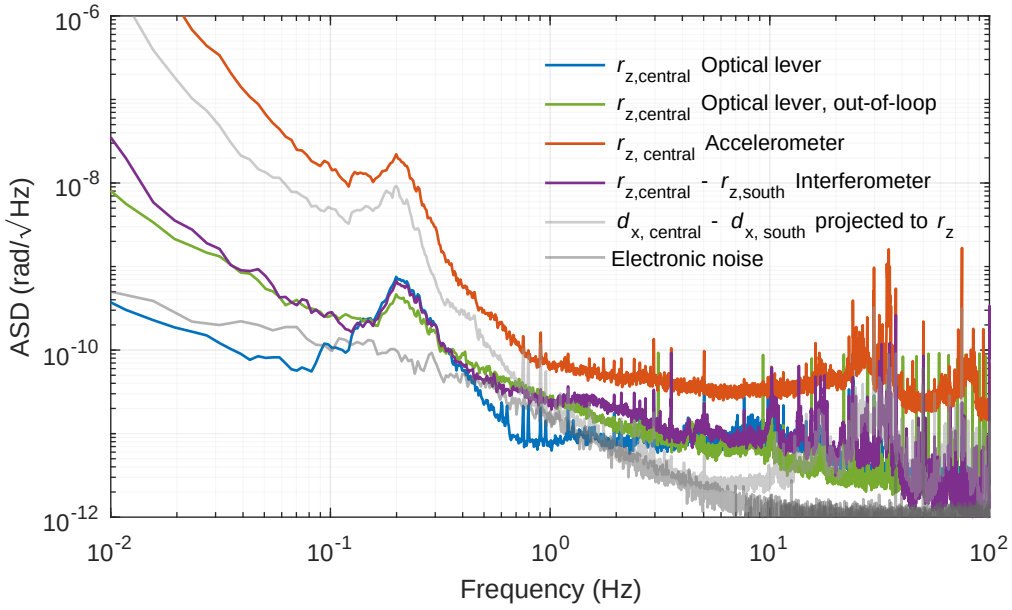

Figure 4.6: Angular displacement ASD of r_z of the central table. In blue, the measurement of the in-loop optical lever as shown before in 4.5 is shown. In green the out-of-loop measurement of the reference optical lever and in purple the measurement of the interferometric reference sensor. The interferometric reference sensor is measuring the differential r_z motion of the two AEI-SAS. They agree up to 10 Hz, with only minor deviations due to the difference of the measurement concept. The out-of-loop optical lever hits its QPD displaced from the center and the calibration is deviating from the in-loop sensor, as it can be seen at the micro-seismic peak at 200 mHz. The accelerometer in red is not sensitive enough to be used as an out-of-loop sensor.

to 300 prad $\mathrm{Hz}^{-1/2}$. The unity gain frequency is at approximately 5 Hz. The optical levers are improving the stability of the r_x and r_z over the full control bandwidth. The motion is suppressed to 10 nrad $\mathrm{Hz}^{-1/2}$ at 10 mHz and to 30 prad $\mathrm{Hz}^{-1/2}$ at 1 Hz. The optical layout of the optical levers is kept simple providing a high flexibility of the beam path. They can therefore be retrofitted easily.

4.1.3 Suspension point motion of the suspended cavities

In section 2.2 the coupling from r_x and r_z to the suspension point of a suspended mirror was explained. Together with the differential longitudinal displacement d_y they displace the suspension point and therefore the mirrors. In this section the stabilization with the Suspension Platform Interferometer and the optical levers are compared to the control of the built-in AEI-SAS sensors by measuring the length fluctuation of the Frequency Reference Cavity. The Frequency Reference Cavity is located at the corners of the optical tables and is shown in 1.1 with the suspension point 870 mm above the optical table [Wes16]. By measuring the length stability of the Frequency Reference Cavity the angular displacement through r_x and r_z is converted to longitudinal displacement of the mirrors. The Frequency Reference Cavity is

transferring its length stability to the laser frequency. The Mode Cleaner Cavity is used as an out-of-loop sensor for the frequency noise and therefore for the cavity length. Figure 4.7 shows the measurement of the Frequency Reference Cavity length by the Mode Cleaner Cavity in four different control states of the active pre-isolation. In the red line the measurement of the cavity length is shown while the rotation around the x-axis r_{x} of both AEI-SAS was stabilized by the geophones. r_{z} is controlled by the optical levers and $d_{\mathrm{y,diff}}$ is controlled by the Suspension Platform Interferometer. For the measurement shown in the yellow line, the r_{x} degree of freedom was controlled by the optical levers and r_{z} was controlled by the accelerometers. For the measurement of the cavity length in the green line the two optical lever controlled r_{x} and r_{z} and the stabilization of d_{y} was controlled by the accelerometers. The optical levers are inertial sensors for each AEI-SAS. The Suspension Platform Interferometer in contrast is a sensor for the differential motion of the two AEI-SAS. The feedback of the Suspension Platform Interferometer is applied to the south AEI-SAS forcing it to follow the central AEI-SAS. The blue line represents a measurement of the Frequency Reference Cavity length displacement, while the Suspension Platform Interferometer and the optical levers are controlling $d_{\mathrm{y,diff}}$, r_{x} and r_{z}. At 200 mHz the suspension point motion is suppressed to 1 nm $\mathrm{Hz}^{-1/2}$. The Suspension Platform Interferometer suppresses the motion by a factor of 1×10^3. If the optical levers were not installed the length stability of the Frequency Reference Cavity would be dominated by the coupling of the r_{x} and r_{z} to the suspension point motion. This is demonstrated by the measurements in the red and yellow line.

The longitudinal Frequency Reference Cavity displacement is shown in figure 4.8 compared to the measurements of the out-of-loop sensors for the Suspension Platform Interferometer and the optical lever at the central AEI-SAS. The motion of the angular displacement of r_{z} is lower than the motion of the other two degrees of freedom over the full control bandwidth ranging from 0.01 Hz to 4 Hz. The coupling to the longitudinal degree of freedom of the Frequency Reference Cavity is lower than for the other two degrees of freedom and it can be neglected. Below 200 mHz the coupling from r_{x} dominates the longitudinal displacement of the Frequency Reference Cavity. The height of the suspension is 870 mm and the displacement of the suspension point is $l_{\mathrm{sus}} \cdot r_{\mathrm{x}}$ [Wes16]. Above 200 mHz the residual $d_{\mathrm{y,diff}}$ motion is the dominant contribution to the displacement of the cavity length. The resonance of the Frequency Reference Cavity suspensions are amplifying the residual motion by a factor of 5×10^2 at 0.66 Hz.

The seismic pre-isolation of the AEI-SAS is enhanced by the use of optical sensors to control the longitudinal displacement of the two optical tables relative to each other $d_{\mathrm{y,diff}}$ and the angular displacement of the central and south AEI-SAS r_{x} and r_{z}. The interferometric readout of the differential motion of the two AEI-SAS relative to each other by the Suspension Platform Interferometer allows to sense and stabilize the differential motion down to 20 pm $\mathrm{Hz}^{-1/2}$ at 10 mHz. The optical levers are stabilizing the r_{x} and r_{z} of the two AEI-SAS. They allow a stabilization of 30 prad $\mathrm{Hz}^{-1/2}$ at a frequency of 1 Hz in both degrees of freedom and 300 prad $\mathrm{Hz}^{-1/2}$ at a frequency of 100 mHz for r_{z} and 1 nrad $\mathrm{Hz}^{-1/2}$ in r_{x} and at a frequency of 10 mHz 10 nrad $\mathrm{Hz}^{-1/2}$ for r_{z} and 40 nrad $\mathrm{Hz}^{-1/2}$ in r_{z}.

The suspension point motion of the Frequency Reference Cavity can be suppressed by a

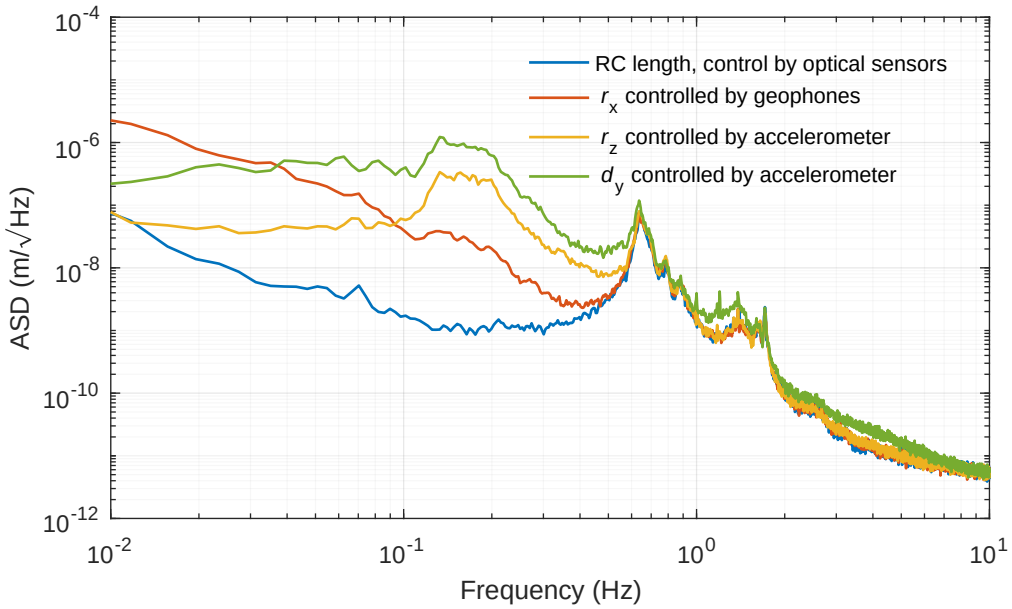

Figure 4.7: Longitudinal displacement ASD of the Frequency Reference Cavity length. The sensors for the feedback to the AEI-SAS units were altered between the optical sensors and the built-in AEI-SAS sensors, to analyzed the effect on the suspension point motion of the mirror suspensions, and in particular of the Frequency Reference Cavity. The blue line shows the suspension point motion of the Frequency Reference Cavity transferred to the longitudinal displacement of the cavity, while the Suspension Platform Interferometer is controlling $d_{y,diff}$ and the optical lever are controlling r_x and r_z at both AEI-SAS. In red the geophone signals were used as error signals for r_x. In yellow the accelerometers were used to stabilize r_z. In green the Suspension Platform Interferometer control of $d_{y,diff}$ was substituted with the local control of the accelerometers at the south table. Below 0.66 Hz the mirror is not isolated by the suspension and follows the displacement of the suspension point. By using the optical sensor the suspension point motion of the Frequency Reference Cavity is reduced to 1 nm $Hz^{-1/2}$ at 120 mHz and to 80 nrad $Hz^{-1/2}$ 10 mHz. The longitudinal stabilization of the Suspension Platform Interferometer is reducing the suspension point motion by a factor of 1×10^3 at 120 mHz. Without the optical lever feedback the stability of the Suspension Platform Interferometer would have been masked by the coupling of r_x and r_z to the longitudinal degree of freedom of the Frequency Reference Cavity. The Frequency Reference Cavity length stability is lower than the out-of-loop readout above 3 Hz.

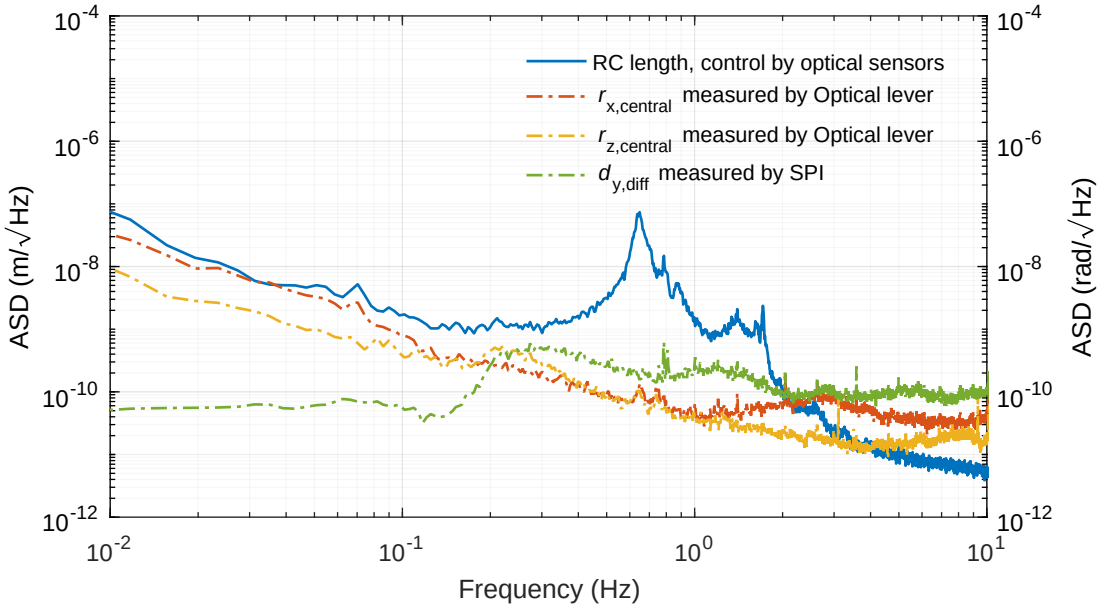

Figure 4.8: Measurement of the longitudinal displacement ASD of the Frequency Reference Cavity length and the residual motion of the AEI-SAS measured by the out-of-loop optical sensors. In blue the measurement of the Frequency Reference Cavity longitudinal displacement measured with the Mode Cleaner Cavity. The r_z motion in the yellow line is lower than r_x and d_y and the coupling to the longitudinal degree of freedom is weaker. The r_x rotational displacement is displacing the suspension point longitudinal with $l_{sus} \cdot r_x$. The Frequency Reference Cavity suspension point is 870 mm above the table top [Wes16]. The r_x is dominating the Frequency Reference Cavity length noise below 200 mHz. Above that, the differential motion of d_y is dominating the suspension point motion.

factor of 1×10^3 at 120 mHz and a factor of 30 at 10 mHz compared to the stabilization with the built-in sensors of the AEI-SAS.

4.2 Single Arm Test

The optical setup and installation of the Single Arm Test was shown in section 3 and the transfer functions of the coil/magnet actuators at the PUM and the ESD mirror were measured. The actuators at the suspensions are required to operate the sub-SQL interferometer and control its degrees of freedom. From the transfer functions of the suspension coil/magnet actuators at the PUM and the ESD at the mirror in figure 3.11 together with the results of the active control of the degrees of freedom of the AEI-SAS in figure 4.2, figure 4.4 and figure 4.6, implies already the feasibility. In this section, the stabilization of the Single Arm Test cavity length to the laser frequency is demonstrated. The length noise of the cavity as well as the suppressed readout signal of the Single Arm Test cavity are presented and the length noise is analyzed.

The error signal generation required to stabilize the cavity, is described in section 3.3. The

photodiode signal measured in reflection of the cavity is frequency mixed with the local oscillator signal and digitized by the CDS. Digital controllers are designed, the feedback signal calculated and converted to a voltage by the CDS. The voltage is converted to a current for the coil/magnet actuators and amplified by a HV amplifier for the ESD by dedicated electronic circuits.

The calculated feedback signal is weighted by the measured actuator transfer function to obtain the feedback signal. The seismic pre-isolation is creating a quiet environment, where already the range of the ESD is sufficient to hold the cavity stabilized for hours. The PUM actuator is extending the duration and reducing the action force at the ESD.

To stabilize the Single Arm Test cavity to the laser frequency a lock acquisition procedure was developed and is implemented by the used of the CDS. This is explained in the next section.

4.2.1 Automated stabilization of Single Arm Test cavity

A photodiode is measuring the transmitted power of the cavity. The signal is also digitized and available in the CDS. The stabilization is automatically started when the power on the photodiode exceeds a reference value. When the cavity feedback exceeds the actuator range the resonance condition is not fulfilled anymore and the stabilization turns off. The Single Arm Test is setup in a seismically isolated environment, with a well stabilized laser frequency leading to long times between the fulfillment of the resonance condition. A ramp signal is applied to the PUM actuator to speed up the time until a next resonance condition is found and the stabilization request is started. As soon as the resonance condition is found the ramp signal stops. When the transmitted power exceeds a reference value and the error signal is crossing zero the lock request is fulfilled. The error signal is applied to the digital filters of the ESD. When the lock request was successful and the error signal Root Mean Square (RMS) is below a threshold additional integrators are applied. This automated switching of filters is preventing the feedback signal from saturation due to transients. It allows an operation of the cavity without manual intervention.

4.2.2 ESD feedback

For the measurement in figure 4.9 the Single Arm Test cavity was stabilized to the laser frequency. The error signal is shown in blue and the feedback signal of the ESD is shown in red. The feedback signal sent to the ESD is weighted by the transfer function measured in 3.11 to calculate the longitudinal displacement of the Single Arm Test cavity. The laser frequency was stabilized to the Frequency Reference Cavity. The Mode Cleaner Cavity is measuring the remaining frequency noise as an out-of-loop sensor and is shown in yellow. The Frequency Reference Cavity is imprinting its fundamental resonance frequency at 0.66 Hz onto the laser frequency. Both the Mode Cleaner Cavity and Single Arm Test cavity feedback are forced to follow these frequency fluctuations and measure it. The Single Arm Test cavity length noise agrees with the Mode Cleaner Cavity from 0.1 Hz to 1 Hz.

The fundamental frequency of the Single Arm Test mirror suspensions is at 0.74 Hz. The suspension resonances are naturally providing gain at the longitudinal resonance frequencies as

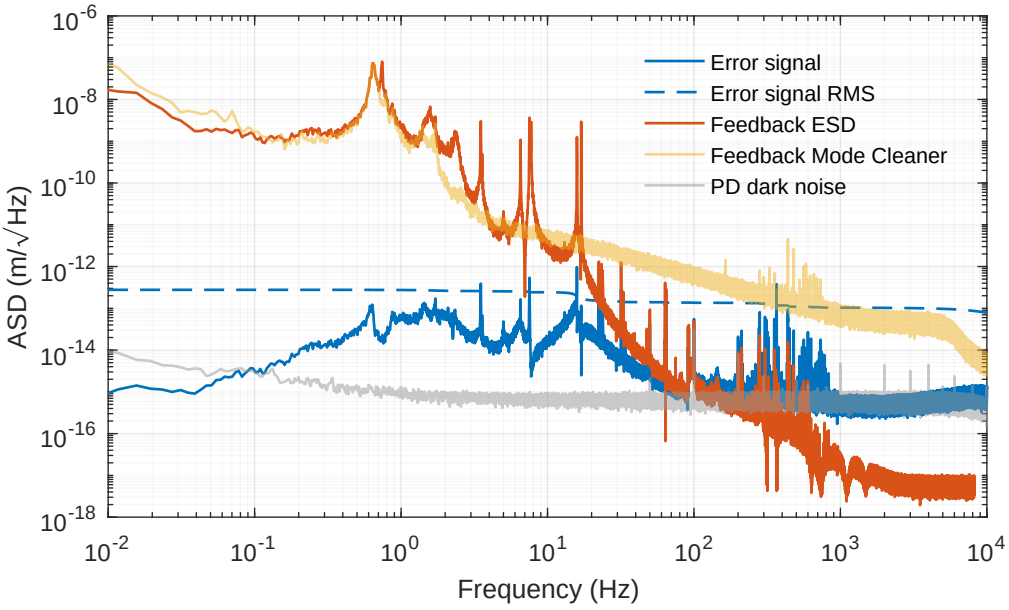

Figure 4.9: Measurement of the displacement ASD of the error and feedback signal of the Single Arm Test cavity. The laser frequency was stabilized to the Frequency Reference Cavity. In yellow the feedback signal of the Mode Cleaner Cavity is shown. It is following the frequency fluctuations of the laser light. Above 3 Hz the frequency noise is below the readout noise. The Single Arm Test cavity feedback signal, in red, agrees with the Mode Cleaner Cavity signal at frequencies from 0.1 Hz to 1 Hz. From 0.74 Hz to 17 Hz the resonance of the Single Arm Test suspensions are dominating the length fluctuations of the cavity. Electronic readout noise in gray is dominating the measurement above the unity gain frequency at 117 Hz. The error signal RMS in the dashed blue line is suppressed to 0.3 pm.

shown by the ESD transfer function. They are well suppressed in the error signal. The resonance peaks in the ESD feedback are introduced by the transfer function. At 3.5 Hz the yaw resonance and at 6.5 Hz, 7.5 Hz, 15.9 Hz and 17 Hz the pitch resonances of the two suspension chains are coupling the the longitudinal readout of the cavity. Above the unity gain frequency of 117 Hz, the error signal is limited by the electronic noise of the readout, shown in gray. Between 200 Hz and 1 kHz peaks are dominating the readout. In the measurement of the Mode Cleaner Cavity peaks from 280 Hz to 700 Hz are visible. They are introduced by the frequency stabilization. Violin modes of the suspension wires of the Single Arm Test suspensions have been identified and their excitation is prevented by notch filters at 312 Hz, 316 Hz, 367 Hz, 634 Hz, 734 Hz, 746 Hz, 1101 Hz, 1116 Hz and 1491 Hz. The lowest two resonances are associated with the violin mode of the suspension wires connecting the PUM with the mirror. The monolithic suspension is designed to have the first violin mode at approximately 1 kHz shifting it outside of the measurement band of the sub-SQL interferometer. The error signal RMS shown in the dashed blue line is suppressed to 0.3 pm.

4.2.3 Penultimate Mass crossover

The ESD actuator has a maximum range of 0.7 µm. To extend the range, the coil/magnet actuators at the PUM are used to stabilize the Single Arm Test cavity below 50 mHz. In figure 4.10 the ASD measurement of the feedback to the suspension actuators is shown. In the blue line the feedback to the ESD is shown. In this measurement the ESD was used as the only actuator to stabilize the Single Arm Test cavity length. In the red line the ESD is shown, this time the feedback to the suspension was distributed to the ESD and the PUM. In yellow line the feedback actuation of the PUM is shown. The cross over frequency was chosen to be at 50 mHz, well below the suspension resonances. To prevent excitation of the pitch resonances the PUM feedback is attenuated above 3 Hz. The feedback of the PUM keeps the ESD at its operating point.

The Single Arm Test demonstrates the feasibility of stabilizing a suspended cavity with the new concept for an ESD. The actuator allows at least a unity gain frequency of up to 117 Hz. The error signal RMS is suppressed below 0.3 pm. The suspension concept and the actuator sizing can be applied for the sub-SQL interferometer.

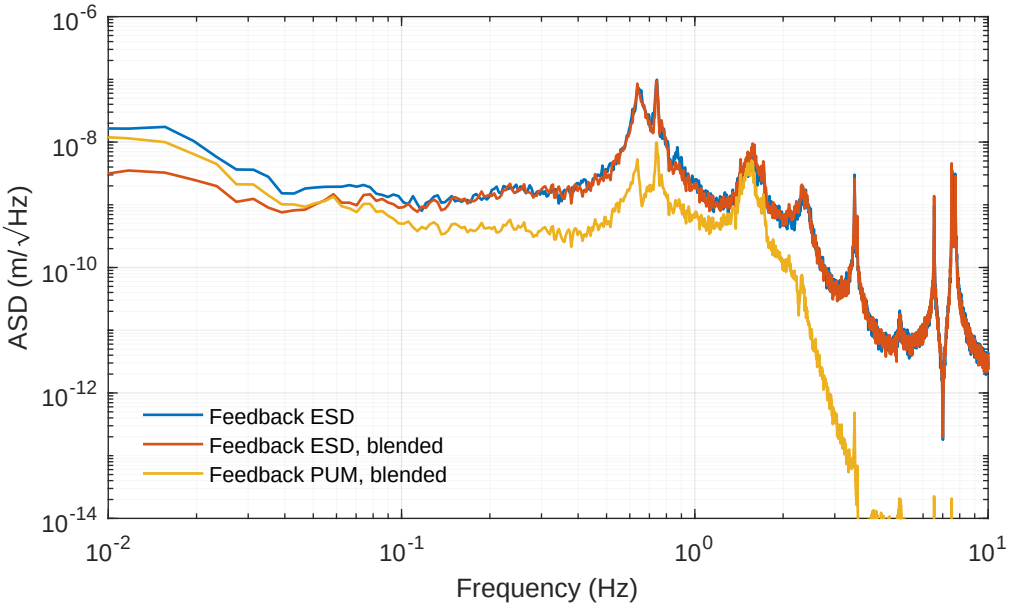

Figure 4.10: ASD of the suspension actuator feedback. In the blue line the feedback signal of the ESD is shown. It is stabilizing the Single Arm Test cavity length to the laser frequency. In the red line the feedback to the ESD is shown, while the cavity length is stabilized by the ESD and the actuators at the PUM. The feedback to the PUM is shown in the yellow line. The cross over frequency is at 50 mHz.

CHAPTER 5

Summary

This thesis addressed the length stabilization at the AEI 10 m-Prototype. Active pre-isolation of the AEI-SAS with optical sensors creates one stable virtual platform. The first experiment built on this platform is the Single Arm Test, proving key technologies for the sub-SQL interferometer.

Optical sensors to stabilize the differential longitudinal motion of two optical tables relative to each other and the inertial motion in the angular displacement around the x- and the z-axis were installed. The Suspension Platform Interferometer consist of heterodyne Mach-Zehnder interferometers, sensing the differential longitudinal displacement of the optical tables. An Optical Path-length Difference Stabilization was implemented improving the readout noise sensitivity of the Suspension Platform Interferometer by a factor of 1×10^3 resulting in $5\,\mathrm{pm\,Hz^{-1/2}}$ at 100 mHz. The stability of the readout is transfered to the two optical tables by active feedback control. The stabilization of the longitudinal differential motion was characterized and is even surpassing the presumed stability reaching $10\,\mathrm{pm\,Hz^{-1/2}}$ below 100 mHz. Hardware modification turned the Suspension Platform Interferometer from a proof of concept experiment into a fully operational sub-system of the sub-SQL interferometer.

Optical levers to sense the angular degrees of freedom of the optical tables inertially were developed and implemented into the feedback control system. Additionally one optical lever and one interferometer served as out-of-loop sensors to monitor the performance and confirm the improved stability.

Stabilizing the optical tables with the Suspension Platform Interferometer and the optical levers suppresses the ground motion. The stability is transfered to all experiments and sub-systems of the AEI 10 m-Prototype. The suspension point motion of the Frequency Reference Cavity was analyzed by measuring its length noise. Altering the optical sensors with the built-in sensors of the AEI-SAS, showed a length noise suppression by a factor of 1×10^3 at 120 mHz down to $1\,\mathrm{nm\,Hz^{-1/2}}$.

The Single Arm Test is a preliminary experiment, to prepare the AEI 10 m-Prototype for the sub-SQL interferometer. Two SQL mirror suspensions were set up with pilot optics and installed in the AEI 10 m-Prototype to characterize the mirror suspensions and its actuation. Two mirror suspensions were set up to form a linear Fabry-Perot cavity with a length of 10.8 m. The mirror is positioned by two types of actuators. Coil/magnet pairs at the Penultimate Mass (PUM) stabilize the low frequency motion. At high frequencies the cavity length is actuated by a new concept for an Electro Static Drive (ESD). Stabilizing the laser frequency of the 35 W Laser system to the Single Arm Test cavity length allowed to characterized the actuators. The

cavity length of the Single Arm Test is stabilized to the laser frequency by using the ESD and the PUM actuator. Due to feedback control provided by the PUM, the ESD can be operated at its optimum operation point and therefore the dynamic range of the ESD is preserved. A control bandwidth of 117 Hz was achieved.

The improved active seismic pre-isolation with the optical sensors even enables stabilizing the Single Arm Test cavity exclusively with the ESD.

The successful installation and operation of the Single Arm Test cavity could verify the feasibility of the stabilization concept between cavity length and laser frequency for the sub-SQL interferometer.

Bibliography

[Aas15] AASI, J. et al.: 'Advanced LIGO'. *Classical and Quantum Gravity* (Mar. 2015), vol. 32(7): p. 074001 (cit. on p. 1).

[Abb16] ABBOTT, B. P. et al.: 'Observation of Gravitational Waves from a Binary Black Hole Merger'. *Physical Review Letters* (Feb. 2016), vol. 116(6) (cit. on p. 1).

[Aff14] AFFELDT, C. et al.: 'Advanced techniques in GEO 600'. *Classical and Quantum Gravity* (Nov. 2014), vol. 31(22): p. 224002 (cit. on pp. 2, 35).

[Ama17] AMARO-SEOANE, P. et al.: 'Laser Interferometer Space Antenna'. (Feb. 2, 2017), vol. (cit. on p. 1).

[Arm16] ARMANO, M. et al.: 'Sub-Femto-*g* Free Fall for Space-Based Gravitational Wave Observatories: LISA Pathfinder Results'. *Physical Review Letters* (June 2016), vol. 116(23) (cit. on p. 1).

[Ast12] ASTON, S. M. et al.: 'Update on quadruple suspension design for Advanced LIGO'. *Classical and Quantum Gravity* (Oct. 2012), vol. 29(23): p. 235004 (cit. on p. 8).

[Aud14] AUDLEY, H. E.: 'Preparing for LISA pathfinder operations: characterisation of the optical metrology system'. PhD thesis. Leibniz Universität Hannover, 2014 (cit. on pp. 14, 18).

[Bar02] BARR, B. W. et al.: 'Silica research in Glasgow'. *Classical and Quantum Gravity* (Mar. 2002), vol. 19(7): pp. 1655–1662 (cit. on p. 1).

[Ber17] BERGMANN, G. et al.: 'Passive-performance, analysis, and upgrades of a 1-ton seismic attenuation system'. *Classical and Quantum Gravity* (Feb. 2017), vol. 34(6): p. 065002 (cit. on p. 13).

[Ber18] BERGMANN, G.: 'Improving the seismic isolation for the AEI 10m prototype'. PhD thesis. Leibniz Universität Hannover, 2018 (cit. on pp. 5, 13, 29, 53, 57, 61).

[Ber06a] BERTOLINI, A., R. DESALVO, F. FIDECARO, M. FRANCESCONI, S. MARKA, V. SANNIBALE, D. SIMONETTI, A. TAKAMORI, and H. TARIQ: 'Mechanical design of a single-axis monolithic accelerometer for advanced seismic attenuation systems'. *Nuclear Instruments and Methods in Physics Research Section A: Accelerators, Spectrometers, Detectors and Associated Equipment* (Jan. 2006), vol. 556(2): pp. 616–623 (cit. on p. 5).

[Ber06b] BERTOLINI, A., R. DESALVO, F. FIDECARO, M. FRANCESCONI, S. MARKA, V. SANNIBALE, D. SIMONETTI, A. TAKAMORI, and H. TARIQ: 'Readout system and predicted performance of a low-noise low-frequency horizontal accelerometer'. *Nuclear Instruments and Methods in Physics Research Section A: Accelerators, Spectrometers, Detectors and Associated Equipment* (Aug. 2006), vol. 564(1): pp. 579–586 (cit. on p. 13).

[Bla01] BLACK, E. D.: 'An introduction to Pound–Drever–Hall laser frequency stabilization'. *American Journal of Physics* (Jan. 2001), vol. 69(1): pp. 79–87 (cit. on pp. 46, 50).

[Bog13] BOGAN, C.: 'Stabilized High Power Lasers and Spatial Mode Conversion'. PhD thesis. Leibniz Universität Hannover, 2013 (cit. on p. 42).

[Bog09] BOGENSTAHL, J., L. CUNNINGHAM, E. D. FITZSIMONS, J. HOUGH, C. J. KILLOW, M. PERREUR-LLOYD, D. ROBERTSON, S. ROWAN, and H. WARD: 'LTP fibre injector qualification and status'. *Journal of Physics: Conference Series* (Mar. 2009), vol. 154: p. 012011 (cit. on p. 16).

[Bor01] BORK, R., R. ABBOTT, D. BARKER, and J. HEEFNER: 'An Overview of the LIGO Control and Data Acquisition System'. *eConf C011127 (2001) TUBI001* (Nov. 9, 2001), vol. (cit. on p. 9).

[Cav81] CAVES, C. M.: 'Quantum-mechanical noise in an interferometer'. *Physical Review D* (Apr. 1981), vol. 23(8): pp. 1693–1708 (cit. on pp. 1, 2).

[Cha16] CHALERMSONGSAK, T., E. D. HALL, G. D. COLE, D. FOLLMAN, F. SEIFERT, K. ARAI, E. K. GUSTAFSON, J. R. SMITH, M. ASPELMEYER, and R. X. ADHIKARI: 'Coherent cancellation of photothermal noise in GaAs/Al0.92Ga0.08As Bragg mirrors'. *Metrologia* (Mar. 2016), vol. 53(2): pp. 860–868 (cit. on p. 8).

[Col13] COLE, G. D., W. ZHANG, M. J. MARTIN, J. YE, and M. ASPELMEYER: 'Tenfold reduction of Brownian noise in high-reflectivity optical coatings'. *Nature Photonics* (July 2013), vol. 7(8): pp. 644–650 (cit. on p. 8).

[Cum12] CUMMING, A. V. et al.: 'Design and development of the advanced LIGO monolithic fused silica suspension'. *Classical and Quantum Gravity* (Jan. 2012), vol. 29(3): p. 035003 (cit. on pp. 1, 35).

[Cum09] CUMMING, A., A. HEPTONSTALL, R. KUMAR, W. CUNNINGHAM, C. TORRIE, M. BARTON, K. A. STRAIN, J. HOUGH, and S. ROWAN: 'Finite element modelling of the mechanical loss of silica suspension fibres for advanced gravitational wave detectors'. *Classical and Quantum Gravity* (Oct. 2009), vol. 26(21): p. 215012 (cit. on p. 8).

[Dah13] DAHL, K.: 'From design to operation: a suspension platform interferometer for the AEI 10 m prototype'. PhD thesis. Leibniz Universität Hannover, 2013 (cit. on pp. 14, 18, 21, 26).

[Gil93] GILLESPIE, A. and F. RAAB: 'Thermal noise in the test mass suspensions of a laser interferometer gravitational-wave detector prototype'. *Physics Letters A* (July 1993), vol. 178(5-6): pp. 357–363 (cit. on p. 8).

[Gon13] GONZÁLEZ-CARDEL, M., P. ARGUIJO, and R. DÍAZ-URIBE: 'Gaussian beam radius measurement with a knife-edge: a polynomial approximation to the inverse error function'. *Applied Optics* (May 2013), vol. 52(16): p. 3849 (cit. on p. 26).

[Goß04] GOSSLER, S., G. CAGNOLI, D. R. M. CROOKS, H. LÜCK, S. ROWAN, J. R. SMITH, K. A. STRAIN, J. HOUGH, and K. DANZMANN: 'Damping and tuning of the fibre violin modes in monolithic silica suspensions'. *Classical and Quantum Gravity* (Feb. 2004), vol. 21(5): S923–S933 (cit. on p. 36).

[Gos02] GOSSLER, S. et al.: 'The modecleaner system and suspension aspects of GEO 600'. *Classical and Quantum Gravity* (Mar. 2002), vol. 19(7): pp. 1835–1842 (cit. on p. 3).

[Goß10] GOSSLER, S. et al.: 'The AEI 10 m prototype interferometer'. *Classical and Quantum Gravity* (Apr. 2010), vol. 27(8): p. 084023 (cit. on pp. 2, 3).

[Grä14] GRÄF, C. et al.: 'Design of a speed meter interferometer proof-of-principle experiment'. *Classical and Quantum Gravity* (Oct. 2014), vol. 31(21): p. 215009 (cit. on pp. 8, 35).

[Grä13] GRÄF, C.: 'Optical Design and Numerical Modeling of the AEI 10 m Prototype sub-SQL Interferometer'. PhD thesis. Leibniz Universität Hannover, 2013 (cit. on pp. 42, 48).

[Har02] HARRY, G. M., A. M. GRETARSSON, P. R. SAULSON, S. E. KITTELBERGER, S. D. PENN, W. J. STARTIN, S. ROWAN, M. M. FEJER, D. R. M. CROOKS, G. CAGNOLI, J. HOUGH, and N. NAKAGAWA: 'Thermal noise in interferometric gravitational wave detectors due to dielectric optical coatings'. *Classical and Quantum Gravity* (Feb. 2002), vol. 19(5): pp. 897–917 (cit. on p. 8).

[Hei04] HEINZEL, G., V. WAND, O. JENNRICH, C. BRAXMAIER, D. ROBERTSON, K. MIDDLETON, D. HOYLAND, A. RÜDIGER, R. SCHILLING, U. JOHANN, and K. DANZMANN: 'The LTP interferometer and phasemeter'. *Classical and Quantum Gravity* (Feb. 2004), vol. 21(5): S581–S587 (cit. on p. 16).

[Hen18] HENNIG, J.-S.: 'Mirror Suspensions for the Glasgow Sagnac Speed Meter'. PhD thesis. University of Glasgow, 2018 (cit. on pp. 8, 35).

[Jun17] JUNKER, J., P. OPPERMANN, and B. WILLKE: 'Shot-noise-limited laser power stabilization for the AEI 10 m Prototype interferometer'. *Optics Letters* (Feb. 2017), vol. 42(4): p. 755 (cit. on p. 7).

[Kaw12] KAWAZOE, F. et al.: 'The AEI 10 m Prototype Interferometer frequency control using the reference cavity and its angular control'. *Journal of Physics: Conference Series* (June 2012), vol. 363: p. 012012 (cit. on pp. 7, 8).

[Kir17] KIRCHHOFF, R., C. M. MOW-LOWRY, V. B. ADYA, G. BERGMANN, S. COOPER, M. M. HANKE, P. KOCH, S. M. KÖHLENBECK, J. LEHMANN, P. OPPERMANN, J. WÖHLER, D. S. WU, H. LÜCK, and K. A. STRAIN: 'Huddle test measurement of a near Johnson noise limited geophone'. *Review of Scientific Instruments* (Nov. 2017), vol. 88(11): p. 115008 (cit. on pp. 5, 13, 32, 60).

[Kog66] KOGELNIK, H. and T. LI: 'Laser Beams and Resonators'. *Applied Optics* (Oct. 1966), vol. 5(10): p. 1550 (cit. on pp. 8, 46).

[Leh16] LEHMANN, J.: 'Charakterisierung und Optimierung der Aktuatoren des Single Arm Tests und dessen Installation im AEI 10 m-Prototypen'. MA thesis. Leibniz Universität Hannover, 2016 (cit. on p. 39).

[Lüc10] LÜCK, H., C. AFFELDT, J. DEGALLAIX, A. FREISE, H. GROTE, M. HEWITSON, S. HILD, J. LEONG, M. PRIJATELJ, K. A. STRAIN, B. WILLKE, H. WITTEL, and K. DANZMANN: 'The upgrade of GEO 600'. *Journal of Physics: Conference Series* (May 2010), vol. 228: p. 012012 (cit. on p. 1).

[McN08] MCNAMARA, P., S. VITALE, and K. DANZMANN: 'LISA Pathfinder'. *Classical and Quantum Gravity* (May 2008), vol. 25(11): p. 114034 (cit. on p. 1).

[Mül03] MÜLLER, G., T. DELKER, D. B. TANNER, and D. REITZE: 'Dual-recycled cavity-enhanced Michelson interferometer for gravitational-wave detection'. *Applied Optics* (Mar. 2003), vol. 42(7): p. 1257 (cit. on p. 3).

[Opp17] OPPERMANN, P.: 'Characterization and stabilization of a high power fiber amplifier laser'. PhD thesis. Leibniz Universität Hannover, 2017 (cit. on pp. 3, 42, 43, 50).

[Pli00] PLISSI, M. V., C. I. TORRIE, M. E. HUSMAN, N. A. ROBERTSON, K. A. STRAIN, H. WARD, H. LÜCK, and J. HOUGH: 'GEO 600 triple pendulum suspension system: Seismic isolation and control'. *Review of Scientific Instruments* (June 2000), vol. 71(6): pp. 2539–2545 (cit. on p. 8).

[Põl14] PÕLD, J. H.: 'Design, Implementation and Characterization of the Advanced LIGO 200 W Laser System'. PhD thesis. Leibniz Universität Hannover, 2014 (cit. on p. 7).

[Rob95] ROBERTSON, D. I., E. MORRISON, J. HOUGH, S. KILLBOURN, B. J. MEERS, G. P. NEWTON, N. A. ROBERTSON, K. A. STRAIN, and H. WARD: 'The Glasgow 10 m prototype laser interferometric gravitational wave detector'. *Review of Scientific Instruments* (Sept. 1995), vol. 66(9): pp. 4447–4452 (cit. on p. 1).

[Rus03] RUSSELL, P.: 'Photonic Crystal Fibers'. *Science* (Jan. 2003), vol. 299(5605): pp. 358–362 (cit. on p. 3).

[Sch17] SCHNABEL, R.: 'Squeezed states of light and their applications in laser interferometers'. *Physics Reports* (Apr. 2017), vol. 684: pp. 1–51 (cit. on p. 1).

[Sho88] SHOEMAKER, D., R. SCHILLING, L. SCHNUPP, W. WINKLER, K. MAISCHBERGER, and A. RÜDIGER: 'Noise behavior of the Garching 30-meter prototype gravitational-wave detector'. *Physical Review D* (July 1988), vol. 38(2): pp. 423–432 (cit. on p. 1).

[Sie86] SIEGMAN, A. E.: *Lasers*. Univ Science Books, 1986 (cit. on p. 48).

[Tak07] TAKAMORI, A., P. RAFFAI, S. MÁRKA, R. DESALVO, V. SANNIBALE, H. TARIQ, A. BERTOLINI, G. CELLA, N. VIBOUD, K. NUMATA, R. TAKAHASHI, and M. FUKUSHIMA: 'Inverted pendulum as low-frequency pre-isolation for advanced gravitational wave detectors'. *Nuclear Instruments and Methods in Physics Research Section A: Accelerators, Spectrometers, Detectors and Associated Equipment* (Nov. 2007), vol. 582(2): pp. 683–692 (cit. on p. 5).

[Vah10] VAHLBRUCH, H., A. KHALAIDOVSKI, N. LASTZKA, C. GRÄF, K. DANZMANN, and R. SCHNABEL: 'The GEO 600 squeezed light source'. *Classical and Quantum Gravity* (Apr. 2010), vol. 27(8): p. 084027 (cit. on p. 2).

[Vah16] VAHLBRUCH, H., M. MEHMET, K. DANZMANN, and R. SCHNABEL: 'Detection of 15 dB Squeezed States of Light and their Application for the Absolute Calibration of Photoelectric Quantum Efficiency'. *Physical Review Letters* (Sept. 2016), vol. 117(11) (cit. on p. 2).

[Veg18] VEGGEL, A.-M. A. van: 'Quasi-monolithic mirror suspensions in ground-based gravitational-wave detectors: an overview and look to the future'. *Philosophical Transactions of the Royal Society A: Mathematical, Physical and Engineering Sciences* (Apr. 2018), vol. 376(2120): p. 20170281 (cit. on p. 8).

[Wan12] WANNER, A., G. BERGMANN, A. BERTOLINI, T. FRICKE, H. LÜCK, C. M. MOW-LOWRY, K. A. STRAIN, S. GOSSLER, and K. DANZMANN: 'Seismic attenuation system for the AEI 10 meter Prototype'. *Classical and Quantum Gravity* (Nov. 2012), vol. 29(24): p. 245007 (cit. on pp. 5, 13, 31).

[Wan13] WANNER, A.: 'Seismic attenuation system (AEI-SAS) for the AEI 10 m prototype'. PhD thesis. Leibniz Universität Hannover, 2013 (cit. on pp. 5, 13, 16).

[War08] WARD, R. L. et al.: 'dc readout experiment at the Caltech 40m prototype interferometer'. *Classical and Quantum Gravity* (May 2008), vol. 25(11): p. 114030 (cit. on p. 1).

[Wes16] WESTPHAL, T.: 'A Coating Thermal Noise Interferometer for the AEI 10 m Prototype facility'. PhD thesis. Leibniz Universität Hannover, 2016 (cit. on pp. 63, 64, 66).

[Wil02] WILLKE, B. et al.: 'The GEO 600 gravitational wave detector'. *Classical and Quantum Gravity* (Mar. 2002), vol. 19(7): pp. 1377–1387 (cit. on p. 1).

[Wit15] WITTEL, H., S. HILD, G. BERGMANN, K. DANZMANN, and K. A. STRAIN: 'New design of electrostatic mirror actuators for application in high-precision interferometry'. *Classical and Quantum Gravity* (Aug. 2015), vol. 32(17): p. 175021 (cit. on pp. 36, 39, 40, 53).

List of Figures

A Appendix

A.1 Iodine Frequency Stabilization of NPRO

The Suspension Platform Interferometer is using a Mach–Zehnder interferometer configuration with an arm length miss match of 23 m. Frequency noise is suppressed by stabilizing with a commercially available frequency stabilization. The LISA group provided an measurement of the phase fluctuations of two of these laser stabilization units relative to each other. In figure A.1 the measurement is projected to the equivalent noise in the measurement interferometers of the Suspension Platform Interferometer.

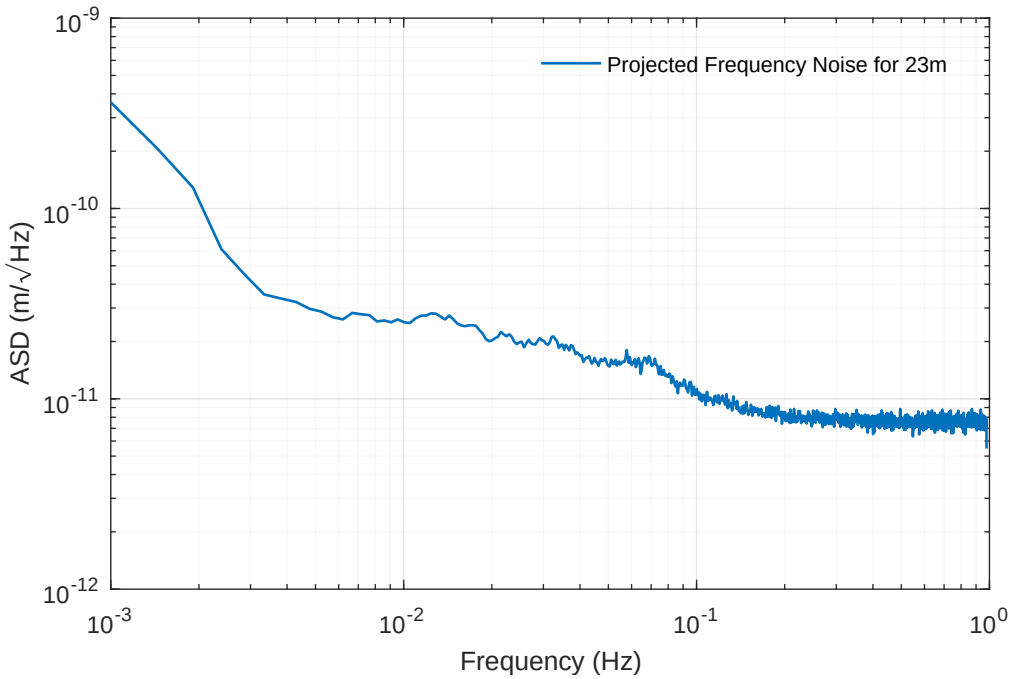

Figure A.1: A measurement of the beat note of two Iodine stabilized lasers, transformed to a noise measurement and projected to the arm length mismatch of the Suspension Platform Interferometer

A.2 Electronics

SAT locking PD

For the readout of the the Single Arm Test a photodiode form the aLIGO PMC was adapted. The transfer function measurement is shown in 3.8 and the schematic in figure A.2. For the Pound-Drever-Hall signal the AC signal of the photodiode is frequency mixed with the local oscillator by an additional board shown in A.3. The DC path of the photodiode is processed by to the board to be converted to a differential signal. The circuit is shown in figure A.4.

Coil/magnet actuator and ESD Driver

The schematics of the coil driver for coil/magnet actuators at the top mass, PUM and the suspended steering mirrors are shown in A.5.

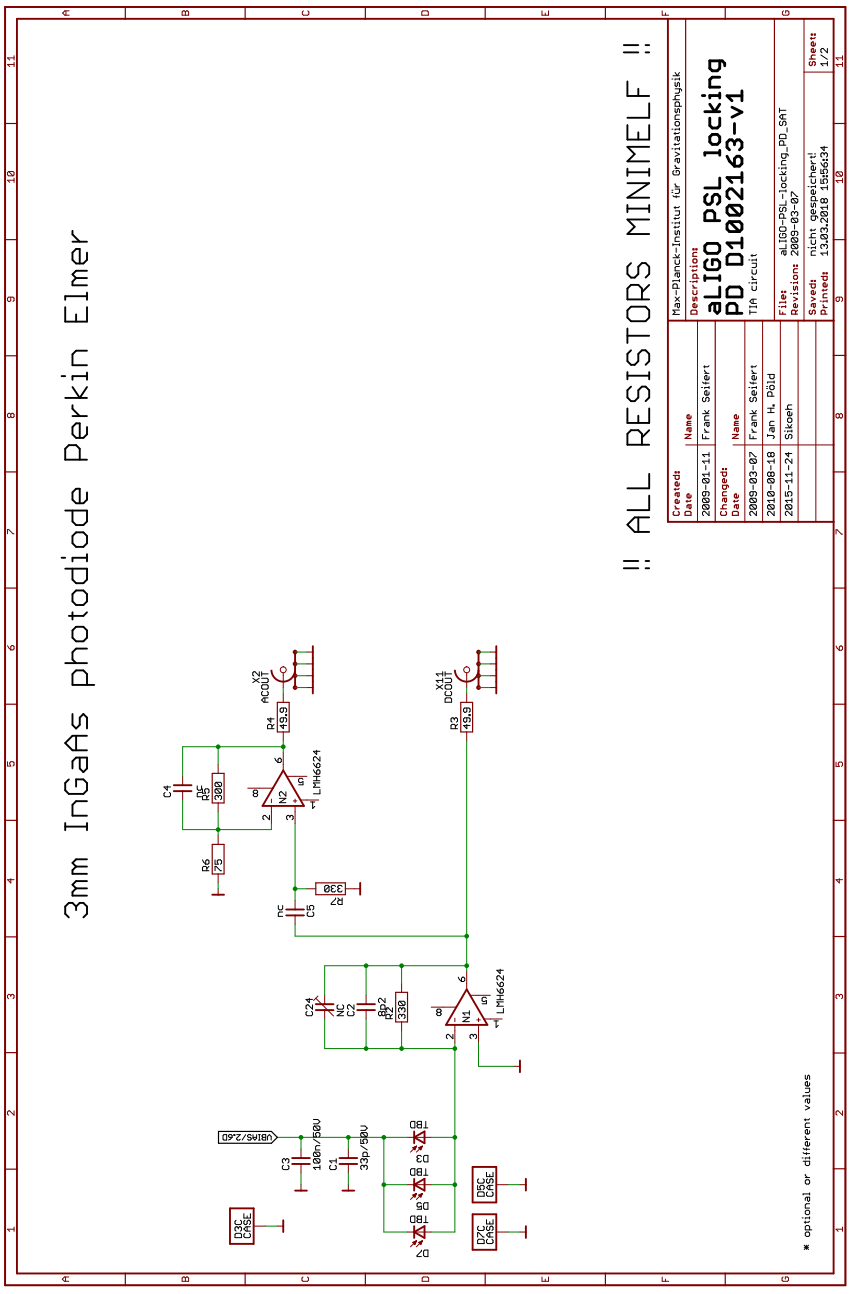

Figure 1: *Project schematics (sheet 1)*

Figure A.2: Schematic of the Single Arm Test locking photodiode.

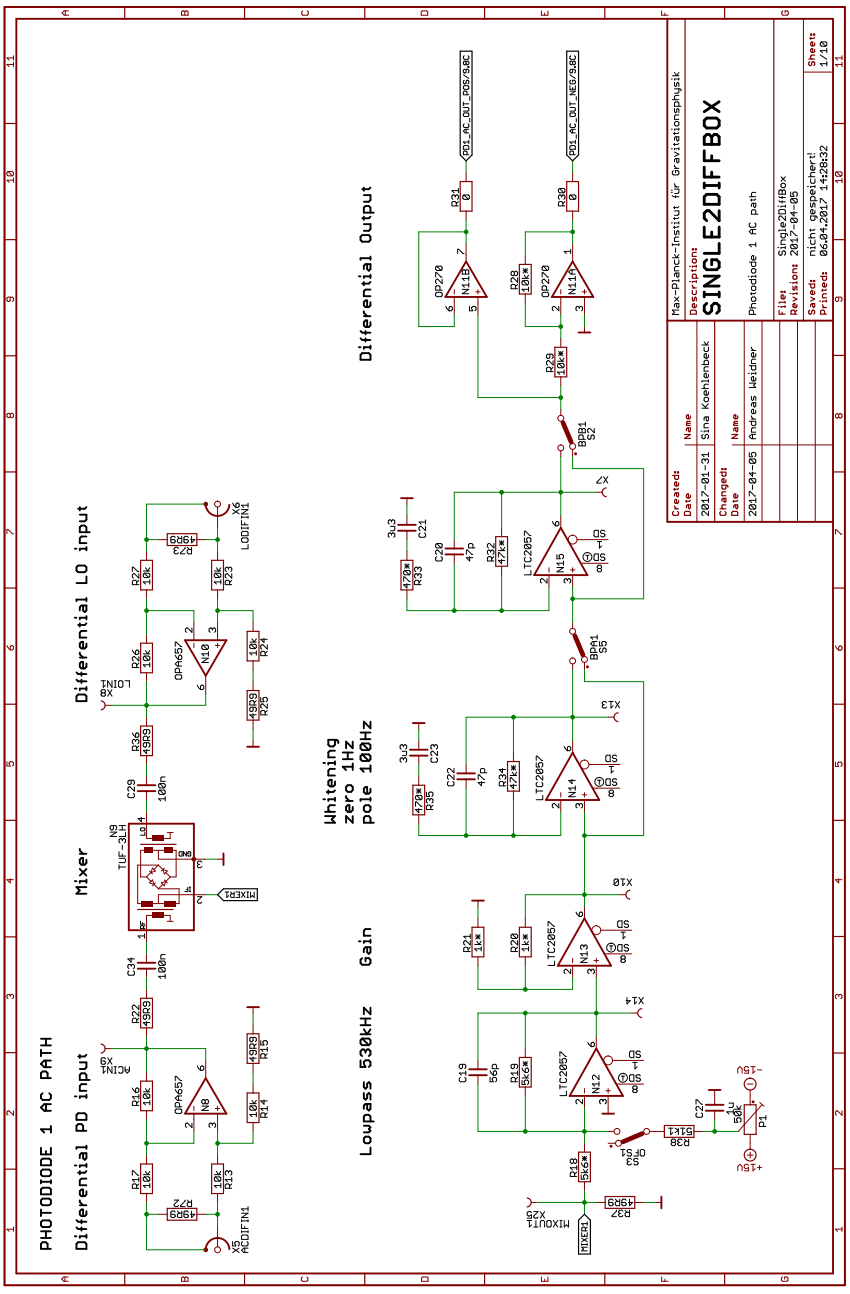

Figure 1: *Project schematics (sheet 1)*

Figure A.3: Schematic of the photodiode to CDS interface the AC-path.

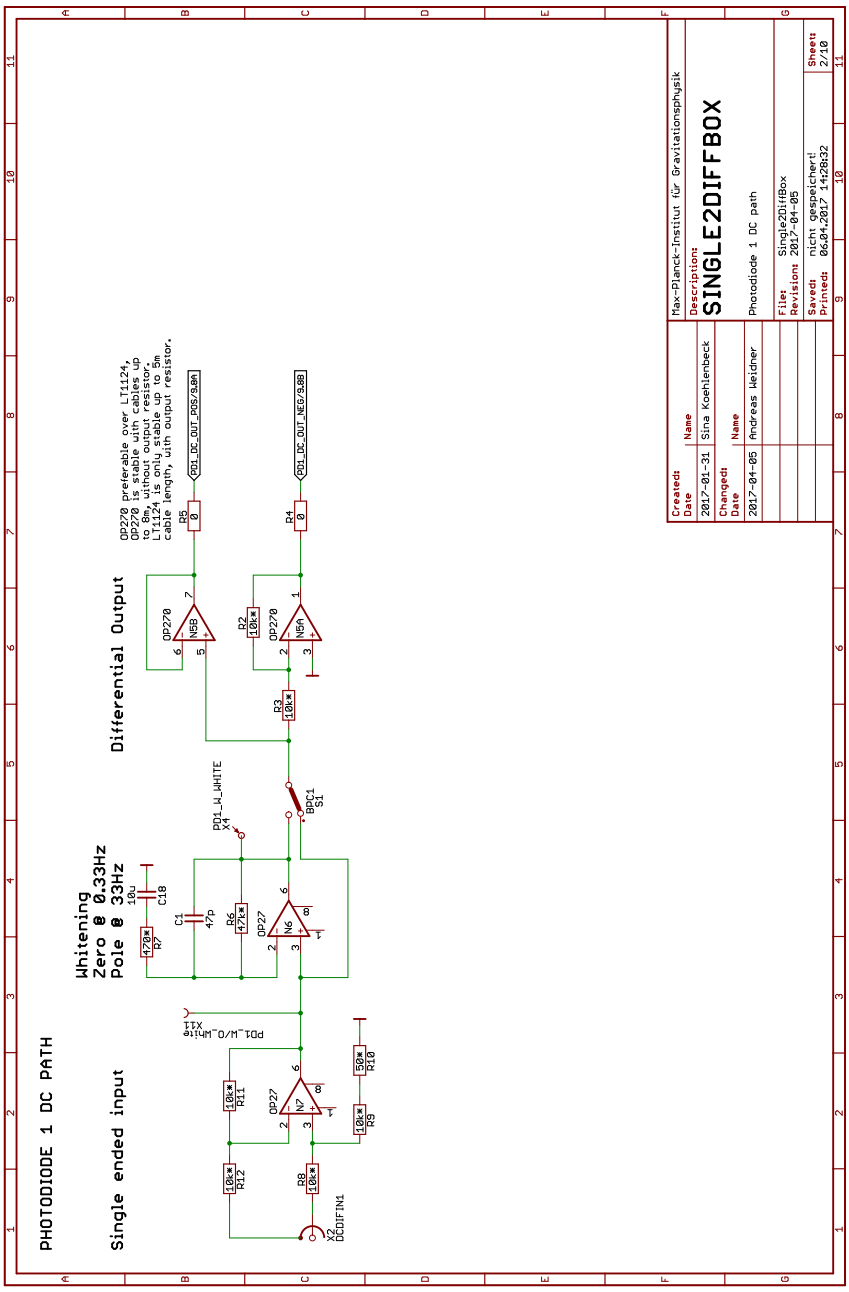

Figure 2: *Project schematics (sheet 2)*

Figure A.4: Schematic of the photodiode to CDS interface the DC-path.

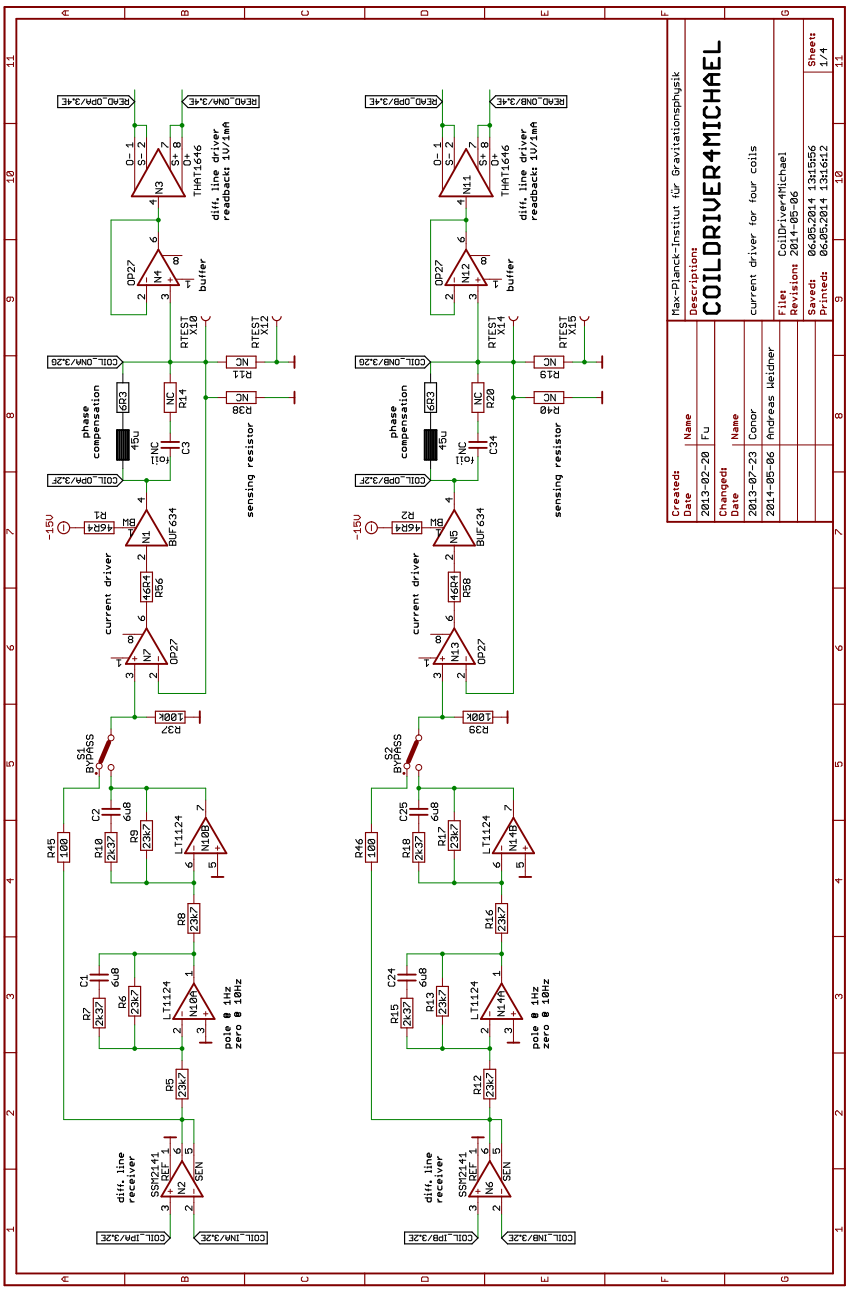

Figure 1: *Project schematics (sheet 1)*

Figure A.5: Coil driver for the suspensions actuators the top mass and Penultimate Mass of the Single Arm Test and the suspended steering mirrors.

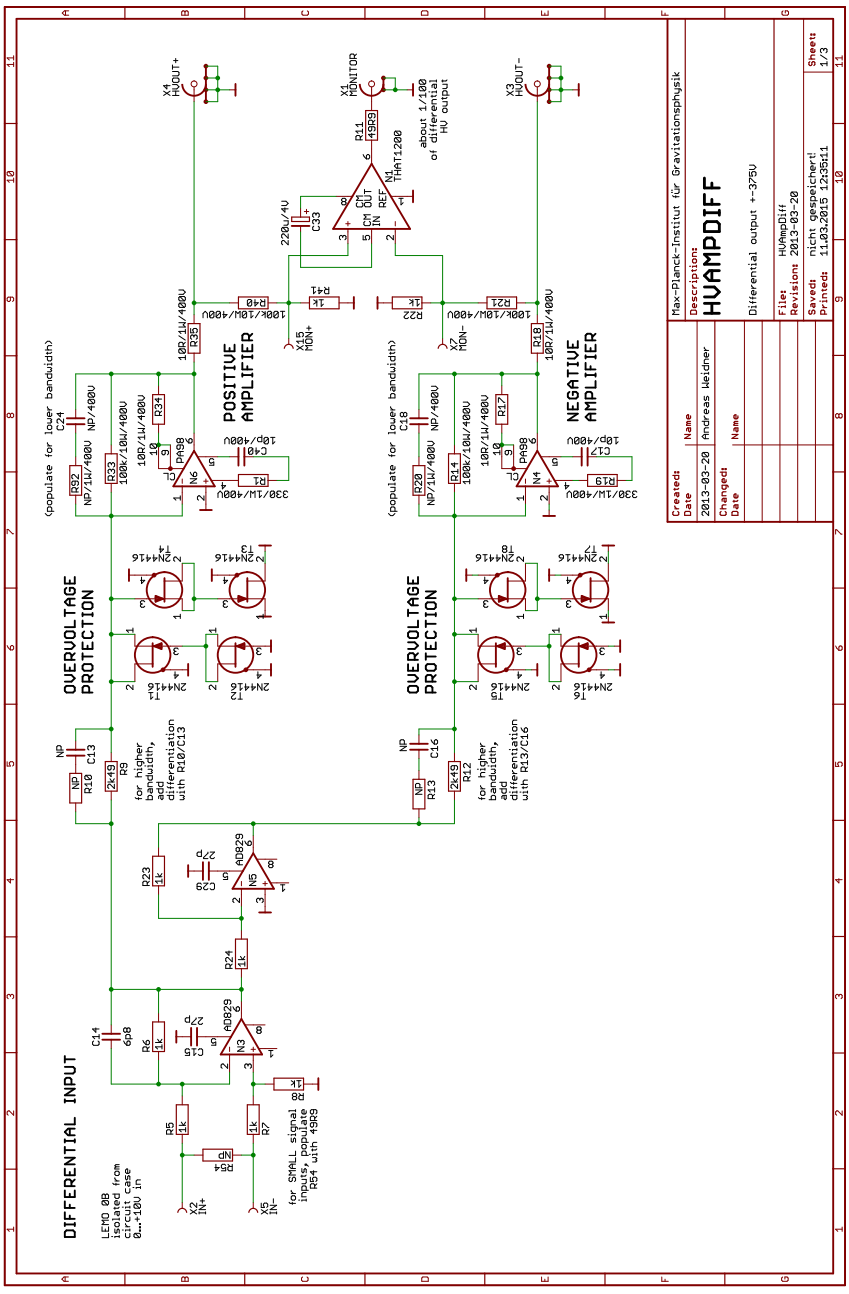

Figure 1: *Project schematics (sheet 1)*

Figure A.6: Schematic of the HV for ESD.

Acknowledgments

I would like thank Prof. Karsten Danzmann and Dr. Harald Lück for the opportunity to write my PhD thesis at the AEI in Hannover.

The AEI is a great place for a PhD student, not only because of its groundbreaking science. The atmosphere and the support of the people in the institute is overwhelming.

I would like to thank all the people of the AEI 10 m-Prototype group who worked with me on our project and especially my former student and now PhD student Johannes Lehmann and the former post-doc Conor Mow-Lowry. Traveling to conferences, opened the view from the busy laboratory work and gave me the possibility to reflect my work. I would like to thank my office colleague and friend Gerald Bergmann in particular for the conversations and the fun times!

Work on the prototype makes use of all the resources AEI has to offer. The support from the mechanical and electrical workshop, especially in "emergencies", was great.

I would also like to thank everyone who supported me in writing and proofreading this work: Vaishali Adya, Stefan Ast, Gerald Bergmann, Manuela Hanke, Steffen Kaufer, Gerrit Kühn, Sean Leavey, Conor Mow-Lowry, Harald Lück, Patrick Oppermann and David Wu.

I would also like to thank Prof. Ken Strain for being the referrer to my thesis and supporting the group with his knowledge every week and Prof. Michèle Heurs, who is also referee and supports me with great advices.

My family supported me during my studies and all the other years and I am very happy to have such a great family!

I thank Patrick Oppermann for supporting my experiments with his knowledge and especially for his support during the last two months!

Much remain unsaid, but I hope you all know how much you have supported me and how grateful I am to you.